

**Development and Characterization of Novel Cellulose-Based Soy Biopolymer  
for Sustainable 3D Printing**

by

Ryan Nodder

A thesis

presented to the University of Waterloo

in fulfillment of the

thesis requirement for the degree of

Master of Science

in

Pharmacy

Waterloo, Ontario, Canada, 2024

© Ryan Nodder 2024

## **AUTHOR'S DECLARATION**

This thesis consists of material all of which I authored or co-authored: see Statement of Contributions included in the thesis. This is a true copy of the thesis, including any required final revisions, as accepted by my examiners. I understand that my thesis may be made electronically available to the public.

## **STATEMENT OF CONTRIBUTIONS**

Ryan Nodder was the sole author of Chapter 1,2 and 4 which were written under the supervision of Dr. Emmanuel Ho.

Within chapter 3, some of the characterization data presented were obtained with assistance from other research groups. SEM imaging and TGA was conducted by Dr. Charles Dal Castel (University of Waterloo, Department of Chemical Engineering). Rheology was conducted by Lian Han of Dr. Tam's research group (University of Waterloo, Department of Chemical Engineering).

## ABSTRACT

Most materials currently used in 3D printing are non-renewable petroleum thermoplastics, which will not support the anticipated growth of 3D printing as the applications and demand of the industry continue to rapidly evolve. In this study, a cellulose-based soy biopolymer (CSBP) feedstock for 3D printing applications is developed. With cellulose-based products accounting for one third of Canada's municipal solid waste, this provides both a solution to the growing problem of environmental pollution and global warming, as well as the need for sustainable materials in 3D printing.

A formulation of soy protein isolate, cellulose and additives has been developed to produce a print media to be used for extrusion 3D printing. A soy-protein component mixed with formulation additives allows for the creation of a self-curing binder, in combination with cellulose as a filler to improve the resulting mechanical properties. A synergistic combination of protein crosslinking, film formation and solvent evaporation is employed to create solid objects with CSBP. Most importantly, this formulation is composed entirely of generally regarded as safe (GRAS) formulation components to become an alternative for extrusion 3D printing that is biodegradable, non-toxic and has environmentally friendly synthesis. The material developed is paste-like in its uncured state and requires a syringe extrusion mechanism for applications in 3D printing. With CSBP established as a 3D printable material through a syringe-based mechanism, multiple physical characterizations are performed to characterize CSBP and provide insights on its overall properties. Furthermore, investigation of some preliminary end-user applications of CSBP were performed to provide insight into the future use of this new biomaterial.

Collectively, this study developed and characterized the use of CSBP feedstock for 3D printing, capable of recycling paper into a new biomaterial. CSBP exhibited a variety of tunable

properties as a function of the curing conditions and time and was found to be naturally biodegradable and biocompatible. Preliminary applications in the adhesive and packaging industries as well as the creation of drug delivery systems were achieved with encouraging initial results. This work highlights a solution to global issues in both the recycling of paper waste and provide a sustainable pathway for the ever-expanding applications of 3D printing.

## **ACKNOWLEDGMENTS**

First and foremost, I would like to thank my supervisor, Dr. Emmanuel Ho, for his mentorship and support through my project. Thank you for allowing me to become a part of your research group, I am grateful for the opportunities you have provided to help me grow not only professionally but personally. In addition, I would like to thank my committee members, Dr. Praveen Rao Perampalli Nekkar and Dr. Mihaela Vlasea, for their insights and support throughout this project.

I would also like to recognize our previous group member, Nischal Ghookal, for working alongside me and assisting with multiple experiments performed throughout this study. It was a pleasure to work with you, and your contributions has greatly enriched this thesis. To the other past and present members of the Ho Research Group that I have had the privilege of working with: Jin Wang, Calvin Wong, Sihan Dong, Alistair Chan, Ethan Watt, Kaidy Orellana, Dr. Chen Sun and David Qi, I am thankful for their friendship and support.

# TABLE OF CONTENTS

<b>AUTHOR'S DECLARATION .....</b>	<b>ii</b>
<b>STATEMENT OF CONTRIBUTIONS .....</b>	<b>iii</b>
<b>ABSTRACT .....</b>	<b>iv</b>
<b>ACKNOWLEDGMENTS.....</b>	<b>vi</b>
<b>LIST OF FIGURES .....</b>	<b>x</b>
<b>LIST OF TABLES .....</b>	<b>xiii</b>
<b>TABLE OF ABBREVIATIONS.....</b>	<b>xiv</b>
<b>1. INTRODUCTION .....</b>	<b>1</b>
<b>1.1 An Introduction to Additive Manufacturing (AM) .....</b>	<b>1</b>
1.1.1 Fused Deposition Modelling (FDM).....	3
1.1.2 Syringe Extrusion 3D Printers in AM .....	4
1.1.3 Syringe Extrusion Mechanisms in AM .....	6
1.1.4 Special Considerations for Printing Pastes .....	6
<b>1.2 Sustainability .....</b>	<b>8</b>
1.2.1 AM and FDM .....	8
1.2.2 Safety of FDM.....	11
1.2.3 Paper Waste .....	11
<b>1.3 Plant Protein Manufacturing.....</b>	<b>12</b>
1.3.1 The Crosslinking Effect .....	12
1.3.2 The Maillard Reaction .....	13
1.3.4 Plant Proteins and AM .....	14
<b>1.4 Soy Protein.....</b>	<b>15</b>
1.4.1 Structure and Crosslinking .....	15
1.4.2 Overview of Soy Protein Biomaterials.....	16
1.4.3 Drug Delivery.....	17
1.4.4 Limitations of Soy Protein Biomaterials .....	18
<b>1.5 Techniques in Material Characterization .....</b>	<b>19</b>
1.5.1 Mechanical Properties .....	19
1.5.2 Degradation Studies.....	20
1.5.3 Drug Delivery Studies .....	21
<b>1.6 Project Overview.....</b>	<b>21</b>
1.6.1 Rationale .....	21
1.6.2 Hypothesis.....	23
1.6.3 Objectives.....	24
<b>2. METHODOLOGY.....</b>	<b>25</b>
<b>2.1 Materials .....</b>	<b>25</b>
<b>2.2 Synthesis of Cellulose-based Soy Biopolymer (CSBP) .....</b>	<b>25</b>
<b>2.3 3D Printing of CSBP.....</b>	<b>27</b>
2.3.1 Rheology.....	28

<b>2.4 Characterizations of CSBP .....</b>	<b>29</b>
2.4.1 CSBP Mechanical Properties .....	29
2.4.2 <i>in vitro</i> Cytotoxicity .....	30
2.4.3 Evaluation of CSBP Biodegradability in Soil.....	31
2.4.4 CSBP Self-Curing and Size Reduction Behavior .....	32
2.4.5 CSBP Thermogravimetric Analysis (TGA).....	32
2.4.6 Water Uptake .....	32
2.4.7 Scanning Electron Microscopy .....	33
2.4.8 Water Contact Angle .....	33
2.4.9 Drug Release Kinetics .....	33
<b>2.5 Applications of CSBP.....</b>	<b>34</b>
2.5.1 Adhesive .....	34
2.5.2 Packaging .....	35
2.5.3 Microneedle Fabrication .....	35
<b>2.6 Statistical Methods.....</b>	<b>37</b>
<b>3. RESULTS AND DISCUSSION .....</b>	<b>38</b>
<b>3.1 Development of CSBP .....</b>	<b>38</b>
3.1.1 Formulation.....	38
3.1.2 Crosslinking .....	39
3.1.3 CSBP Structure and Film Formation .....	41
3.1.4 Self-Curing Behavior of CSBP .....	42
3.1.5 Heat Cured CSBP .....	44
<b>3.2 3D Printing of CSBP via a Syringe-Based 3D Printer .....</b>	<b>46</b>
3.2.1 Rheology of CSBP .....	48
<b>3.3 Mechanical Properties of CSBP .....</b>	<b>49</b>
3.3.1 Tensile Strength .....	49
3.3.2 Compressive Strength .....	51
3.3.3 The Impact of Humidity on Mechanical Strength .....	53
<b>3.4 <i>in vitro</i> Cytotoxicity of CSBP.....</b>	<b>53</b>
<b>3.5 CSBP Degradation.....</b>	<b>55</b>
3.5.1 TGA.....	55
3.5.2 Biodegradation in Soil .....	57
<b>3.6 Water Properties.....</b>	<b>60</b>
<b>3.7 Drug Release Kinetics .....</b>	<b>62</b>
<b>3.8 Heat Cured CSBP Mechanical Properties .....</b>	<b>66</b>
<b>3.9 CSBP Characterization Summary .....</b>	<b>68</b>
<b>3.10 CSBP Applications.....</b>	<b>69</b>
3.10.1 Paper-Based Adhesive.....	69
3.10.2 Sustainable and Biodegradable Packaging Alternative .....	70
3.10.2 Microneedles for Drug Delivery .....	72
<b>4. CONCLUSIONS AND FUTURE DIRECTION .....</b>	<b>76</b>
<b>4.1 Conclusions .....</b>	<b>76</b>
<b>4.2 Limitations .....</b>	<b>79</b>

4.3 Future Directions .....80  
*REFERENCES* ..... 82

## LIST OF FIGURES

<b>Figure 1: Recyclability and Biodegradability of the 3 Most Common FDM Filaments.....</b>	<b>9</b>
<b>Figure 2: General Protein-Protein Crosslinking Mechanism. Made using BioRender.....</b>	<b>13</b>
<b>Figure 3: Maillard Reaction Process. Made using BioRender.....</b>	<b>14</b>
<b>Figure 4: Circular Production of CSBP Diagram. Made with BioRender.....</b>	<b>22</b>
<b>Figure 5: Summary of CSBP Paste Synthesis. Made with BioRender.....</b>	<b>27</b>
<b>Figure 6: Disulfide Bond Formation Mechanism. Made using BioRender.....</b>	<b>40</b>
<b>Figure 7: SEM of Soy Protein Isolate and Microcrystalline Cellulose. (A) SEM of Soy Protein Isolate. (B) SEM of Microcrystalline Cellulose.....</b>	<b>41</b>
<b>Figure 8: SEM of Self-cured CSBP Cross Sections. (A) CSBP at 5.0kx magnification. (B) CSBP at 1kx magnification.....</b>	<b>42</b>
<b>Figure 9: CSBP Self-Curing Weight and Volume Change as a Function of Relative Humidity. (A) CSBP self-curing weight change, evaluated from 10-90% RH. (B) CSBP self-curing volume change, evaluated from 10-90% RH....</b>	<b>43</b>
<b>Figure 10: 3D Printed Heat Cured CSBP Dogbone. Samples was 3D printed and heat cured at 200°C for ....minutes.....</b>	<b>45</b>
<b>Figure 11: Syringe-based 3D Printer used in the 3D Printing of CSBP. FelixFood Single Head 3D Printer.....</b>	<b>46</b>
<b>Figure 12: 3D Printed CSBP Objects. (A) Pyramid printed using base CSBP and 18Ga syringe nozzle (B) Bird printed using base CSBP and 18Ga syringe nozzle (C) Hexagon structure printed using 10% diluted CSBP and 20Ga syringe nozzle (D) Bird silhouette printed using 10% diluted CSBP and 20Ga syringe nozzle. The different color of each object is due to the addition of a water-based pigment to the CSBP formulation.....</b>	<b>47</b>

**Figure 13: Rheology of CSBP for 3D Printing.** Shear rates were recorded from 0.1 to 1000 s<sup>-1</sup> but excluded after 10 s<sup>-1</sup> for better viewing.....49

**Figure 14: Comparison of CSBP Tensile Strength by Self-curing Duration and Relative Humidity.** \*\*p<0.01, \*\*\*p<0.001, \*\*\*\*p<0.0001. Data represents the mean +/- SD (n=3). Error bars are displayed when possible.....50

**Figure 15: Comparison of CSBP Compressive Strength by Curing Time and Humidity. (A) 10% deformation compressive strength of CSBP. (B) 35% deformation compressive strength of CSBP.** \*\*p<0.01, \*\*\*p<0.001, \*\*\*\*p<0.0001. Data represents the mean +/- SD (n=3). Error bars are displayed when possible.....52

**Figure 16: in vitro Cytotoxicity Evaluation of CSBP via Elution-based MTS Assay.** Data represents the mean +/- SD (n=3). .....54

**Figure 17: TGA of Self-cured CSBP.** Samples were tested from 0 to 600°C in N<sub>2</sub> conditions. Formulation components are identified according to the obtained literature values in Table 6.....56

**Figure 18: Soil Biodegradation of Self-cured CSBP. (A) Percent mass remaining of self-cured CSBP over a period of 80 days. (B) Weekly degradation rate of self-cured CSBP samples, expressed as a percentage.** Error bars smaller than the data point symbols are not shown....57

**Figure 19: Visual Representation of Self-cured CSBP Soil Biodegradation Study. (A) Visual representation of CSBP soil biodegradation over time (B) Picture of CSBP with visible growth after first 7 days of soil burial and prior to cleaning.....59**

**Figure 20: Comparison of Self-cured CSBP Soil Biodegradation to Other Thermoplastics.** Comparative mass remaining after 80 days of soil burial for PLA, ABS and CSBP with control. Data represented is the mean +/- SD (n=3). .....59

**Figure 21: CSBP Water Uptake by Curing Condition. Data represents the mean +/- SD (n=3). \*\*p<0.01, \*\*\*p<0.001.....61**

**Figure 22: Comparison of Self-cured and Heat Cured CSBP Water Contact Angles. (A) Self-cured CSBP Water Contact (B) Heat cured CSBP Water Contact.....62**

**Figure 23: Fluorescein Standard Curve in PBS. 6.25 µg/mL – 50 µg/mL, R2 >0.99.....63**

**Figure 24: Fluorescein Release Kinetics from CSBP after 48 Hours in PBS (pH 7.2, 37°C). (A) Fluorescein release kinetics by total released. (B) Fluorescein release kinetics by percent released. (C) Fluorescein-loaded CSBP scaffold. Data represents the mean +/- SD (n=3)....64**

**Figure 25: Comparison of CSBP Mechanical Properties by Curing Condition. The comparison between compressive strength is not direct, and instead between compressive strength at 35% deformation for self-cured CSBP and compressive strength of heat cured CSBP. \*\*p<0.01, \*\*\*\*p<0.0001.....67**

**Figure 26: Preliminary CSBP Packing Peanut Design. (A) Air-based CSBP packing peanut with inserts removed (B) Comparison of CSBP packing peanut size, prior to insert removal, to other common polystyrene packaging peanuts.....71**

**Figure 27: CSBP-PVA Microneedle Macroscopic Appearance and SEM Imaging. (A) image of the CSBP-PVA microneedles using an iPhone and 3x optical zoom. (B) SEM image of the CSBP-PVA microneedle with a magnification of 503x. (C) Image of an array of the CSBP-PVA’s microneedles at a magnification of 100x.....73**

**Figure 28: Insertion Analysis of CSBP-PVA Microneedles. (A) Penetration of 3 layers of Parafilm M with a CSBP-PVA microneedle. (B) Penetration of porcine stratum corneum with CSBP-PVA microneedle.....74**

## LIST OF TABLES

<b>Table 1: Overview of Some Additive Manufacturing (AM) Technologies.....</b>	<b>2</b>
<b>Table 2: Protein Fraction Composition of Soy Protein.....</b>	<b>15</b>
<b>Table 3: Printing Parameters for CSBP Using a Syringe-based 3D Printer.....</b>	<b>28</b>
<b>Table 4: CSBP Formulation Components' Thermal Degradation Obtained from Literature.....</b>	<b>56</b>
<b>Table 5: Summary of CSBP Characterizations.....</b>	<b>69</b>
<b>Table 6: CSBP Preliminary Adhesive Strength by Dilution.....</b>	<b>69</b>
<b>Table 7: CSBP Preliminary Packaging Results.....</b>	<b>72</b>
<b>Table 8: A List of Potential Future Characterizations for CSBP.....</b>	<b>81</b>

## TABLE OF ABBREVIATIONS

<b>3D</b>	Three Dimensional
<b>ABS</b>	Acrylonitrile-butadiene-styrene
<b>AM</b>	Additive Manufacturing
<b>ASTM</b>	American Society for Testing and Materials
<b>CAD</b>	Computer-aided Design
<b>CSBP</b>	Cellulose-based Soy Biopolymer
<b>DDS</b>	Drug Delivery System
<b>DI</b>	Deionized
<b>FDM</b>	Fused Deposition Modelling
<b>GC</b>	Gas Chromatography
<b>GRAS</b>	Generally Regarded as Safe
<b>HEPA</b>	High-efficiency Particulate Arrestance
<b>HPLC</b>	High-performance Liquid Chromatography
<b>ISO</b>	International Organization for Standardization
<b>ODT</b>	Optimal Degradation Temperature
<b>PBS</b>	Phosphate Buffered Saline
<b>PET</b>	Polyethylene Terephthalate
<b>PETG</b>	Polyethylene Terephthalate Glycol
<b>PETT</b>	Polyethylene Cotrimethylene Terephthalate
<b>PLA</b>	Polylactic Acid
<b>RH</b>	Relative Humidity
<b>SD</b>	Standard Deviation
<b>SEM</b>	Scanning Electron Microscopy
<b>SLA</b>	Stereolithography
<b>SPI</b>	Soy Protein Isolate
<b>TEM</b>	Transmission Electron Microscopy
<b>TGA</b>	Thermogravimetric Analysis
<b>UFP</b>	Ultrafine Particles
<b>UTM</b>	Universal Testing Machine
<b>VOC</b>	Volatile Organic Compounds

# 1. INTRODUCTION

## 1.1 An Introduction to Additive Manufacturing (AM)

The creation of objects through the successive formation of layers is referred to as three dimensional (3D) printing or additive manufacturing (AM), and has become a widely popular technology in the last few decades.<sup>1</sup> Unlike traditional forms of manufacturing that rely on techniques such as stamping or injection molding to create objects into a mold using force, AM instead creates physical objects through the continuous addition of material.<sup>1</sup> The recent rise of interest in AM is due not only to the unique advantages and opportunities it presents in commercial industries, but also its potential applications in healthcare and immense research potential.<sup>1</sup> Compared to more traditional forms of manufacturing, AM has several unique advantages within the supply chain matrix such as resource efficiency, production flexibility and customizability.

### 1) Material and Machine Efficiency

AM offers a unique advantage in the supply chain through its efficiency of both materials and parts.<sup>1,2</sup> Unlike processes such as sheeting or injection mold which often leave an excess of material once production is complete, AM processes are built layer-by-layer and therefore can greatly reduce wasted material.<sup>2</sup> As a result of the layer-by-layer mechanism of AM, these processes are extremely efficient in their need for parts and alternate machinery.<sup>1</sup> If we consider a traditional form of manufacturing such as the sheeting of metal, different machines are responsible for the curling, laser cutting, and punching during production.<sup>3</sup> Furthermore, there are several other complimentary components such as coolants, fixtures, cutting tools and molds that are needed for continued production. AM does not require these additional resources and devices for production, providing much more efficient machine use.<sup>1,4</sup>

## 2) Production Flexibility and Customizability

Production flexibility and the customization of products to fit consumer need and demand is made easy by AM processes, as products can be produced on a made-to-order basis.<sup>5</sup> Furthermore, this production flexibility may even greatly reduce the need for other types of costs for businesses such as inventory and warehouse space costs.<sup>4</sup> Among this, the seamless customization of products allows for small quantity production of products such as prototypes, most importantly without the need for new auxiliary resources (such as molds).<sup>1,4</sup> Some of the common processes used in different AM technologies are outlined in the following table:

**Table 1: Overview of Some Additive Manufacturing (AM) Technologies<sup>6</sup>**

<b>Technology</b>	<b>Mechanism of Action</b>
<b>Fused Deposition Modelling (FDM)</b>	Polymer is heated and extruded in consecutive layers, solidifying layer-by-layer to form a final object. FDM is the most common form of AM.
<b>Stereolithography (SLA)</b>	A beam of UV light interacts with a vat of photosensitive resin, hardening the resin as it interacts with it.
<b>Binder Jetting</b>	An inkjet deposits a liquid binding agent onto a thin layer of powder.
<b>Electron Beam Direct Beam Manufacturing</b>	Use of a high energy electron beam to fuse together layers of powdered metal for the construction of metal parts
<b>Polyjetting</b>	A combination of binder jetting and SLA in which a photopolymer is jetted upon a build plate and subsequently cured with the use of UV light
<b>Laminated Object Manufacturing</b>	Use of an adhesive-coated material such as paper, metal or plastic laminate as a medium. Sheets are glued together and cut using a laser cutter or knife to form objects.

Being that AM contains a broad range of processes and technologies, the materials used also vary greatly and include but are not limited to: polymer thermoplastic filaments, metals, ceramics, resins, nylons, powders, pastes and more.<sup>6,7</sup> Being that the scope of AM is broad and there are many diverse processes, a summary to fused deposition modelling (FDM) and syringe extrusion mechanisms of AM will be provided to establish the AM fields related to this study.

### **1.1.1 Fused Deposition Modelling (FDM)**

The most common type of AM is a form of 3D printing called fused deposition modelling (FDM), which involves the creation of physical objects through the heated extrusion of thermoplastic filaments.<sup>8</sup> FDM works by having thermoplastic filament pass through a heated nozzle, commonly referred to as the hot head, which melts the filament and allows it to flow and be extruded onto the build platform where it cools and resolidifies to form a layer.<sup>8,9</sup> FDM is the most used AM process in both industry and with consumers, with a reported 51% of AM products relying on the use of FDM technology and polymer-plastic filaments.<sup>9</sup> FDM printing applications range from industrial production of everyday objects to drug delivery scaffolds and tablets as a result of the thermoplastic filaments' diversity.<sup>7,10,11</sup>

FDM printers can print several different types of thermoplastic filaments, which vary in the resulting post-print properties.<sup>12</sup> Among FDM filaments, perhaps the most commonly used and well-known material is polylactic acid (PLA).<sup>13,14</sup> PLA has quickly become the most popular thermoplastic used for FDM printers in the last two decades, due to its production being environmentally preferred over other filaments, as well as its ease of use in FDM 3D printers.<sup>13</sup> PLA is based off of renewable resources such as corn and sugar cane, and involves multiple reactions for the isolation of lactide which is then polymerized into a PLA powder that is made into a filament.<sup>13</sup> The second most common filament used for FDM prints is acrylonitrile-butadiene-styrene polymer (ABS), which often has superior mechanical properties to PLA although dependent on the use of fossil fuels for its formation.<sup>15,16</sup> Beyond ABS and PLA, the third most common thermoplastics in FDM are polyethylene terephthalate glycol (PETG) and its variations polyethylene terephthalate (PET) and polyethylene cotrimethylene terephthalate

(PETT), which is more ductile and naturally transparent compared to other FDM thermoplastics.<sup>17,18,19</sup>

### **1.1.2 Syringe Extrusion 3D Printers in AM**

Syringe extrusion mechanisms of AM are a relatively new expansion to the AM field, and as a result there are few 3D printers capable of syringe extrusion that are widely commercially available. In fact, the current state of syringe extrusion mechanisms of AM can be grouped into three main categories that each differ in their functionality and uses:

#### 1) Food 3D Printing

The most common and feasible form of syringe extrusion for AM is food 3D printing, which has rapidly gained commercial and scientific interest in the last decade.<sup>20</sup> The increasing interest in food 3D printing comes from the potential for creating personalized food and nutrition, as well as accommodating several types of dietary restrictions.<sup>20</sup> For example, it is estimated that up to 60% of people at nursing homes have difficulty chewing and swallowing food, and as a result are provided with unappetizing foods.<sup>21</sup> This has been shown to cause a loss of appetite and subsequent nutritional deficiencies, however, with food 3D printing, these problems can be addressed through the creation of customized food that is both appetizing and easy to swallow.<sup>20,21</sup>

Food 3D printers are capable of printing a wide variety of foods, and work through extrusion-based mechanisms similar to FDM.<sup>20</sup> Where this technology differs from FDM printing is in the type of extrusion, as a syringe system is used in place of a hot head.<sup>20,21</sup> This means that the resulting prints of a food 3D printer often do not cure immediately after being extruded, unlike FDM. Foods suitable for use in syringe-based food 3D printing must be processed into a paste with rheology favourable for consistent extrusion through a nozzle, and mechanical integrity for layer formation.<sup>20</sup> Besides from the rheology of the food, several other properties such as syringe and

build platform temperature are important for each food that is being extruded.<sup>20,22</sup> The syringe and build plate temperature used for most foods is room temperature extrusion, however, for some foods such as chocolate, heated extrusion is used to facilitate the flow of the paste.<sup>20,21</sup>

## 2) 3D Bioplotter

Another form of syringe extrusion within AM is the use of a 3D bioplotter, which is a newer technology first created in 2003 that allows for the printing of cells, hydrogels and other novel biomaterials.<sup>23</sup> Much of the research interest with 3D bioplotters is with respect to the immense potential for the biomedical applications of AM such as bone regeneration through tissue scaffolds, drug releases, organ printing, cartilage formation and more.<sup>23,24</sup> Bioplotters may vary in their exact printing mechanism depending on the print mediums, however, most commonly involve the use of one or multiple syringes to extrude media with a piston or sterile compressed gas.<sup>23,25,26</sup> The extrusion mechanisms used in bioplotters is syringe-based, however, in some cases the nozzle diameter used is in the micro-meter range opposed to millimeter gauge nozzles used in food 3D printing.<sup>23,27,28</sup> The future applications and potential for bioplotters to change modern medicine is of great interest and has received a high amount of research interest since being developed.<sup>23,24</sup>

## 3) Other Syringe-based 3D Printers

While food 3D printers and bioplotters make up most syringe-based printers that are commercially available, it is worth mentioning that some other forms of syringe-extrusion 3D printers are commercially available or have been reported in literature. For example, companies have developed syringe extrusion mechanisms that can be substituted onto a FDM printer in place of the hot head. In this case, a syringe 3D printer is not commercially available, but instead an existing FDM printer can be re-engineered to accommodate syringe-based 3D printing. The conversion of a FDM printer into a syringe-extrusion printer is also the most common method used

by researchers to create their own syringe 3D printer for research, and several articles have been published outlining this process.<sup>29,30,31</sup> The underlying mechanism of FDM and syringe-extrusion based 3D printing is similar, and the substitution of a hot-head for syringe system as well as adjustments to the g-codes can successfully convert a FDM printer to print using a syringe-based mechanism.<sup>29,31</sup>

### **1.1.3 Syringe Extrusion Mechanisms in AM**

The type of syringe-based mechanism used in AM varies depending on the print media used and falls into three general categories. The most common mechanism used in syringe-based extrusion is the use of a syringe plunger or piston which is compressed downward by a stepper motor to force the media through the nozzle. This is the most common mechanism for food 3D printers and syringe-based 3D printers created by researchers.<sup>26,32-34</sup> Another form of mechanical extrusion, a screw-type mechanism, may be used for AM and works by a stepper motor rotating a screw to drive print media downwards through the nozzle.<sup>35</sup> This screw-type mechanism is seldom used in syringe-based 3D printing processes beyond food 3D printing, due to its overall complexity and several limitations.<sup>35</sup> A pneumatic system in which compressed air or gas is used to create pressure for the extrusion of print media rather allows the printing of higher viscosity print media than the two aforementioned mechanical methods.<sup>26,35</sup> A pressure based system for syringe-based AM also allows for easier control of potential contaminants through the use of sterilized air or gases in bioprinting.<sup>26</sup>

### **1.1.4 Special Considerations for Printing Pastes**

Although the 3D printing of pastes and slurries is achievable through mechanisms like that used in FDM, pastes behave differently when extruded and have special limitations that must be considered prior to use:

### 1. Consistent Extrusion and Viscosity

In FDM printing, thermoplastic filament is melted into a liquid prior to extrusion by the hot-head, however, pastes are instead semi-solid during extrusion and have greater viscosity.<sup>9</sup> This presents a potential issue with extrusion, as pastes capable of being 3D printed must have rheology that allows for consistent extrusion through a syringe pump.<sup>36</sup> If a paste is too viscous, it will jam the syringe preventing consistent extrusion, while pastes that are too fluid may extrude as liquid and have trouble forming physical structures with subsequent layers.<sup>36</sup>

### 2. Mechanical Integrity

Pastes that are suitable for use in syringe-based 3D printing must have mechanical integrity and self-supporting stability after being extruded, to support the extrusion of successive layers that do not undergo any external curing stimuli.<sup>36</sup> That is, a paste must be able to support its own structure with the addition of additional layers to prevent sag or buckling.<sup>20,36</sup> If the mechanical integrity of the paste is low, the weight of additional layers will cause the resulting structure to become deformed.<sup>36</sup>

### 3. Layer Lines and Resolution

For a paste to be suitable for use in AM, it must be able to form an appropriate final product. Specifically, it must have sufficient resolution to create the desired final product and limited definition lines.<sup>36,37</sup> Layer lines, sometimes referred to as definition lines, are horizontal lines that appear in the final print of an object and are often a result of the over-extrusion of material, and are an indication of the overall resolution of the 3D printed object.<sup>37</sup>

#### 4. Support and Overhang

With the computer-aided design (CAD) aspect of 3D printed pastes, there are two main limitations to syringe-based 3D printing applications: support and overhang. AM works through the creation of objects layer-by-layer; however, most objects are not built with this considered and instead have longer segments at unequal points vertically. Being that FDM printers work layer-by-layer, they are not capable of printing on air and instead rely on the use of printed support structures to accommodate these conditions.<sup>38</sup> With syringe-based 3D printing, support structures are extremely difficult to integrate due to the nature of pastes' mechanical integrity, and overhang between layers must be minimal to avoid sagging.

### **1.2 Sustainability**

#### **1.2.1 AM and FDM**

There is a growing belief that AM is a promising suitor for creating and sustaining a future global circular economy.<sup>39</sup> A circular economy refers to an industrial economy that is fully restorative, and is based upon ultimate resource efficiency and the elimination of waste.<sup>39</sup> Currently, there are two main issues AM faces with respect to creating a circular economy: the use of petroleum thermoplastics, and the use of fossil fuel plants to power 3D printers.<sup>40</sup> This section will focus on the first of two issues, the use of petroleum thermoplastics with respect to FDM sustainability.

One major hurdle FDM faces with creating a circular economy is its reliance on petroleum-based thermoplastic filaments, mainly ABS and PET associated filaments, as these are produced from exhaustible petroleum resources.<sup>39-41</sup> It is estimated that 4% of global oil and gas production is used for the synthesis of non-renewable plastic feedstock, with an additional 3-4% being used to provide the energy needed for manufacturing.<sup>42</sup> With a grim warning from the United Nations

in their annual climate report released on March 20<sup>th</sup> 2023, it is evident that there is an immediate need for a drastic reduction of carbon emissions and use of non-renewable petroleum resources by 2035 to prevent impending climate disaster.<sup>43</sup> Furthermore, although offering advantages in the supply chain matrix FDM is not void of waste material, as a study assessing material waste under real-world conditions found that 34% of material used in FDM prints were wasted in an open studio setting.<sup>44</sup> With FDM accounting for over half of all AM usage, it is integral that more sustainable processes and materials are developed to reduce the use of demand for petroleum thermoplastics and carbon emissions associated with production.<sup>9</sup>

While the sustainability of current FDM thermoplastic filaments' raw materials is problematic, there are also issues with respect to the recyclability and biodegradability of these materials, beginning with the fact that only 9% of the plastic used in Canada is recycled.<sup>45</sup> A summary of the reported recyclability and biodegradability of the three most common materials used in FDM prints is provided in Figure 1 below:

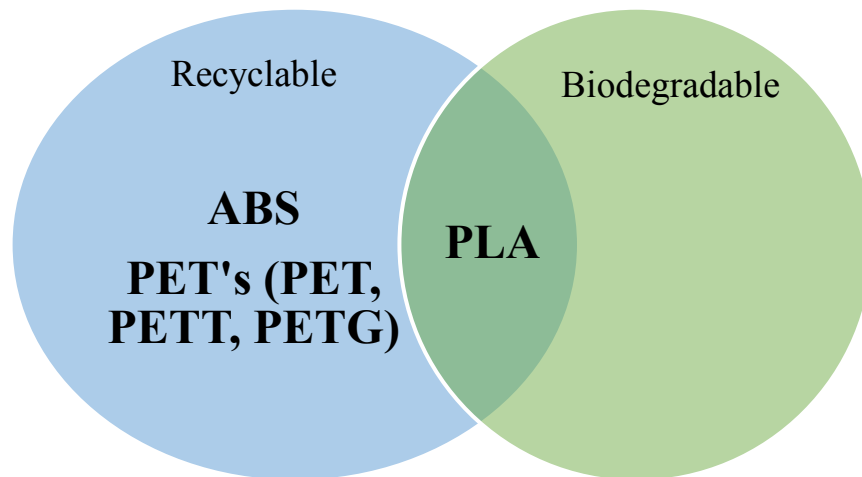


**Figure 1: Recyclability and Biodegradability of the 3 Most Common FDM Filaments<sup>46-48</sup>**

While it appears that the use of ABS, PLA, and PET's (PET, PETT, PETG and other PET plastics) in FDM prints may be sustainable due to the noted recyclability and biodegradability,

these listed properties have major limitations to consider. Firstly, it is often promoted that PLA is both recyclable and biodegradable, however, both of these properties are only achieved under specific and controlled conditions.<sup>47,49</sup> The recyclability of PLA is misleading as it is not collected by municipal recycling programs and as there is no resin identification number associated with it, as well as no other programs currently in place to collect it.<sup>50,45</sup> There is also a common misconception with the biodegradability of PLA, as it is widely believed that biodegradable materials are instead compostable and can be disposed of and reduced by the natural environment.<sup>51,52</sup> This is not the case for PLA, as it instead requires the use of industrial composting that combines the use of specific temperature and humidity as well as the presence of PLA-degrading microorganisms such as *Pseudonocardiaceae* species, none of which are available at municipal recycling stations.<sup>47,51</sup> Despite major limitations to both the listed recyclability and biodegradability of PLA, its environmentally-friendly properties are often wrongly communicated within the AM community and may even be used as a form of greenwashing.<sup>53,54</sup> It is worth noting that PLA is still a much more environmentally-preferred thermoplastic than other materials used in FDM due to its use of renewable raw material for production, however, with a lack of infrastructure to support its recycling and biodegradability the current sustainability of PLA still remains limited.<sup>53</sup>

Like PLA, ABS lacks an identification number for street-collection recycling, although PET's are a commonly recycled plastic and identified by #1 in the identification system for municipal recycling.<sup>50</sup> Due to the production of PLA and PET's relying on the use of petroleum based materials, neither are biodegradable.<sup>46,48</sup>

### **1.2.2 Safety of FDM**

With a rapid increase in the popularity of FDM printing in the last decade, the development of low-cost 3D printers has become widely available for use by both small businesses and hobbyists who may lack the resources that industrial companies have to ensure safe usage.<sup>55</sup> With the production and processing of thermoplastics, potentially carcinogenic volatile organic compounds (VOC) and ultrafine particles (UFP) are emitted into the air during thermal degradation.<sup>55-57</sup> A study assessing the thermal degradation of PLA, ABS and PET filaments using thermogravimetric analysis (TGA) and VOC emission test procedures revealed that all three thermoplastics undergo partial decomposition and emit VOC at their FDM print temperatures.<sup>55</sup> The resulting gas chromatography (GC) analysis of this research showed that ABS emits much higher quantities of VOCs than PLA, nylon, PET, with nylon and PET being much lower due to a higher thermal stability.<sup>55</sup> The publication highlighted is just one of the multiple evaluations that have been conducted to evaluate the safety of FDM with respect to its VOC and UFP emission. Since the thermal degradation of thermoplastic filament is necessary for FDM, the release of VOC and UFP is not preventable and instead should be managed using special filters.<sup>55,58</sup> While high-efficiency particulate arrestance (HEPA) filters are sometimes used in FDM to manage the UFP emitted during printing, they cannot remove particles smaller than 0.3µm and gaseous pollutants such as VOCs.<sup>55,56,58</sup> FDM processes must be improved to develop safer operating procedures to limit the operator's exposure to VOC and UFP during production, as many commercially available 3D printers do not come with protective filters.

### **1.2.3 Paper Waste**

In 2018, paper fibres accounted for the largest amount of total waste diverted by material in Canada at 36%, and continues to account for a large proportion of global landfills.<sup>59</sup> Despite

global recycling efforts, paper waste is still a large contributing factor to solid waste due to limitations associated with the recycling of paper. Many types of paper, such as those that have been treated, coated, laminated or touched by food waste cannot be reused, which prevents them from being recycled.<sup>60,61</sup> It is highly unlikely that paper waste will be fully eliminated by established recycling programs, and instead interest has emerged upon finding new ways to recycle paper waste into new products.<sup>62,63</sup>

### **1.3 Plant Protein Manufacturing**

With increasing environmental concerns and the depletion of non-renewable resources, great importance has been placed on new sustainable solutions for products used in our everyday life.<sup>64</sup> The need for green biomaterials as an alternative to petroleum plastics is clear, and researchers have begun to evaluate the potential of plant proteins as a source of plastic products.<sup>64-66</sup> Plant proteins refers to a category of proteins encompassing multiple different natural protein sources such as soy proteins, wheat protein and glutens, corn zein, casein and more.<sup>64</sup> There are several different processes that can utilize the properties of plant proteins to create different products, however, a common approach is the creation of biopolymers using crosslinking.<sup>65,66</sup> The creation of biopolymers uses the crosslinking effect to polymerize protein monomers into networks of crosslinked proteins, and has shown great promise in creating new biomaterials.<sup>64,67,68</sup>

#### **1.3.1 The Crosslinking Effect**

Protein crosslinking is a process by which covalent bonds are formed between proteins, called intermolecular crosslinking, or intramolecular crosslinking between polypeptide chains of the same protein.<sup>69-71</sup> In nature, these crosslinks are crucial for maintaining protein conformation and structure, and play a role in biological processes such as ageing.<sup>69,72</sup> The crosslinking of proteins is not limited to the natural crosslinking of proteins to provide function, and can also be

selectively introduced using multiple methods.<sup>71</sup> Changes in temperature, pH, oxidizing conditions, the additional of chemical agents or enzymes may be used to induce protein crosslinking through changing the protein structure (often denaturation) and exposing additional functional groups.<sup>28,71,73</sup> Interest in protein crosslinking is not limited to the synthesis of plant protein plastics, as crosslinked proteins can take on different forms and applications.<sup>73</sup>

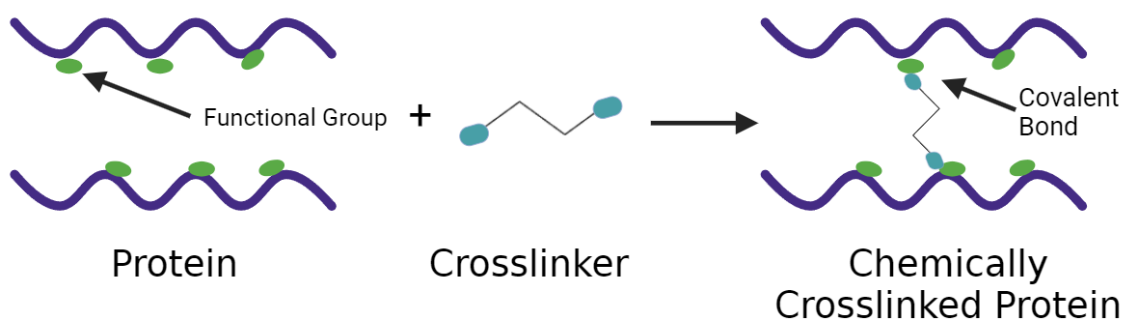


**Figure 2: General Protein-Protein Crosslinking Mechanism. Made using BioRender.**

Crosslinking agents are common reagents in plant protein materials that are used to induce protein crosslinking by binding to functional groups of two protein strands to form a crosslink between them, as shown in Figure 2.<sup>74</sup> The specific binding sites and interactions of the crosslinking effect is specific to the plant protein of interest, and thus crosslinking agents used can vary greatly in chemical composition and their interactions.<sup>73</sup>

### 1.3.2 The Maillard Reaction

The Maillard reaction, or sometimes referred to as glycosylation, has been extensively used throughout the food industry since its original discovery by Louis Camille Maillard in 1912.<sup>75</sup> The Maillard reaction is a complex browning process that occurs when a protein source is in the presence of reducing sugars and heat, and undergoes a series of reactions.<sup>75</sup> First, a condensation reaction between the carbonyl group of a reducing sugar and a free amino group, either from a residue or the core amino group, forms a Schiff base that self-rearranges into a Amadori or Heyns

product.<sup>75</sup> After this, an intermediate reaction occurs and the Amadori/Heyns product undergoes dehydration and fission to form highly reactive compounds, which then reacts in the third stage of the reaction to form a wide variety of end compounds.<sup>75</sup> The most notable end products of the Maillard reaction, melanoidins, are a group of nitrogenous polymers formed during this process and contribute to the brown appearance and aroma of many foods, such as coffee.<sup>75,76</sup>

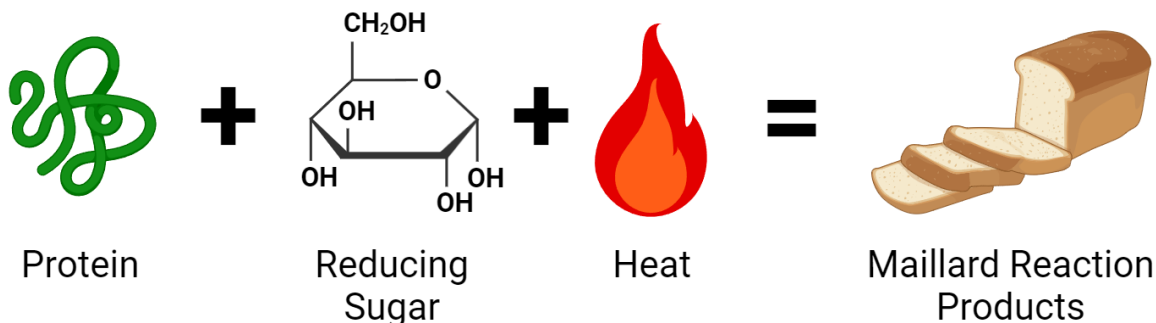


**Figure 3: Maillard Reaction Process. Made using BioRender.**

While the most common uses of the Maillard reaction comes from the food industry, researchers have begun to access the potential for the Maillard reaction as a mechanism for biopolymer synthesis. These types of products rely on the non-enzymatic and green synthesis of biopolymers using Maillard-type crosslinking, by using the covalent bonds formed in the initial Maillard condensation reaction to create biomaterials with applications such as drug delivery scaffolds and films.<sup>75,77</sup>

### 1.3.4 Plant Proteins and AM

Interest in integrating biomaterials with AM has rapidly emerged in the 21<sup>st</sup> century and become an increasingly popular approach to expanding the potential applications of plant-proteins.<sup>22,78,79</sup> Currently, the most common approach to AM and plant proteins is in the food 3D printing industry for the creation of edible foods, however, recently researchers have evaluated the potential biomedical and commercial applications of plant proteins with AM.<sup>28,78,80</sup> With

increasing research in developing regenerative medicine through tissue engineering, there is a need for biocompatible and biodegradable scaffold materials.<sup>81,82</sup> Many plant proteins have good biocompatibility and cytoaffinity due to their biological nature, which makes them strong candidates for the fabrication of tissue scaffolds and other biomedical applications using AM.<sup>82,83</sup>

## 1.4 Soy Protein

Experimentation with soy protein materials have been of interest for their potential commercial uses for nearly a century, dating back to the soybean car experiments of Henry Ford in the late 1930's.<sup>84</sup> Interest in soy protein plastics has re-emerged in the last few decades, as researchers aim to develop biomaterials that can ultimately reduce the need for petroleum-based resources.<sup>84,85</sup> Soybeans are one of the most agriculturally produced plants worldwide, due to its prominent role in the oilseed industry.<sup>84,85</sup> The potential for soy protein-based plastics that rely on the crosslinking effect use the isolated protein component of soy, which is extracted from soybean meal.<sup>85</sup> This soy protein isolate (SPI) is highly refined, consisting of greater than 90% protein which is favourable for introducing protein crosslinking.<sup>85</sup>

### 1.4.1 Structure and Crosslinking

**Table 2: Protein Fraction Composition of Soy Protein**<sup>85-87,88,89</sup>

<b>Protein Fraction</b>	<b>Molecular Weight (g/mol)</b>	<b>Properties</b>
<b>Bowman-Bark Trypsin Inhibitor</b>	24,000	- Can form dimers and trimers - High cystine content
<b>Kunitz Trypsin Inhibitor</b>	21,000	- Disulfide linkages - Single reactive site
<b>Hemagglutinin</b>	100,000-110,000	- No disulfide crosslinks
<b>Lipoxygenase</b>	102,000	- Can be dissociated into two fragments
<b>7S Globulin</b>	180,000 - 210,000	- Can dissociate into smaller subunits (2S, 5S) at acidic pH
<b>11S Globulin</b>	330,000 – 350,000	- Easily dissociates into 7S globulin fragments

Soy protein is not a simple protein but instead an assortment of multiple types of protein fractions.<sup>85</sup> Some of the protein fractions that make up soy protein are listed in Table 2 with their molecular weight and some of the relevant binding and dissociation properties. Soy protein is known to be hydrophilic and hygroscopic, and over 60% of its functional groups are hydrophilic.<sup>85,90</sup> Of soy proteins' functional groups, lysine (5.50 molar %) and arginine (5.56 molar %) are of great interest for inducing amino soy protein crosslinking, due to additional available amine groups.<sup>85,91-93</sup>

Currently, the most common application of soy protein crosslinking is with the creation of edible films.<sup>87,94</sup> The basis of soy protein film production is a three step process: soy protein functional groups are disrupted and exposed by changing the conditions, polymer chains are arranged, and films are produced by forming a 3D network of new interactions after the disrupting agent is removed.<sup>85,94</sup> Common additives for soy protein films include hydroxyl agents such as glycerol and sorbitol, as well as other compounds with active carboxyl and hydroxyl groups.<sup>85,86,94,95</sup>

#### **1.4.2 Overview of Soy Protein Biomaterials**

Currently, soy protein biomaterial development has been of interest to many researchers for the creation of new green biomaterials, with multiple different approaches to how soy protein can be used in synthesis.<sup>85,96</sup> Many of SPI's properties such as biodegradability, biocompatibility, renewability, processability and its inexpensive nature make it a great candidate for material development and research across a wide range of industries.<sup>85,96,97</sup>

Soy protein-based materials have been evaluated for their potential in film formation, through crosslinking mechanisms involving the use of heat, pressure, enzymes or pH.<sup>80,94,96,98</sup> This film formation is reliant on variable crosslinking mechanisms with soy protein in combination with

the external stimuli and a diverse range of crosslinkers added to the formulation.<sup>71,73,95</sup> Multiple modification methods have been developed to facilitate various methods of crosslinking and dictate the end properties of SPI-based materials, such as lipid and oil integration, fillers, radiation and enzymatic action.<sup>96</sup>

One promising approach to overcome some of the deficiencies associated with SPI-based materials is with the use of a filler. Fibrous materials such as cellulosic and glass fibres have been integrated in SPI-based materials to increase properties such as mechanical strength, water resistance and bond strength, while food-based emulsifiers are sometimes used in the creation of food-based soy materials in AM.<sup>28,96,99–101</sup> These filler materials used in SPI-based biomaterials may interact with the SPI molecules to form networks and physical crosslinks, as well as allow for the deposition of SPI along the filler to create a film layer.<sup>96,99</sup>

When evaluating soy-based materials and their applications in AM, research has been largely focussed upon the use of SPI in food 3D printing. This is because most of the processes and methodology used for SPI-based biomaterials and crosslinking require molding methods or external stimuli that is not compatible with 3D printers. Thus, the current 3D printing of SPI is largely based on the fabrication of foods. SPI-based biomaterials have been successfully 3D printed by multiple researchers using a syringe-based mechanism or food 3D printer to create various types of edible final objects.<sup>28,79,101,102</sup>

### **1.4.3 Drug Delivery**

The use of SPI in the creation of various drug delivery systems (DDS) such as matrices, nanoparticles, and hydrogels has gained popularity in the past few decades alongside other natural polymers.<sup>103–105</sup> SPI has emerged as a candidate for the development of new DDS as it is FDA approved for its health benefits and has established bioactivity and biocompatibility for potential

applications such as tissue and bone engineering.<sup>83,97,106,107</sup> Much of the work conducted thus far on SPI-based DDS involve production methods and synthesis that rely on the creation of scaffolds and porous networks of SPI, through the use of protein crosslinking.<sup>104-106</sup>

With the creation of SPI-based DDS, many of the research conducted thus far relies on the hygroscopic nature and swelling properties of SPI to facilitate the release of drug from a scaffold.<sup>104-106</sup> As SPI swells when immersed in water or other aqueous media, this causes the expansion of the scaffold which opens up channels for diffusion.<sup>104,105</sup> As SPI is known to create porous scaffolding matrices when crosslinked to form a polymeric network, the porosity of SPI DDS may be used to modulate the resulting release of drug.<sup>104,108</sup> Other properties, such as polymer and drug dissolution in media, also play a part in the release kinetics of SPI DDS.<sup>105</sup> Research conducted thus far on the creation of a DDS with SPI-based materials have been focused on an evaluation of the initial 24-48 hour release profile, and these materials commonly exhibit a rapid release within the first 24 hours of immersion in media.<sup>104,105,107</sup>

#### **1.4.4 Limitations of Soy Protein Biomaterials**

Experimentation with creating soy protein plastics has been able to produce promising biomaterials with applications throughout a wide range of industries, however, there are two main limitations within most soy protein materials currently preventing the advancement and wide stream adoption of soy protein plastics.<sup>73,85</sup>

1. **Hydrophilicity:** Due to the hydrophilic nature of soy protein, resulting soy protein plastics are often water soluble and swell when submerged in water, causing the material to weaken.<sup>64,80,85</sup>
2. **Mechanical Properties:** Developing biopolymers as a potential replacement for petroleum thermoplastics is difficult with respect to achieving similar tensile strength and mechanical properties, as plant protein plastics are mechanically inferior to their synthetic

counterparts.<sup>85,94,109</sup> Much research has been done with soy protein plastics in hopes to improve the mechanical strength of products, and it has been found that compounds such as ethylene glycol and structurally-related compounds can be used to increase the properties of soy-protein plastics.<sup>67,85,110</sup> Regardless of the addition of formulation additives and plasticizers, many studies have observed soy-protein plastics to be brittle when processed at high temperatures.<sup>67,70,85</sup> Unfortunately, many of the most effective crosslinking agents are synthetic, nonbiodegradable or toxic, which makes them an inadequate option for creating sustainable biomaterials.<sup>91,111,112</sup> Although it is unlikely that soy protein plastics will be capable of mechanical strength equal to that of many petroleum-based products, soy protein plastics still have great potential for real-world applications that may help to decrease the use of non-renewable plastics.<sup>66,70,85</sup>

## **1.5 Techniques in Material Characterization**

With the creation of any new material, multiple characterizations can be performed to evaluate the properties and assess potential end applications. The methodology described in the following sections are not an exhaustive list to the potential material characterizations that can be performed but are instead introduced as a preface to characterizations performed in this study.

### **1.5.1 Mechanical Properties**

The most expansive category for the characterization of newly synthesized materials is the resulting mechanical properties, as these tests communicate many of the physical properties of the material and can provide detailed results for many different end applications of a material.<sup>113</sup> The term mechanical properties as a whole is not a single property but instead a family of material properties such as plasticity, brittleness, creep, hardness, strength, stiffness and many more, each with different testing procedures.<sup>113,114</sup> The two main mechanical properties evaluated in this study

were the tensile strength, or sometimes referred to as break strength, and the compressive strength of a material. The tensile strength can be measured using a universal testing machine (UTM), and is used to describe the maximum load a material can withstand with tension to obtain values such as ultimate tensile strength, elongation at break and tensile yield strength, depending on the material and testing procedure.<sup>113,115</sup> Compressive tests allow for a determination of properties such as compressive strength and modulus of elasticity through evaluating the compression of a specimen under load.<sup>113,116</sup>

### **1.5.2 Degradation Studies**

When creating biomaterials for the elimination of single-use non-renewable plastic materials, the degradation properties of the material become an integral point of evaluation. For the biodegradation of a material, degradation may be measured in different systems such as in soil, aqueous environment and composting conditions.<sup>117</sup> Despite protocols outlined in the American Society for Testing and Materials (ASTM) D5988-18 and ISO (International Organization for Standardization) 17556:2019 for the standardization of biodegradation testing in soil, aqueous and compost, the exact protocols used by researchers show little standardization.<sup>117</sup> For evaluating the biodegradation of biomaterials in soil specifically, a literature review conducted by Pires et al. found that more studies employed a mass loss-based procedure, in lieu of the ASTM or ISO protocols.<sup>117</sup> Another form of degradation that is commonly evaluated in materials science is the thermal degradation of a material, using thermogravimetric analysis (TGA). This allows for an understanding of the thermal limits before degradation begins to occur and to find the optimal degradation temperature of a material (ODT).

### **1.5.3 Drug Delivery Studies**

Properties related to evaluating the drug delivery potential of a material vary greatly depending on the DDS, release mechanism, model drug and material, however, as SPI-based materials are often based upon release related to swelling and porosity, characterization centered around evaluating water properties, release kinetics, and microstructure of the material may be performed.<sup>104,105</sup> The water properties, which includes terms such as water uptake/absorption, swelling properties and water vapour permeability are often characterized by looking at mass increase when exposed to water, by methods of immersion or using an environmental chamber.<sup>90,104,118</sup> The porosity of a material may be measured using a pycnometer, or imaging with methods such as scanning electron microscopy (SEM) or transmission electron microscopy (TEM) may be used to visualize the resulting microstructure of the biomaterial for a better understanding of its drug delivery potential. Evaluating the drug release of a DDS is highly dependent on the system and experimental conditions (*in vitro*, *ex vivo*, *in vivo*), however, evaluating preliminary release kinetics is commonly completed with dissolution studies and observation methods such as absorbance-based detection or high-performance liquid chromatography (HPLC).<sup>107,119–121</sup>

## **1.6 Project Overview**

### **1.6.1 Rationale**

With an estimated 9 billion people expected to be living on earth by 2050 and with our current patterns of production and consumption, it is evident that there will be a drastic increase in the demand for resources and raw materials.<sup>66,122</sup> With the production of petroleum filaments accounting for approximately 8% of global oil and gas consumption, the need for biomaterials and sustainable solutions is crucial to reducing the use of non-renewable plastics in everyday life.<sup>41,42</sup> While one can propose that the emergence of current bioplastics such as PLA be used to alleviate

the demand of petroleum thermoplastics, this relies on the use of corn, cassava, and sugarcane as a source of lactide monomers.<sup>8,123</sup> Thus, the ethics behind the worldwide production of PLA must be put into question, as it takes 2.7 kg of corn to produce 1kg of PLA.<sup>8,124</sup> With a rapidly growing population, the consequences of diverting a large portion of one of the world's most important food crops to manufacture plastics must be heavily considered from an ethical and logistical standpoint. Therefore, there is still a need for the development of new sustainable biomaterials and processes that fit the ideal goal of a future circular economy.<sup>66</sup>

This study is designed to develop and characterize the first ever cellulose-based soy biopolymer (CSBP) feedstock composed of generally regarded as safe (GRAS) components for sustainable extrusion-based 3D printing applications. With a reliance on renewable resources and the creation of a biodegradable material, there is potential for CSBP to become a circular product, that is, one that may be used in a circular economy (Figure 4).

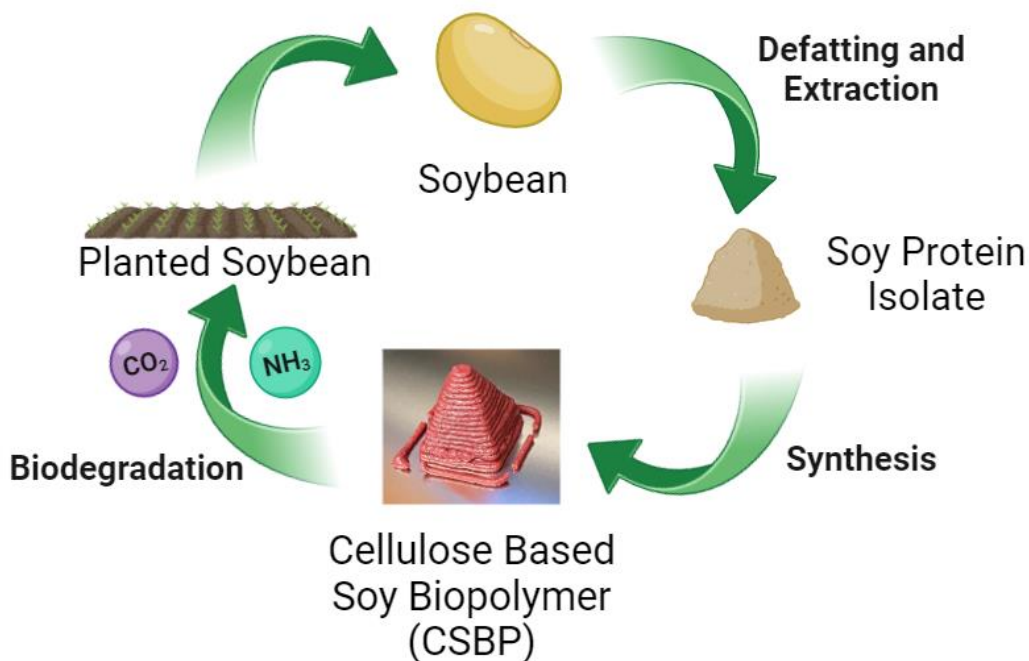


**Figure 4: Circular Production of CSBP Diagram. Made with BioRender.**

A formulation consisting of a soy protein source, cellulose fibres, and additives was developed to produce a feed material to be used for sustainable syringe-based 3D printing. Two different types of paper, brown obtained from paper towel, and white obtained from blank printer paper, were evaluated as a proof of concept to demonstrate CSBP's potential for the recyclability of paper.

The created CSBP formulation relies on the crosslinking of proteins, and SPI will be used as the plant protein source to achieve this. SPI is used as it is highly refined and consists of greater than 90% soy protein, which allows for a higher degree of crosslinking.<sup>85</sup> The soy protein-based binder relies firstly on the cross-linking effect from a condensation reaction between the protein's amino groups and the added crosslinking agents to produce a self-curing product. Secondly, film formation with cellulose fibres is used to increase the resulting mechanical properties and water resistance of CSBP, through interactions with SPI and cellulose. Finally, solvent evaporation allows for the use of CSBP in a 3D printer as it can be extruded as a fluid paste before solidifying into a solid object after extrusion. Soy protein was selected as the plant protein source for some of the following advantages:

- 1) Inexpensive and abundantly produced<sup>85</sup>
- 2) Established applications in 3D printing<sup>28,36,79</sup>
- 3) Biocompatibility and biodegradability<sup>106</sup>
- 4) Extensive research history of soy protein biomaterials<sup>86,109</sup>

### **1.6.2 Hypothesis**

This project hypothesizes that the development of CSBP, a novel cellulose-based soy biopolymer, reliant on a synergistic combination of protein crosslinking, film formation and

solvent evaporation, can provide a non-cytotoxic and sustainable alternative to petroleum-based materials, with potential applications in drug delivery as well as other commercial industries.

### **1.6.3 Objectives**

1. Development of CSBP using a combination of protein crosslinking, film formation and solvent evaporation.
2. Integration of CSBP with a syringe-based 3D printer
3. Characterizations of CSBP: mechanical strength (compression, tensile), degradation, cytotoxicity, water properties, release kinetics, self-curing.
4. Preliminary investigation of potential applications of CSBP: microneedles, adhesion, packaging.

## 2. METHODOLOGY

### 2.1 Materials

Soy Protein Isolate (92% protein content) was purchased from MP Biomedicals. Citric Acid (>99.5%), glycerol (>99%), microcrystalline cellulose (microcrystalline powder, 20 µm), carnauba wax (refined), fluorescein sodium salt, polyvinyl alcohol was purchased from Sigma Aldrich Canada. Promega CellTiter 96™ AQueous One Solution Cell Proliferation Assay (MTS), 0.25% trypsin-EDTA was purchased from Thermo Fischer. Heat-inactivated fetal bovine serum (FBS), penicillin/streptomycin 100x, and 0.4% trypan blue was purchased from Fischer Scientific.

### 2.2 Synthesis of Cellulose-based Soy Biopolymer (CSBP)

The synthesis of CSBP is outlined as a 6-step process:

#### 1. Preparation of Plant Protein Component

The first step to CSBP synthesis is the creation of the plant protein component of the formulation. SPI is weighed out and added to deionized (DI) water to create a mixture of 20% weight/volume (w/v) soy protein solution. From here, a denaturation step is performed by heating the soy protein solution to 80°C for 20 minutes using a hot plate, to expose additional soy protein functional groups (such as lysine and arginine) to molecular interactions. With the denatured SPI mixture prepared, formulation additives can now be added.

#### 2. Preparation of Formulation Additives

Two additives are dissolved in solution to prepare the active component to be used with the soy protein component to form the final binder. For this, a hydroxyl and carboxyl containing compound are used. For the carboxyl component, citric acid dissolved in a ratio of 60% w/v with DI water. A hydroxyl compound, glycerol, is added to the citric acid solution at 25% w/v to DI water as an additional additive.

### 3. Combination of Final Binder

The additives prepared in step 2 are added to the soy protein solution from step 1. A mixture of protein component to additives are used in a 1:1.2 ratio to create a final binder solution.

### 4. Preparation of Cellulose Base

The second component of CSBP is the use of a cellulose base in combination with the binder prepared in step 3 to create CSBP paste. For the recycling of paper as the cellulose component of this material, paper must be powdered prior to its use in the formulation, using a cryogenic mill or pulping machinery. In this study, microcrystalline cellulose (MCC) powder was used as a cellulose source in place of powdered recycled paper for characterizations, due to the low yield of powdering paper using a cryogenic mill and the high quantities of cellulose needed to make CSBP for characterizations.

### 5. Final Preparation of CSBP

The final binder made in step 3 is mixed with the cellulose component from step 4. The soy protein binder can be integrated with the cellulose source in a 4:1 (binder : cellulose) ratio to create the final CSBP paste. A ratio of 1g MCC to 4g final binder is optimal for producing a paste with favourable rheology for consistent extrusion 3D printing. CSBP was made in batches of approximately 150g and used on the same day of preparation for the 3D printing of objects used in this study.

### 6. Curing of CSBP Paste

Two different forms of curing for CSBP were used throughout the study. Firstly, CSBP paste is capable of self-curing into a final, solid object. This was performed at controlled temperatures and relative humidity throughout the study and listed alongside each characterization.

Although CSBP has self-curing properties, it is also capable of heat-curing to form a different type of final object. The heat curing of CSBP is achieved by placing it in a lab oven at 200°C for 20 or more minutes to fully solidify the object. The exact heat curing time depends on the dimensions of the object being heat cured due to the need for heat penetration throughout the entire CSBP structure. CSBP samples were checked every 5 minutes of heat curing, to observe browning and ensure no pyrolysis of the sample.

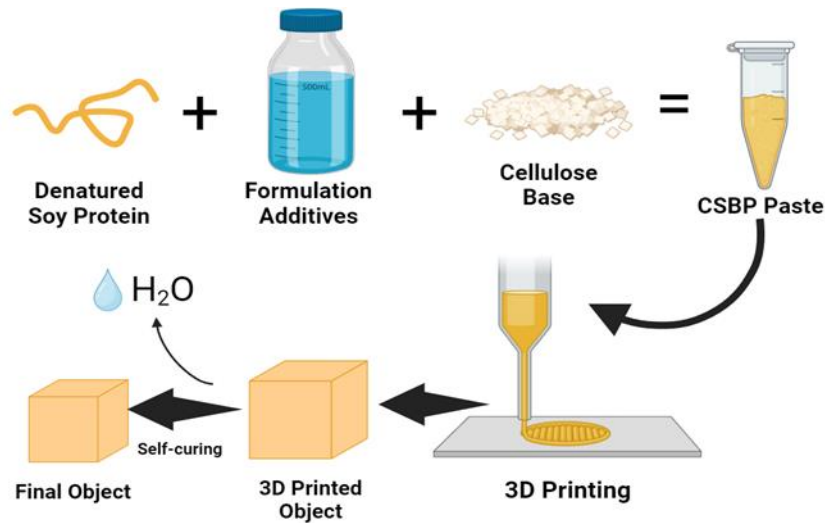


**Figure 5: Summary of CSBP Paste Synthesis. Made with BioRender.**

### 2.3 3D Printing of CSBP

CSBP paste was prepared according to the process outlined in section 2.2. Once prepared, CSBP paste was thoroughly mixed before being loaded into a 100mL syringe and placed into a FelixFood 3D printer. Objects to be printed were designed with SOLIDWORKS and sliced on Simplify3D using a printer profile designed for the FelixFood 3D printer. The 3D printing settings used for CSBP are as follows:

**Table 3: Printing Parameters for CSBP Using a Syringe-based 3D Printer**

<b>3D Printing Parameter</b>	<b>Value</b>	<b>Definition</b>
Nozzle Diameter	1.03mm (18Ga)	Diameter of extruded nozzle
Layer Height	0.50mm	Thickness of each printed layer
Extrusion Multiplier	0.95	Multiplier for all extrusion movements. Used for flowrate tweaking
Retraction Distance	1.0mm	How much material to pull back into nozzle
Extra Restart Distance	0.04mm	Extra extrusion distance on top of initial retraction amount
Retraction Vertical Lift	0.50mm	Distance nozzle will lift from surface of a part during a retraction move
Retraction Speed	300mm/min	Extruded speed for retraction movements
Coating Distance	1.25mm	Distance nozzle will stop extruding prior to the end of a loop
Wipe Distance	2.0mm	Total distance for wipe movement
First Layer Height	200%	Height of first printed layer. Remaining layers are 100% height
Outline Overlap	50%	Percentage of extrusion width that will overlap with outline perimeter. Used to ensure infill bonds to outline

Other parameters such the interior infill and skirt are dependent on the object being printed and have not been included. A consistent flowrate was established using the extruder prior to the initiation of a print file. The heating of the bed and syringe were not used for the 3D printing of CSBP in this study. Every characterization performed in this study, except for release kinetics, microneedles and packaging application studies, was done by 3D printing CSBP samples at 18Ga.

### **2.3.1 Rheology**

Rheology was performed on CSBP using a Kinexus Prime ultra+ rheometer (courtesy of Dr. Michael Tam's Research Group, University of Waterloo Department of Chemical Engineering). Two formulations developed for 3D printing, baseline CSBP as described in section 2.2 and 10% water-diluted CSBP, for 18Ga and 20Ga nozzle diameter prints respectively, were tested from 0.1 to 1000 PaS (shear rate). The diluted CSBP variant is not characterized throughout

the remainder of this study as it shows weaker resulting mechanical properties, however, it has increased precision for 3D printing.

## **2.4 Characterizations of CSBP**

With the completion of CSBP synthesis and 3D printing, a new material capable of printing through a syringe-based 3D printer has been developed and a range of characterizations were performed to evaluate its potential applications. Most importantly, the mechanical properties of CSBP were accessed to determine the strength and limitations of this new material, as well as its performance with different curing conditions. Beyond mechanical properties, properties relating to the sustainability and GRAS nature of this material such as biodegradability and cytotoxicity were evaluated.

### **2.4.1 CSBP Mechanical Properties**

To characterize and quantify the mechanical properties of 3D printed CSBP, a universal testing machine (UTM) was used to perform tests for tensile and compressive strength. A CellScale UniVert 1kN UTM (purchased from Waterloo, Ontario) was used to carry out the following tests:

#### ***1. Tensile Strength***

To evaluate the tensile strength of self-cured CSBP, two different atmospheric curing conditions were considered, 10% and 55% relative humidity (RH). Tensile bars (50 x 15 x 10 mm) of CSBP were 3D printed using a FelixFood 3D printer and self-cured at room temperature (22°C) and either 10% or 55% RH using a desiccator (10% RH) or environmental chamber (55% RH). Two different self-curing time points of 7 days and 14 days were tested for tensile strength, to understand when CSBP becomes fully cured. 24-hour self-cured CSBP could not be evaluated as it is too soft to be held by the tensile grips. Once cured, samples were tested for tensile strength using a CellScale UniVert mechanical tester at a rate of 2.50mm/min (n = 5).

The tensile strength of heat cured CSBP was also evaluated in addition to self-curing. CSBP tensile bars (50 x 15 x 5mm) were 3D printed and allowed to cure at 10% RH for 24 hours before being heat cured at 200°C for 30 minutes. Heat cured CSBP samples were tested using a CellScale UniVert at a rate of 2.50mm/min (n = 5).

## **2. Compression**

To evaluate the compressive strength of self-cured CSBP, two different conditions were considered, 10% and 55% RH. CSBP compression samples adhering to the dimensions listed in ASTM D695 (12.7 x 12.7 x 25.4 mm) were 3D printed using a FelixFood 3D printer and self-cured at room temperature (22°C), and either 10% or 55% RH using a desiccator (10% RH) or environmental chamber (55% RH). Three different self-curing time points of 24 hours, 7 days and 14 days were tested for compressive strength. Once cured, samples were tested using a CellScale UniVert mechanical tester for 10% and 35% deformation over a course of 90 seconds (n = 5).

The compressive strength of heat cured CSBP was also evaluated in this study. CSBP compression samples were 3D printed and allowed to cure at room temperature, 10% RH for 24 hours before being heat cured at 200°C for 30 minutes. The heat cured CSBP samples were tested according to the procedure outlined in ASTM D695 (n = 5).

### **2.4.2 *in vitro* Cytotoxicity**

To evaluate the *in vitro* cytotoxicity of CSBP, an elution-based MTS cell viability assay was performed to ensure that CSBP was biocompatible over three different exposure times. CSBP samples of 1000 mg weight were 3D printed using a FelixFood 3D printer and self-cured for 14 days at room temperature (22°C) and 10% RH. After self-curing was complete, samples were dried for 24 hours at 100°C in a lab oven. Samples were then sterilized by exposure to UV light for 24 hours, followed by a 70% ethanol wash and rinsed 3 times with PBS. Once complete, samples

were immersed into 10mL of complete EMEM media, containing base EMEM with 10% heat-inactivated fetal bovine serum and 1% penicillin/streptomycin. The overall concentration of CSBP in cell media was 100mg/mL. Cell media containing CSBP sample was then stored in a 4°C fridge until time for CSBP sample to be removed. At set time points of 1, 7 and 30 days, the CSBP samples were removed from the cell media.

CRL 2522 cells, a line of skin fibroblasts, were seeded into a 96-well plate at a density of 5000 cells/well and incubated at 37°C and 5% CO<sub>2</sub> for 24 hours. After the fibroblasts had incubated and adhered to the bottom of the wells, cell media was extracted and replaced with treatment media, and cells were again incubated for 24 hours (n = 3). After incubation with the treatment media, treatment media was removed from each well and washed with PBS. A Promega CellTiter 96 TM AQueous Solution Proliferation Assay was then used to conduct the MTS assay, using the manufacturer's outlined protocol. Absorbance readings from the MTS reagent were evaluated using a Varioskan microplate reader.

#### **2.4.3 Evaluation of CSBP Biodegradability in Soil**

15 x 15 x 5 mm samples of CSBP were 3D printed using a FelixFood 3D printer and self-cured at room temperature (22°C), 10% RH for 14 days. After self-curing was complete, samples were dried using a vacuum drying oven, weighed to obtain an initial weight, and buried (5 cm depth) in jars containing fresh samples of soil obtained from Victoria Park in Kitchener, Ontario and kept at room temperature (22°C), 60% RH (n = 3). Weekly, CSBP samples were removed from soil, brushed, and dried for 24 hours prior to obtaining weights. After the weights were obtained, samples were re-buried into fresh soil samples. Soil biodegradation was recorded weekly until the sample could no longer be found in the soil. A negative control containing CSBP without soil as well as ABS and PLA were also evaluated alongside CSBP as a comparison.

#### **2.4.4 CSBP Self-Curing and Size Reduction Behavior**

To assess the self-curing properties of CSBP, the size reduction and weight loss were evaluated as a function of relative humidity (RH). To accomplish this, 15 x 15 x 5 mm CSBP samples were 3D printed using a FelixFood 3D Printer and allowed to cure at different humidities: 10%, 30%, 50%, 70%, and 90% RH. Room temperature (22°C) was maintained for each humidity tested. After time points of 0, 1, 3 and 7 days the volume and weight of each self-cured CSBP sample was measured using a digital scale and caliper (n= 3).

#### **2.4.5 CSBP Thermogravimetric Analysis (TGA)**

TGA was conducted by Dr. Charles Dal Castel as part of the University of Waterloo Analytical Facilities Lab (TA instruments Q500). 10mg samples of 14-day self-cured 10% RH CSBP were tested, and TGA was performed from 0 to 600°C in N<sub>2</sub> conditions (n = 5).

#### **2.4.6 Water Uptake**

Water uptake was evaluated to determine how much water CSBP absorbs when saturated. To do this, CSBP samples (15 x 15 x 5 mm) were 3D printed using a FelixFood 3D Printer and self-cured at 10% RH and room temperature (22°C) for 14 days. In total, 4 different conditions were evaluated for the impact of curing conditions on CSBP water uptake: self-cured CSBP, 150°C heat cure for 10 minutes, 200°C heat cure for 30 minutes and a thin carnauba wax coating on CSBP to represent a negative control. To create a thin carnauba wax coating around CSBP, carnauba wax was heated to 80°C and CSBP samples dipped to form an exterior coating.

After the samples were conditioned, they were placed in a room temperature (22°C), 95% RH environment using a Thermo Forma Environmental Chamber 3911 for 24 hours. After 24 hours at 95% RH, the weight of each CSBP sample was taken (n = 3).

#### **2.4.7 Scanning Electron Microscopy**

Scanning Electron Microscope Imagery was performed by Dr. Charles Dal Castel as part of the University of Waterloo Analytical Facilities. Images were taken of the surface of 14 day self-cured 10% RH CSBP samples using a Tescan VEGA TS-5130.

#### **2.4.8 Water Contact Angle**

Water contact angle was conducted using a Ramé-Hart 190 Contact Angle Goniometer. CSBP samples (15 x 15 x 5 mm) were 3D printed using a FelixFood 3D Printer and self-cured at 10% RH and room temperature (22°C) for 14 days. CSBP samples were then evaluated for their water contact angle. Heat-cured CSBP samples were prepared and tested by heating the self-cured CSBP samples in a 200°C lab oven for 30 minutes before water contact analysis. Samples were positioned on the stage of the goniometer and a drop of DI water was placed upon the surface to examine the angle between the surface of CSBP and the droplet (n = 3).

#### **2.4.9 Drug Release Kinetics**

The release kinetics of fluorescein from CSBP was evaluated using fluorescein as a model drug and evaluating CSBP as a function of self-curing time. To incorporate fluorescein into the CSBP formulation, the synthesis of CSBP was carried out as outlined in section 2.2, with the addition of fluorescein sodium salt to the final binder. Fluorescein was added at a weight of 0.633% of the entire CSBP formulation. The remaining steps of CSBP synthesis (outlined in section 2.2) were carried out and the fluorescein-containing CSBP was placed in a fridge at 4°C for self-curing.

At time points of 24 hours, 7 days, and 14 days, 50mg samples of fluorescein loaded CSBP were cut, weighed, placed into a glass jar and filled with 2.5 mL of phosphate buffered saline (PBS) to initiate release. These quantities were determined to produce absorbance readings over the limit of detection, which was taken as five times the standard deviation of the blank<sup>125</sup>. The

fluorescein-loaded CSBP scaffolds were created by molding CSBP into a long rectangular prism shape (50x2.5x2.5mm), before cutting out pieces with a length of approximately 2.5mm. Release sample jars were incubated at 37°C and 5% CO<sub>2</sub> during release. At set time points (15 minutes, 30 minutes, 45 minutes, 1, 2, 4, 8, 12 and 24 hours), the full volume (2.5 mL) of PBS was removed from the jar, replaced with fresh PBS, and pipetted into a microcentrifuge tube. Each release extraction timepoint was centrifuged at 10,000 RPM for 10 minutes to remove any CSBP particulate, and the resulting supernatant was extracted into a fresh microcentrifuge tube. Absorbance readings for the release samples were then plated onto a 96 well plate at a volume of 100 uL/well and evaluated using a Varioskan microplate reader at an absorbance wavelength of 470nm. Release kinetics was performed in triplicate (n = 3 scaffolds for each self-curing timepoint), and each release time point was performed in triplicate when plating absorption readings. The resulting absorbance values was the average of each scaffolds average release at a given time.

## **2.5 Applications of CSBP**

### **2.5.1 Adhesive**

Preliminary adhesive testing was conducted on CSBP for its potential as a sustainable alternative to current adhesives for paper-based materials. CSBP paste was prepared in three forms to evaluate the impact dilution may have on the resulting adhesive strength: baseline CSBP (as outlined in section 2.2), 10% diluted CSBP (9 parts CSBP, 1 part water), and 25% diluted CSBP (3 parts CSBP, 1 part water). DI water was used for each dilution. Once prepared, a 1 x 1 inch square was measured in the center of cut cardboard strips and CSBP paste was applied uniformly across the measured area. The cardboard strip (containing a 1 x 1 inch square of CSBP paste in the center) was then placed downwards onto a small cardboard box, and a 500g weight was placed

atop the cardboard strips for 24 hours to facilitate adhesion. The adhered cardboard strips were tested the subsequent day for their adhesive strength, on a pass-fail criterion (n = 3). This was conducted by lifting the box with increasing weights placed inside (intervals of 200-250g). The weight at which the CSBP cardboard strip failed (detached) was recorded as the failure weight.

### **2.5.2 Packaging**

The packaging potential of CSBP was evaluated by attempting to emulate the specific dimensions and compressive properties of currently used polystyrene packaging peanuts. CSBP hollow cylinders with a diameter of 25mm and height of 30 mm were 3D printed using a FelixFood 3D Printer and a 14Ga syringe nozzle – a larger diameter syringe nozzle was used to ease the creation of a hollow cylindrical structure. After being printed, CSBP packaging peanuts self-cured at room temperature, 10% RH for 24 hours. Since CSBP is still soft yet forms a defined shape after 24 hours of self-curing, rectangular inserts were carefully cut and removed from the CSBP peanuts to decrease both the density and compressive strength. After inserts were removed, CSBP packaging peanuts were cured at room temperature, 10% RH for an additional 13 days to allow for 14 total days of self-curing. The compressive strength, recovery, and density of CSBP and polystyrene packaging peanuts was then determined and compared (n = 3). Mechanical testing was performed using a CellScale UniVert 1 kN to determine compressive strength at 35% deformation.

### **2.5.3 Microneedle Fabrication**

Microneedles were created with CSBP with the use of a modified formulation. The CSBP formulation and microneedle fabrication method proceeds as follows, and was adapted from a validated protocol for microneedle fabrication conducted by Babity et al.:<sup>126</sup>

1. Preparation of final binder: The CSBP binder solution was prepared as outlined in step 1 and 2 of section 2.2.

2. Integration of polyvinyl alcohol (PVA): CSBP binder was placed into a lab oven set to 70°C, and PVA was added to form a final w/w ratio of 9:1 CSBP to PVA. The CSBP-PVA blend was mixed periodically for 2 hours, or until PVA had fully dissolved into the CSBP binder.
3. Addition of MCC: MCC was added in a 1:2 ratio to form the final CSBP-PVA solution for casting. The solution was kept at 70°C until poured into the mold.
4. Microneedle Casting and Formation: Microneedles molds were secured in a 6-well cell culture plate using tape, and the CSBP-PVA solution was poured into the mold. The well plate was covered with parafilm and centrifuged at 2500g for 5 minutes. After one cycle, the plate was rotated 180° and CSBP-PVA solution was recast atop the mold and centrifuged again using the same settings. This was repeated for 8 total cycles. After the last cycle was completed, one final addition of cast solution was reapplied to the mold and the cell culture plate was stored in a desiccator at 10% RH for 48 hours.

CSBP-PVA microneedles were evaluated for their structure and mechanical integrity, using SEM and insertion analysis. SEM was performed using a Tescan VEGA TS-5130. Insertion analysis was conducted using a CellScale UniVert 1 kN mechanical tester. To evaluate insertion, CSBP-PVA microneedles were positioned downward and adhered to the top compressive plate of the UTM, and pressed downward for 30 seconds at a force of 32N. 32N was selected as it is equivalent of the force that would be exerted by a human thumb applying a microneedle.<sup>127</sup> The CSBP-PVA microneedles were pressed into Parafilm M that had been folded eight times to form consecutive layers, and porcine stratum corneum that was dermatomed to a thickness of 350 µm.

## 2.6 Statistical Methods

All studies were conducted in triplicate or greater. Outliers were removed prior to statistical analysis. An outlier was defined as a data point that was 1.5 times greater or less than the interquartile range of the dataset. Data was statistically analyzed using t-tests when applicable ( $\alpha = 0.05$ ).

### 3. RESULTS AND DISCUSSION

#### 3.1 Development of CSBP

##### 3.1.1 Formulation

CSBP was successfully developed as a biopolymer paste capable of either self-curing or heat-curing to form a final object, each of which rely on different molecular interactions. CSBP consists of a soy protein source combined with MCC, DI water, and additives with hydroxyl and carboxyl functional groups. The CSBP formulation ratios were developed to create a paste capable of syringe extrusion for 3D printing applications, whilst gaining its mechanical strength once cured.

For the plant protein component of CSBP, multiple food protein sources may be used, however, soy protein isolate was selected due to its high protein content (92%) to increase crosslinking interactions.<sup>85</sup> Other sources of soy protein with a lower protein content can be used for the protein component of this formulation, which include but are not limited to soy flour, defatted soy flour and soy concentrate.

The crosslinking agents added to the CSBP formulation were glycerol and citric acid, although the inclusion of additional additive(s) to the formulation can also change the resulting properties of the product. For example, additives such as ethylene glycol-based compounds are commonly used as a plasticizer in soy-protein materials to increase the strength of the material by inserting within the polymer chain of crosslinked soy protein monomers.<sup>70</sup> Other ethylene glycol compounds such as polyethylene glycol, triacetin and other structurally related compounds may be used instead, as well as other known plant-protein additives.<sup>70</sup> Glycerol and citric acid were selected as they are both naturally occurring compounds that are GRAS, which fit the goal to create a new sustainable biomaterial.

The cellulose component of CSBP serves as an emulsifier or filler and may be comprised of paper such as white or brown, as well as other types of paper fibres and materials containing cellulose. To recycle paper into its formulation, CSBP requires the paper become processed into a powder. This involves the use of a cryogenic mill to induce the grinding and subsequent powdering of paper, however, other methods such as thermos-mechanical pulping can also process paper into a powder for use in the CSBP formulation. Beyond the use of white and brown paper in CSBP, other cellulose sources such as MCC (used all throughout this study) and paper pulp can be substituted for the cellulose component of the material. This study only performed characterizations on CSBP using MCC as the cellulose component, as other non-cellulose filler material will lead to changes in the molecular interactions and end properties of the material.

### **3.1.2 Crosslinking**

Unlike most polymers in which monomers undergo a reaction to yield a crystalline and/or consistent crosslinked structure with a specific mechanism, the crosslinking of soy protein as used in CSBP is amorphous and relies on multiple crosslinking mechanisms commonly used in soy protein-based biomaterials. Firstly, soy protein can form crosslinks with itself, however, this process is scarcely spontaneous, and denaturation is needed to unfold soy protein and expose more functional groups.<sup>85,95,128,129</sup> Soy protein self-crosslinking with disulfide bonds is a common redox reaction and results from the oxidation of sulfhydryl groups on the soy protein's cysteine residues, resulting in the formation of a S-S bond.<sup>130</sup> Disulfide bond formation is a major contributor to overall protein structure and occurs spontaneously during protein folding, therefore, the denaturation of protein is a useful step to initiate self-crosslinking.<sup>128,131</sup>

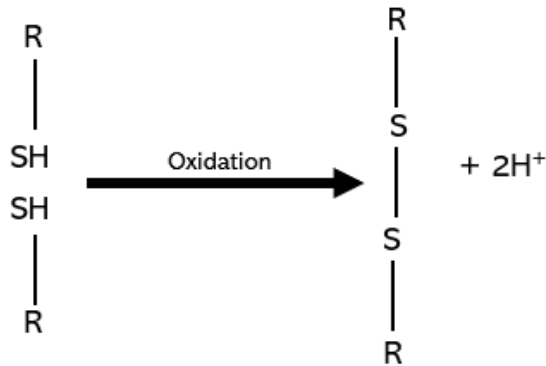


**Figure 6: Disulfide Bond Formation Mechanism. Made using BioRender.**

Relying on denatured soy protein self-crosslinking in its own would produce a final product with a very low degree of crosslinking, so, additional crosslinking agents were added to the CSBP formulation. Glycerol is a non-toxic, naturally occurring triol, and has been used by previous researchers as a plasticizer for soy protein-based films. Glycerol reacts with the carboxyl and amino groups of SPI monomers to form hydrogen bonds, inserting itself between protein chains and increasing chain mobility, allowing for less brittle SPI biomaterials.<sup>98,132,133</sup> In addition to glycerol, citric acid is a non-toxic naturally occurring crosslinking agent that interacts with amino groups and was incorporated into the CSBP formulation.<sup>134</sup> As determined by studies conducted by Xu et al., the citric acid crosslinking mechanism is a nucleophilic substitution with a carboxyl group on citric acid and a free amine group (lysine, arginine, alpha amino group) to form a new amide bond.<sup>134</sup> The additives included in the CSBP formulation, citric acid and glycerol, can form crosslinks in the presence of denatured soy protein's exposed functional groups to form a polymer network, and have each been used by previous researchers looking to change the mechanical properties of SPI-based materials.<sup>98,134,135</sup> These crosslinking mechanisms are integral to the self-curing of CSBP, however, CSBP may also be crosslinked using heat and will be discussed in section 3.1.4.

### 3.1.3 CSBP Structure and Film Formation

The structure of soy protein-based materials is often porous due to its amorphous structure and protein aggregation after denaturation, creating void space.<sup>108,136,137</sup> As seen in a SEM of the topology of raw SPI in Figure 7A, the protein appears to have an amorphous shape and size.<sup>136</sup> In Figure 7B, the SEM of MCC shows the irregular and sharp appearance of MCC fibres.<sup>138</sup>

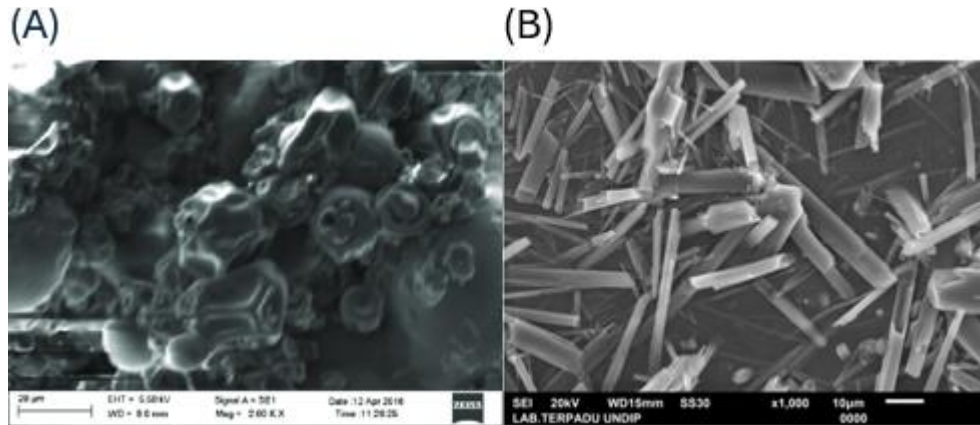


**Figure 7: SEM of Soy Protein Isolate and Microcrystalline Cellulose. (A) SEM of Soy Protein Isolate.<sup>136</sup> (B) SEM of Microcrystalline Cellulose.<sup>138</sup>**

In the SEM images of self-cured CSBP in Figure 8A, there is a noticeable difference in the appearance of SPI when compared to the SEM of raw SPI, due to the addition of MCC as an emulsifier. The MCC (20μm fibre size) included into the CSBP formulation causes the deposition of SPI around each cellulose fibre to form a film. Research conducted by O'Dell et al. on creating SPI adhesives with glass fibre support shows a similar interaction as seen in the SEM of CSBP, as the SPI showed uniform distribution and film formation throughout glass fiber support.<sup>99</sup> The SEM images of CSBP also show an expected porous structure, a common feature of SPI-based biomaterials.<sup>108,139,140</sup>

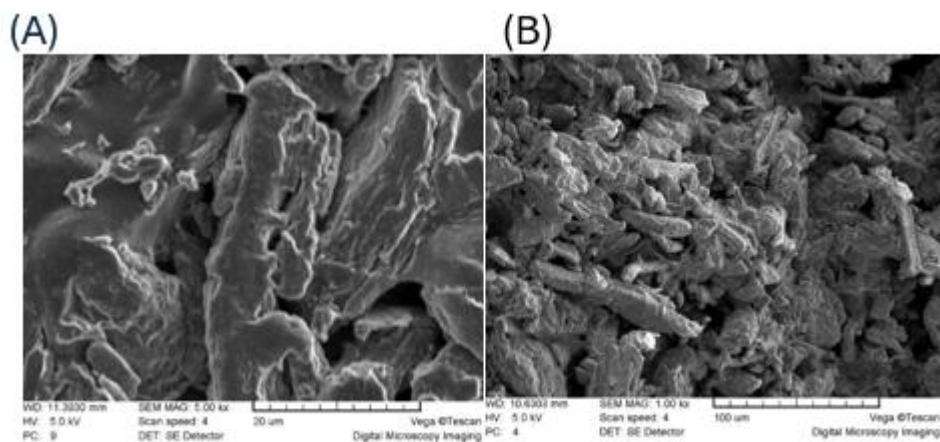


**Figure 8: SEM of Self-cured CSBP Cross Sections. (A) CSBP at 5.0kx magnification. (B) CSBP at 1kx magnification.**

The SPI-MCC film formation in CSBP helps to reinforce the final CSBP object by decreasing the porosity and increasing mechanical strength through interactions between MCC fibres and soy protein.<sup>139</sup> Several potential interactions such as hydrogen bonding, imine linkages and ionic attraction have been highlighted as plausible interactions between cellulose fibres and SPI, as well as the formation of amide bonds between cellulose and SPI via amidification.<sup>139</sup> Future work should be conducted on obtaining SEM images for CSBP paste prior to self-curing, as well as SEM images of the specific SPI and MCC reagents used in CSBP. This way, the appearance of CSBP prior to SPI-MCC film formation can be observed with both SPI and MCC dispersed throughout the paste.

#### **3.1.4 Self-Curing Behavior of CSBP**

Once CSBP paste has been produced, it can undergo self-curing to form a solid, final object without the use of heat or any additional catalysts. However, this process is reductive in nature due to the evaporation of water, as the dimensions and weight of freshly printed CSBP paste is greater than the final self-cured product. Therefore, it is important to characterize the self-curing behavior of CSBP to ensure that if needed, objects of specific dimensions or weight can be created. To

evaluate any potential impact that the humidity of the surrounding environment may have on CSBP self-curing, weight and volume change was measured as a function of humidity and shown in Figure 9.

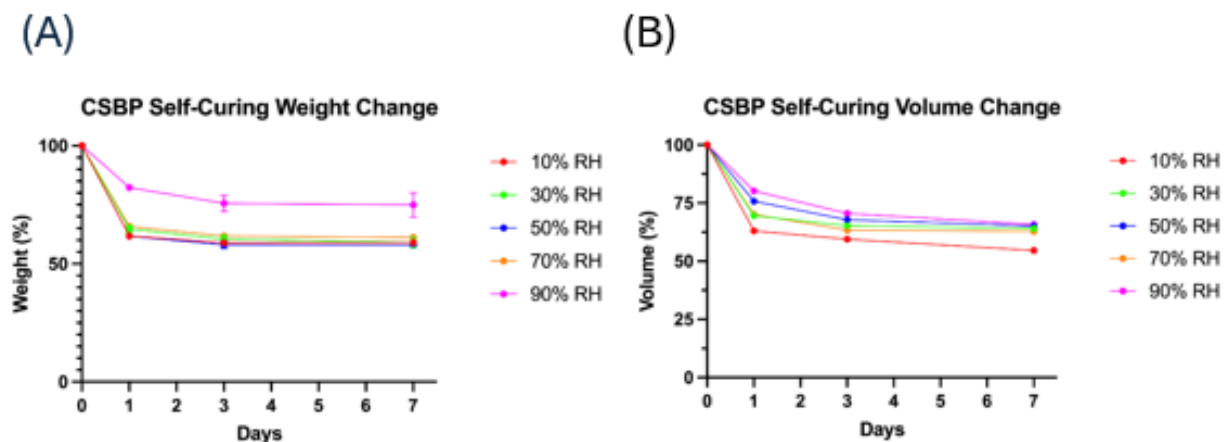


**Figure 9: CSBP Self-Curing Weight and Volume Change as a Function of Relative Humidity. (A) CSBP self-curing weight change, evaluated from 10-90% RH. (B) CSBP self-curing volume change, evaluated from 10-90% RH.**

As shown in Figure 10A, the weight change of self-cured CSBP shows little deviation at  $59.3 \pm 1.33\%$  of the initial printed weight between 10% and 70% RH, except for self-curing at 90% RH which reduced to  $74.9 \pm 5.22\%$  of its initial weight. The reduced weight loss of CSBP at 90% RH is a result of the uptake of water by the porous CSBP structures at 90% RH, as there was no significant difference in the volume of these samples at this humidity. In addition, the conditioning of samples at 95% RH is a common method used for the determination of the water uptake of biomaterials, meaning that exposure to 90% RH likely caused a similar uptake of water and impacted the recorded weight at 90% RH.<sup>141,142</sup>

For the change in volume with self-curing humidity, Figure 9B shows that self-cured CSBP will shrink to an average of  $64.44 \pm 1.31\%$  of its original volume from 30-90% RH, and  $54.66 \pm 3.71\%$  of its original volume at 10% RH. This difference may be accounted for by the

difference in the curing apparatus for the samples at 10% RH and 30-90% RH, as samples were stored in a desiccator for 10% RH but stored in a humidity controlled environmental chamber for 30-90% RH, due to limitations with decreasing the RH of the environmental chamber below 30% RH. It is possible that the active absorption of moisture using a desiccant system may have resulted in the further reduction of CSBP sample volume. For both the weight and volume change of CSBP as a function of RH, 14-day self-cure timepoints were evaluated and no difference was observed.

The reductive nature of CSBP self-curing is a result of both the loss of DI water by evaporation and SPI film formation around MCC fibres. As a fresh paste, the CSBP formulation components have not yet interacted with each other and exist as a mixture. As CSBP begins to self-cure, SPI interacts with the MCC fibres to form a film, creating void space and the reduction of the overall volume and weight of the object. The evaporation of water present in the CSBP formulation also contributes to the final object's weight and volume loss.

### **3.1.5 Heat Cured CSBP**

The curing temperature and time applied to CSBP can alter the desired end properties of the material, as the use of high temperature heat curing creates a more rigid object. In this study, the properties of a heat cured variation of CSBP was considered for its use in creating a stronger and more water-resistant final product. For this, CSBP paste was printed and placed into a lab oven at 200°C for 20-60 minutes depending on the sample dimensions, for the induction of the Maillard reaction. Although the Maillard reaction typically occurs at approximately 160-180°C, a higher temperature was employed to allow for the penetration of heat throughout the entire CSBP structure.<sup>143</sup> The use of heat in the processing of SPI-based materials is an approach used by some researchers on SPI-based plastics, and the resulting properties of the heat cured SPI-based material is often rigid but brittle<sup>86,144,145</sup>. The induction of the Maillard reaction in CSBP is indicated by the

presence of melanoidins which produce the brown appearance of the heat cured samples, seen in Figure 10.<sup>75</sup>



**Figure 10: 3D Printed Heat Cured CSBP Dogbone. Samples was 3D printed and heat cured at 200°C for 30 minutes.**

With the visible production of melanoidins as well as a distinct baking aroma that occurs during heat curing, it is evident that the Maillard reaction is taking place when heat curing CSBP. However, the CSBP formulation was not originally intended to produce Maillard-type reactions when heat cured, as the formulation consists of none of the typical reducing sugars that are needed for their carbonyl groups. It is possible then that the presence of reducing sugars needed for Maillard-type reactions in heat cured CSBP may be a result of alterations to the chemical composition of cellulose, or the thermal degradation of citric acid and glycerol, which can form reactive carbonyl-containing compounds in their degradation pathways.<sup>146,147</sup> The thermal degradation of glycerol produces multiple reactive aldehyde and ketone-containing compounds, while citric acid may degrade into aconitic acid then acetone, which contains a carbonyl group.<sup>146,147</sup> Although neither of these decomposition products fit the typical description of a reducing sugar such as glucose and fructose, the presence of these carbonyl compounds may still facilitate the Maillard reaction or react with each other to form other unknown compounds that contribute to the Maillard reaction. Future work must be conducted to better understand and describe the specific interactions that occur within heat cured CSBP.

### 3.2 3D Printing of CSBP via a Syringe-Based 3D Printer

The first step in the 3D printing of the CSBP paste was the selection of a 3D printer with a syringe-based mechanism of extrusion. For this, a FelixFood single-head 3D printer was selected to print this material (Figure 11) for its customizable interface for integrating new materials with syringe 3D printing, as well as the bed (maximum 105°C) and syringe (maximum 60°C) heating potential.

For the 3D printing of CSBP paste, the printing parameters were developed to be able to consistently 3D print objects out of an 18Ga syringe nozzle using a baseline CSBP formulation. In addition to 3D printing at 18Ga, a variation of CSBP consisting of a 10% dilution with DI water was developed to successfully print through a 20Ga syringe nozzle, providing prints with greater detail. Some of CSBP's 3D printed structures are outlined in Figure 12.



***Figure 11: Syringe-based 3D Printer used in the 3D Printing of CSBP. FelixFood Single Head 3D Printer.***

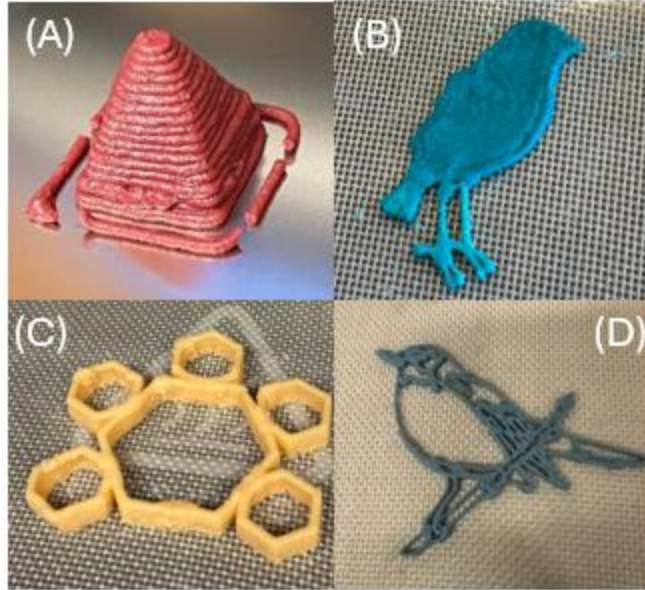


**Figure 12: 3D Printed CSBP Objects. (A) Pyramid printed using base CSBP and 18Ga syringe nozzle (B) Bird printed using base CSBP and 18Ga syringe nozzle (C) Hexagon structure printed using 10% diluted CSBP and 20Ga syringe nozzle (D) Bird silhouette printed using 10% diluted CSBP and 20Ga syringe nozzle. The different color of each object is due to the addition of a water-based pigment to the CSBP formulation.**

The 3D printing of CSBP with upwards of a 20Ga syringe nozzle is a workable quality for the fabrication of many objects, however, there remains disadvantages when compared to the capabilities of common FDM printers. Firstly, the internal syringe nozzle diameter of typical FDM printer is around 22Ga (0.400mm), a value that is lower than that of the 20Ga (0.603 mm) maximum capability of CSBP. This difference is a direct result of the different mechanisms between FDM and the 3D printing of CSBP, as since FDM works by melting thermoplastics filament into a liquid prior to extrusion, it allows for a lower viscosity print media which may print through a finer nozzle. This difference in 3D printing mechanism also allows FDM to have a much more precise layer height of 0.1 – 0.2mm, while the lowest established layer height for 3D printing with CSBP in this study is 0.5mm. As there is no melting of the CSBP paste into a liquid form to

reduce its viscosity, there is limitations with respect to the precision of CSBP 3D printed objects when compared to FDM. The 3D printing of CSBP was established to successfully create the necessary objects for the characterizations and applications to be performed in the remainder of the study and was not further investigated to achieve higher print quality. Therefore, there is still potential to greatly improve the 3D printing of CSBP with optimization of both the print parameters and formulation.

### **3.2.1 Rheology of CSBP**

The rheology of CSBP is displayed in Figure 13, for the base-CSBP formulation used throughout the entirety of this study as well as the 10% diluted CSBP used in higher quality 3D printing. The results shows that CSBP behaves as a shear-thinning, non-Newtonian fluid which reinforces its suitability for use in a syringe-based 3D printer. With a shear-thinning fluid, viscosity decreases as shear rate increases, meaning the use of a pressure-based system for extrusion allows CSBP to function as a fluid when extruded from a syringe nozzle, whilst maintaining the ability to form solid layers once extruded.<sup>148</sup> As expected, the 10% diluted CSBP formulation shows lower viscosities than the base CSBP formulation at any given shear rate, as the higher ratio of liquid to solid in the formulation decreases the overall viscosity of the paste and increase extrudability.

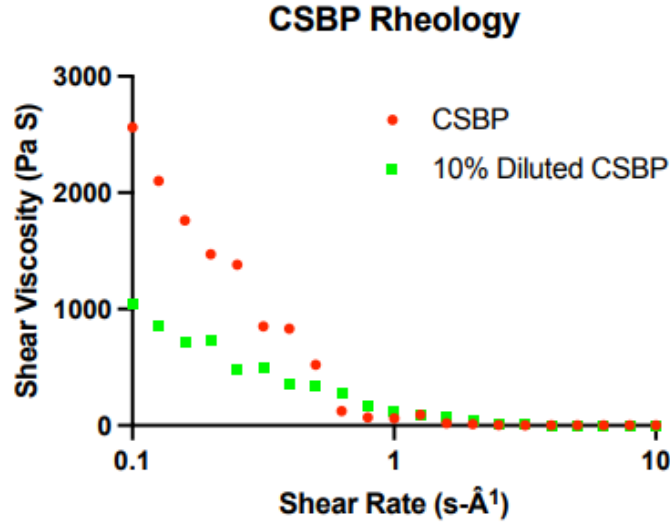


**Figure 13: Rheology of CSBP for 3D Printing. Shear rates were recorded from 0.1 to 1000 s-Â¹ but excluded after 10 s-Â¹ for better viewing.**

### 3.3 Mechanical Properties of CSBP

#### 3.3.1 Tensile Strength

The tensile strength of CSBP was recorded for two different time points of self-curing (7 days, 14 days) as well as two different humidities (10% and 55% RH). These humidity values were selected to represent the two humidities that are common indoors throughout the year, as winter humidity stayed constant at 10% while summer humidity values ranged from 50 to 60%. Evaluating self-cured CSBP mechanical strength as a function of RH will help to evaluate how atmospheric water content may impact the mechanical properties of CSBP, as soy-based materials are known to have poor water resistance and thus are often processed using heat.<sup>85,86,149</sup>

The results shown in Figure 14 indicate that CSBP has a much greater tensile strength after 7 days of self-curing at 10% RH when compared to 7 days of self-curing 55% RH, and this trend is consistent with the 14-day self-curing data. When preparing and handling the samples, there was a distinct difference between the 10% RH and 55% RH samples – samples cured at 55% RH were

much softer and pulled apart with minimal force while the 10% RH samples were much firmer. Tensile data was also recorded for 21 days of self-curing and there was no difference in the results.

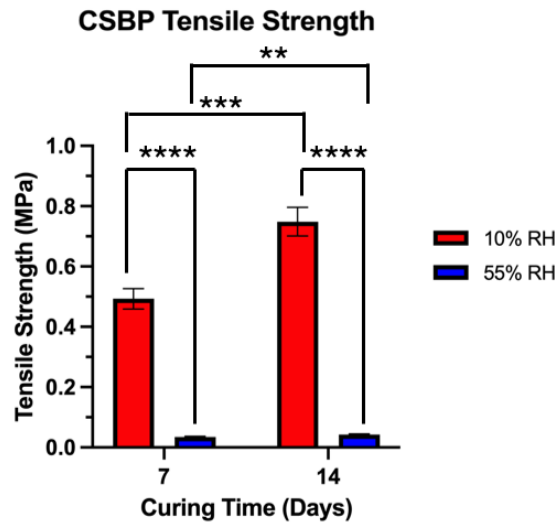


**Figure 14: Comparison of CSBP Tensile Strength by Self-curing Duration and Relative Humidity. \*\* $p < 0.01$ , \*\*\* $p < 0.001$ . \*\*\*\* $p < 0.0001$ . Data represents the mean  $\pm$  SD (n=3).**

**Error bars are displayed when possible.**

Comparing the tensile strength of self-cured CSBP to two common FDM filaments, PLA (39.9– 52.5 MPa) and ABS (18.8 – 24.9 MPa), it has significantly lower strength and failed to reach 1.0 MPa after 14 days of self-curing<sup>150</sup>. Ultimately, this is an expected result as SPI-based materials are not expected to surpass the mechanical strength of currently used synthetic plastics and polymers, but to instead provide a sustainable and biodegradable alternative, among other advantages. The tensile strength of self-cured CSBP is also lower than that of other SPI-based materials that have been created, as some researchers have been able to create SPI-based biomaterials with tensile strength upwards of 15 MPa.<sup>151,152</sup> However, this is not a direct comparison to self-cured CSBP as most of the recent developments in SPI-based materials has been largely concentrated on thin film formation and not AM, which often uses processes such as synthetic additives, nanoparticles, and most commonly thermal treatment in curing to create

stronger films.<sup>153</sup> The self-cured CSBP created in this study differs in that it can instead create objects of varying dimensions through AM, consists of entirely GRAS components, and requires minimal processing as SPI-MCC film formation and crosslinking is not driven by specific catalysts or stimuli. Factors such as the ambient-active self-curing method of CSBP and weaker crosslinkers that are GRAS can be attributed to the overall lack of mechanical strength when compared to other SPI-based materials.

### **3.3.2 Compressive Strength**

Since the self-curing of CSBP produces a non-rigid material with compressibility and recovery, compression was evaluated by looking at the compressive strength at 10% and 35% deformation. ASTM D695 is not suitable for non-rigid materials as failure becomes difficult to accurately define, thus deformation testing is a much better indication of CSBP's compressive properties. Three different self-curing time points of 24 hours, 7 days and 14 days were tested for compressive strength, to understand when CSBP becomes fully cured.

A comparison of CSBP self-cured compressive strength in Figure 15 shows that CSBP has the greatest compressive strength at 35% deformation of 6.843 +/- 0.608 MPa after 14 days of self-curing at 10% RH. The impact of RH on the resulting compressive strength of CSBP is consistent with the results obtained for tensile strength, as CSBP conditioned to self-cure at 55% RH had much lower compressive strength for both 10% and 35% deformation, apart from 24 hours of self-curing. Additional CSBP samples were tested after 21 days of self-curing and there were no further increases in compressive strength. The results of a Welch's multiple t-test show that there was a significant difference in compressive strength between 10% and 55% RH at 7 and 14 days of self-curing.

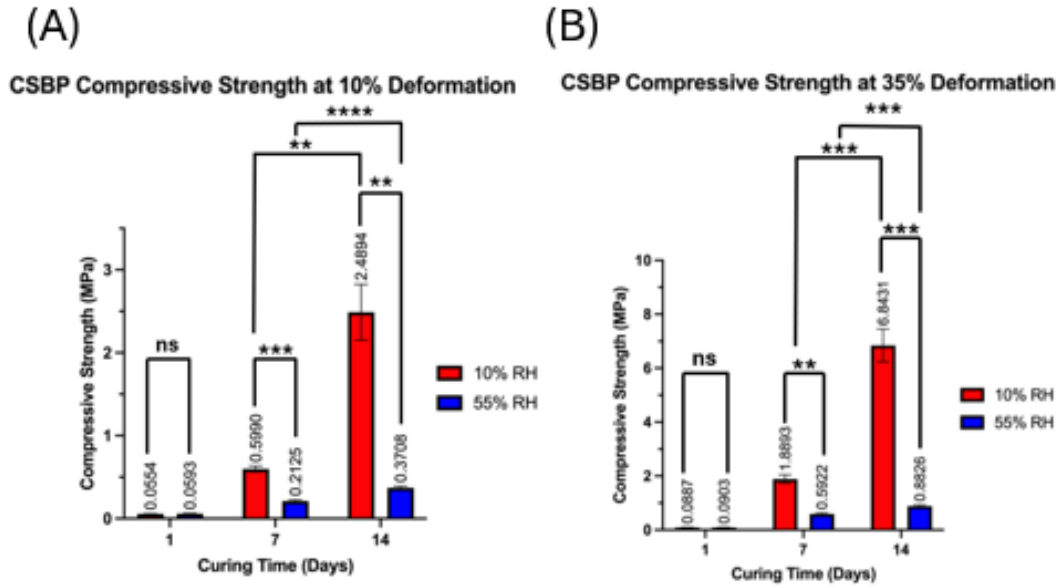


**Figure 15: Comparison of CSBP Compressive Strength by Curing Time and Humidity. (A) 10% deformation compressive strength of CSBP. (B) 35% deformation compressive strength of CSBP.  $**p<0.01$ ,  $***p<0.001$ ,  $****p<0.0001$ . Data represents the mean  $\pm$  SD (n=3). Error bars are displayed when possible.**

Many materials used in FDM are rigid thermoplastics, so, the compressive strength of non-rigid self-cured CSBP cannot be directly compared. The results show that the impact of the surrounding RH for CSBP self-curing does not significantly impact the resulting compressive properties of the material in the first 24 hours of self-curing, which is likely due to the lack of fully formed molecular interactions within CSBP at this time point. Reinforced by the tensile and compressive data, it is evident that much of CSBP's mechanical strength does not develop from its self-curing within the first 24 hours of being produced. This means that many of the interactions within CSBP, mainly SPI-MCC film formation and crosslinking, have not yet fully occurred and therefore there is less disruption and ultimately reduction in mechanical performance with a greater moisture content. Further testing on self-cured CSBP such as SEM imaging could be conducted at the 24-hour self-cure timepoint could be conducted reinforce this finding.

### **3.3.3 The Impact of Humidity on Mechanical Strength**

As expected, the surrounding RH of self-curing CSBP had a major impact on the resulting mechanical strength of the final object. The poor water resistance of SPI-based materials has been well documented by previous researchers, and much of the current research conducted is designed to overcome this shortcoming.<sup>85,118,149</sup> The impact of water on CSBP's mechanical strength is due to molecular interactions occurring with water and the individual formulation components, as well as interactions present in self-cured CSBP. Firstly, glycerol and SPI are known to be hygroscopic, which may have a negative impact on the mechanical strength of self-cured CSBP as the formulation components swelling may causing degradation and the disruption of bonds.<sup>90,154-156</sup> The swelling properties of SPI-based materials, although a detriment to the mechanical strength when exposed to water, makes them great candidates for drug delivery and will be discussed in section 3.7. The presence of moisture can also disrupt key molecular interactions which result in the reduced mechanical strength of CSBP at higher RH, as water may trigger amide hydrolysis and the disruption of ionic interactions and hydrogen bonding, disrupting SPI-MCC film formation and crosslinking.<sup>139,157,158</sup>

### **3.4 *in vitro* Cytotoxicity of CSBP**

A cytotoxicity assay was conducted to provide a biocompatibility evaluation of CSBP and provide insight on its suitability for the creation of medical devices and drug delivery systems.<sup>68,159</sup> To do this, an elution-based MTS assay was performed to ensure that CSBP did not release hazardous byproducts when immersed in medium, with the results shown in Figure 16. The resulting cell viability after 1, 7, and 30 days of elution in cell media is 114.65 +/- 4.47%, 106.63 +/- 10.78% and 83.90 +/- 19.43% respectively.

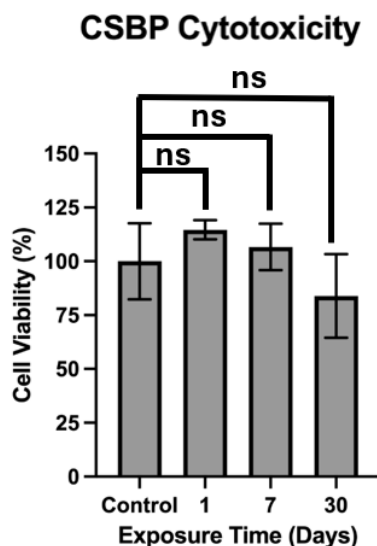


**Figure 16: *in vitro* Cytotoxicity Evaluation of CSBP via Elution-based MTS Assay.**

**Data represents the mean +/- SD (n=3).**

Looking at the MTS assay results of the elution-based cytotoxicity assay performed on CSBP, there is no significant change in cell viability for 1 and 7 days of immersion of medium. After 30 days of elution in media, the viability of the cells may appear lower with a value of 83.90 +/- 19.43%, however, this difference is not statistically significant (df = 5.946, t = 1.226, P>0.05). The biocompatibility of CSBP was an expected result as all of the formulation components are GRAS compounds that have common uses in the food, pharmaceutical and cosmetics industry that rely on consumers consuming these compounds.<sup>160-162</sup>

When cells were seeded into wells with the elution media and observed under a microscope, small fragments of CSBP that had detached during elution were floating in the media, which could have impacted the resulting absorbance readings as they remained in the wells once the elution media was removed. These CSBP fragments present in the elution media were not visible in the 1-day exposed media, but instead present scarcely throughout the 7-day media, and much more in the 30-day media. With a higher quantity of CSBP detached fragments in the 30-day elution media, it is possible that these artifacts may contribute to lower absorbance readings during the MTS assay

or cause physical damage to the cells. Future studies that want to evaluate CSBP cytotoxicity should be conducted using a well plate with an insert to directly test CSBP samples and limit the potential for disruption in absorbance readings, or by the centrifugation of elutions.

The cell viability of 1- and 7- day CSBP elution media in the MTS assay was slightly above the cell viability of the positive control, however, it was not a statistically significant difference ( $p>0.05$ ). It is possible that the partial degradation of CSBP in media releases free amino acids that may contribute to cell growth and the increased cell viability of these samples. This concept is supported by a review conducted by Gupta et al. on soy protein hydrolysates, the products formed during soy protein hydrolysis, which found that these compounds can significantly enhance cell growth and alter cell functionality.<sup>163</sup> The results obtained for the cytotoxicity test of CSBP produces the same outcome as other research conducted on SPI-based materials' cytotoxicity, as two studies conducted found no significant difference in cell viability when compared to control unless their SPI-based formulations incorporated a known cytotoxic component.<sup>164,165</sup>

### **3.5 CSBP Degradation**

#### **3.5.1 TGA**

TGA was performed to evaluate the thermal degradation of self-cured CSBP. The results are shown in Figure 17 with a summary of each formulation components' degradation temperature obtained from literature in Table 4. TGA was performed in triplicate, however, the results from a single run are presented for easier viewing.

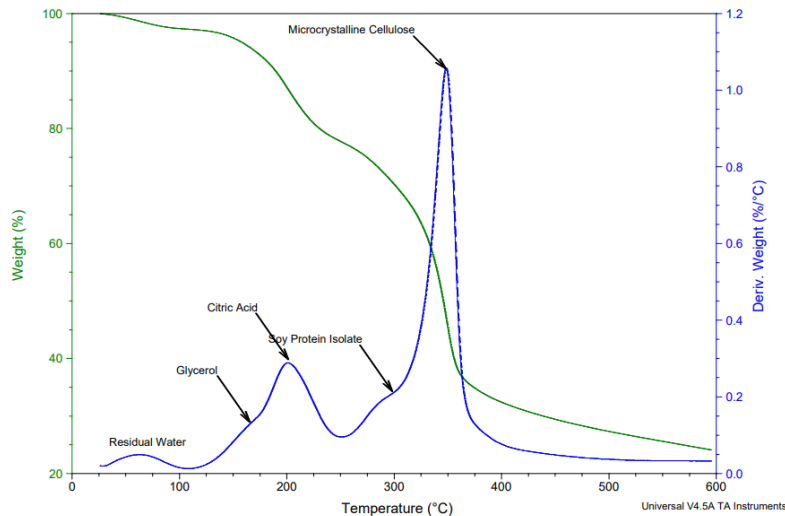


**Figure 17: TGA of Self-cured CSBP. Samples were tested from 0 to 600°C in N<sub>2</sub> conditions. Formulation components are identified according to the known literature values in Table 4.**

As seen in the TGA results, self-cured CSBP has an ODT of 342.1 +/- 0.948°C and produces the expected degradation peaks as each peak corresponds to literature values obtained for the individual CSBP formulation components. TGA was not conducted for heat cured CSBP but would be expected to follow a similar degradation pattern as self-cured CSBP beginning at 200°C, excluding the creation of any Maillard reaction products.

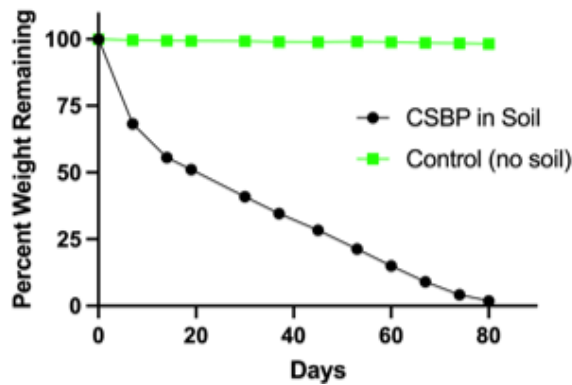
**Table 4: CSBP Formulation Components’ Thermal Degradation Obtained from Literature**

Formulation Component	Thermal Degradation Peak Range (°C)
Soy Protein Isolate (SPI)	267-367 <sup>166</sup>
Citric Acid	160 <sup>167</sup>
Glycerol	200-250 <sup>168</sup>
Microcrystalline Cellulose (MCC)	353 <sup>169</sup>

### 3.5.2 Biodegradation in Soil

The soil biodegradation of CSBP was conducted using a soil burial test, a technique most commonly used for biomaterial degradation testing.<sup>117</sup> From the soil burial test conducted, self-cured CSBP lost 98.13 +/- 0.63% of its weight in 80 days, compared to 1.76 +/- 0.057% for the negative control (no soil).

(A)  
**CSBP Soil Biodegradation by Percent Mass Remaining**



(B)  
**Change in CSBP Biodegradation Rate**

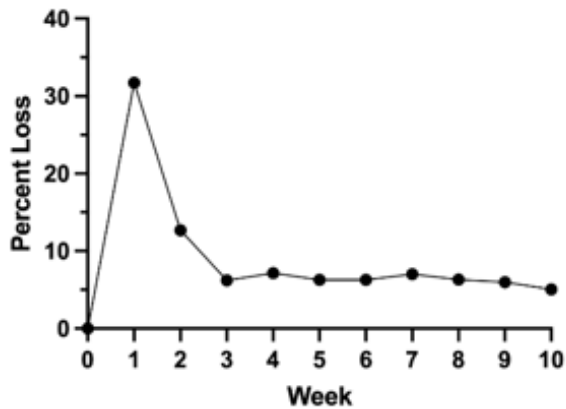


**Figure 18: Soil Biodegradation of Self-cured CSBP. (A) Percent mass remaining of self-cured CSBP over a period of 80 days. (B) Weekly degradation rate of self-cured CSBP samples, expressed as a percentage. Error bars smaller than the data point symbols are not shown.**

The slight decrease of self-cured CSBP's weight in the negative control is likely the result of additional weight loss due to self-curing that took place beyond 14 days, or, due to slight degradation because of the conditioning of the samples (22°C, 60% RH). In the soil biodegradation results of self-cured CSBP, there is a greater loss of weight in the first two weeks, accompanied by visible fungal growth shown in Figure 19B that appeared only within the first two weeks. Unfortunately, to obtain accurate weekly weight values for CSBP the fungal growth had to be removed from the samples, but it is worth considering that since many fungi are decomposers, this removal could have led to slower degradation than would be obtained if samples were left untouched underground.<sup>170</sup> The natural biodegradability of CSBP can be attributed to the accessible breakdown of the formulation components, as each component can be broken down into simple sugars or carbon by common soil bacteria and fungi. The soy protein and cellulose component of the CSBP formulation is susceptible to degradation by proteases and cellulases, enzymes that break down proteins and cellulose respectively, present in soil bacteria and fungi.<sup>171-</sup>  
<sup>173</sup> Citric acid and glycerol are known to be readily degradable in soil by multiple genus' of bacteria and fungi, and are reduced to their carbon sources.<sup>174-176</sup>

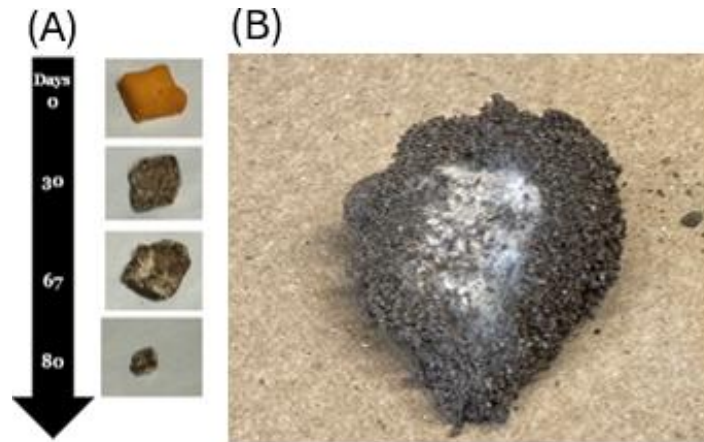


**Figure 19: Visual Representation of Self-cured CSBP Soil Biodegradation Study. (A) Visual representation of CSBP soil biodegradation over time (B) Picture of CSBP with visible growth after first 7 days of soil burial and prior to cleaning.**

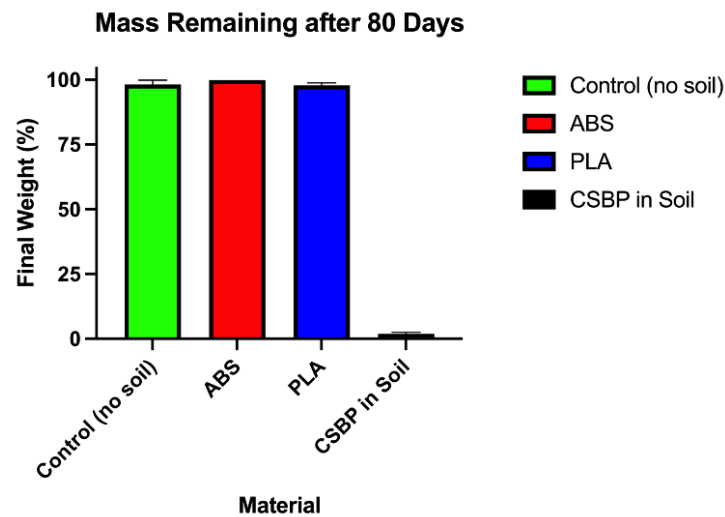


**Figure 20: Comparison of Self-cured CSBP Soil Biodegradation to Other Thermoplastics. Comparative mass remaining after 80 days of soil burial for PLA, ABS and CSBP with control. Data represented is the mean +/- SD (n=3).**

Through a comparison of the soil biodegradation of CSBP to other commonly used thermoplastics in AM, ABS and PLA, CSBP is the only material to show a significant loss in weight. As discussed in section 1.2, ABS is not biodegradable and the biodegradability of PLA is

reliant on highly controlled composting parameters, which reinforces this result. Heat cured CSBP was not evaluated for its soil biodegradability, further, no currently published research thus far on Maillard-type biomaterials could be found that evaluates these compounds' biodegradability in soil. Presumably, since heat cured CSBP works through Maillard-type reactions and products, the biodegradation in soil may be like that of protein rich baked foods, however, additional biodegradation testing should be conducted before making any conclusions.

### **3.6 Water Properties**

The water properties of CSBP were evaluated by looking at both its water uptake and contact angle, to quantify the water resistance of CSBP with different curing temperatures. The water properties of self-cured CSBP were only evaluated for 14-day, 10% RH self-cured CSBP and referred to as “Self-Curing” in the resulting figures to represent fully self-cured CSBP's water properties. Results of water uptake studies (Figure 21) showed that CSBP has a higher water uptake of 47.49 +/- 1.55% compared to that of heat cured (200°C, 30 minutes) CSBP at 11.73 +/- 0.46%. An intermediate condition (150°C, 10 minutes) was tested with the intention of creating a hardened exterior shell to CSBP to decrease the water uptake of CSBP. This intermediate curing condition showed a decreased water uptake of 37.01 +/- 1.33%, which was a significant difference when compared to self-cured CSBP ( $df = 3.907$ ,  $t = 8.887$ ,  $p = <0.01$ ).

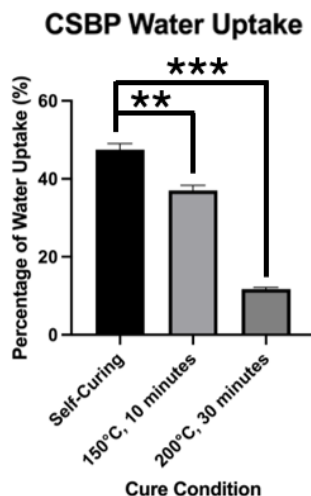


**Figure 21: CSBP Water Uptake by Curing Condition. Data represents the mean +/- SD (n=3). \*\*p<0.01, \*\*\*p<0.001.**

The water uptake of CSBP demonstrates the known impact of heat-curing on the resulting water resistance of SPI-based materials as previous studies have successfully used heat-based processes to effectively increase water resistance.<sup>145,177</sup> As mentioned in section 3.3.3, the SPI and glycerol component of CSBP are hygroscopic compounds, which contributes to the water uptake of CSBP.<sup>90,154–156,178</sup> Furthermore, the porous structure of CSBP as shown in the SEM results (Figure 8) also contributes to the water uptake of self-cured CSBP, and is a characteristic common to protein-based biomaterials.<sup>108,179</sup> The full heat curing of CSBP shows a significantly lower water uptake than self-cured CSBP, which can firstly be attributed to the thermal degradation of two hygroscopic additives, citric acid and glycerol. This is because, as shown in the TGA results (Figure 17), the heat cured variation of CSBP is processed at 200°C, which is above the degradation temperature of both citric acid and glycerol.<sup>167,168</sup> It is also likely that the porosity of CSBP is greatly altered by heat-curing and should be evaluated directly by conducting SEM and porosity calculations for each curing condition to better understand this difference. One study conducted by Zadeh et al. accessing Maillard reaction scaffolds have found that the induction of

the Maillard reaction can cause thicker pore walls, which in return would decrease porosity and pore size.<sup>77</sup> If this same mechanism occurs for heat cured CSBP, this could explain why water uptake decreases as the material becomes less porous.

The water contact angle results of self-cured and heat cured CSBP reinforce the water uptake results, as self-cured CSBP has a water contact angle of  $23.60 \pm 2.09^\circ$  and heat cured CSBP has a higher contact angle of  $74.87 \pm 5.76^\circ$ . This indicates that although CSBP remains hydrophilic regardless of curing conditions since both contact angles are below  $90^\circ$ , heat cured CSBP is less hydrophilic than self-cured CSBP.

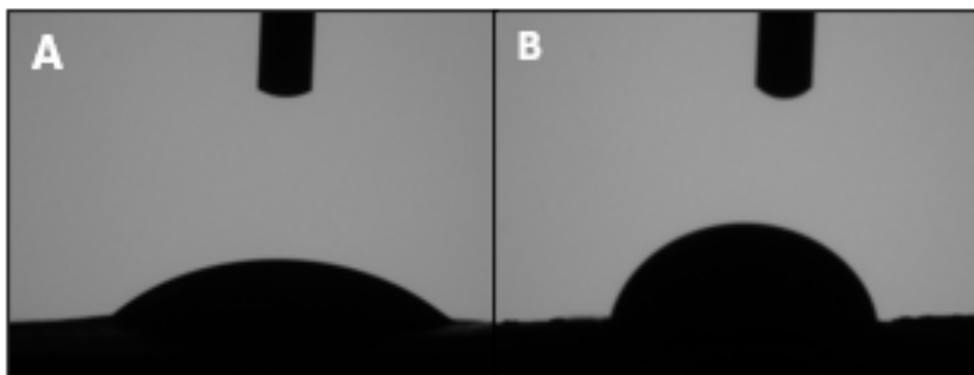


**Figure 22: Comparison of Self-cured and Heat Cured CSBP Water Contact Angles. (A) Self-cured CSBP Water Contact (B) Heat cured CSBP Water Contact.**

### **3.7 Drug Release Kinetics**

The use of plant proteins presents an advantage when considering the potential for medical applications and the development of medical devices, as plant-based proteins are ideal biomaterials due to their natural binding sites and bioactivity *in vitro* and *in vivo*.<sup>97,180</sup> Furthermore, soy protein has been recently evaluated for its potential in creating scaffolds for tissue regeneration, and has shown promising bioactivity for uses in regenerative medicine.<sup>81,83,97,106</sup>

CSBP as characterized throughout this study has shown to be biodegradable, porous, non-cytotoxic and hygroscopic which makes it an ideal candidate for a biodegradable DDS.

Furthermore, research has already been conducted on new types of soy-based materials for biodegradable scaffolds, due to advantages such as mediation of cell adhesion and growth, high drug binding capacity, and biocompatibility.<sup>104,120</sup> To gain a fundamental understanding of how CSBP may be used as a drug delivery system, release kinetics from CSBP was evaluated as a function of curing time using fluorescein as a model drug. Fluorescein was selected for its high fluorescent sensitivity and hydrophilicity, which allowed for easy integration and detection with CSBP scaffolds. The results of fluorescein release kinetics from CSBP are shown in Figure 24. Heat cured CSBP's release kinetics were not evaluated as the high temperature used in curing exceeds the thermal degradation of most pharmaceutical compounds, which limits its potential as a DDS.

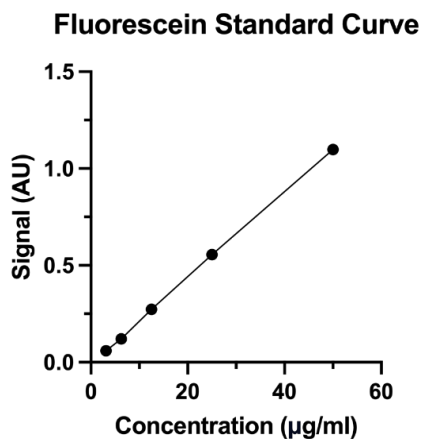


**Figure 23: Fluorescein Standard Curve in PBS. 6.25 µg/mL – 50 µg/mL,  $R^2 > 0.99$ .**

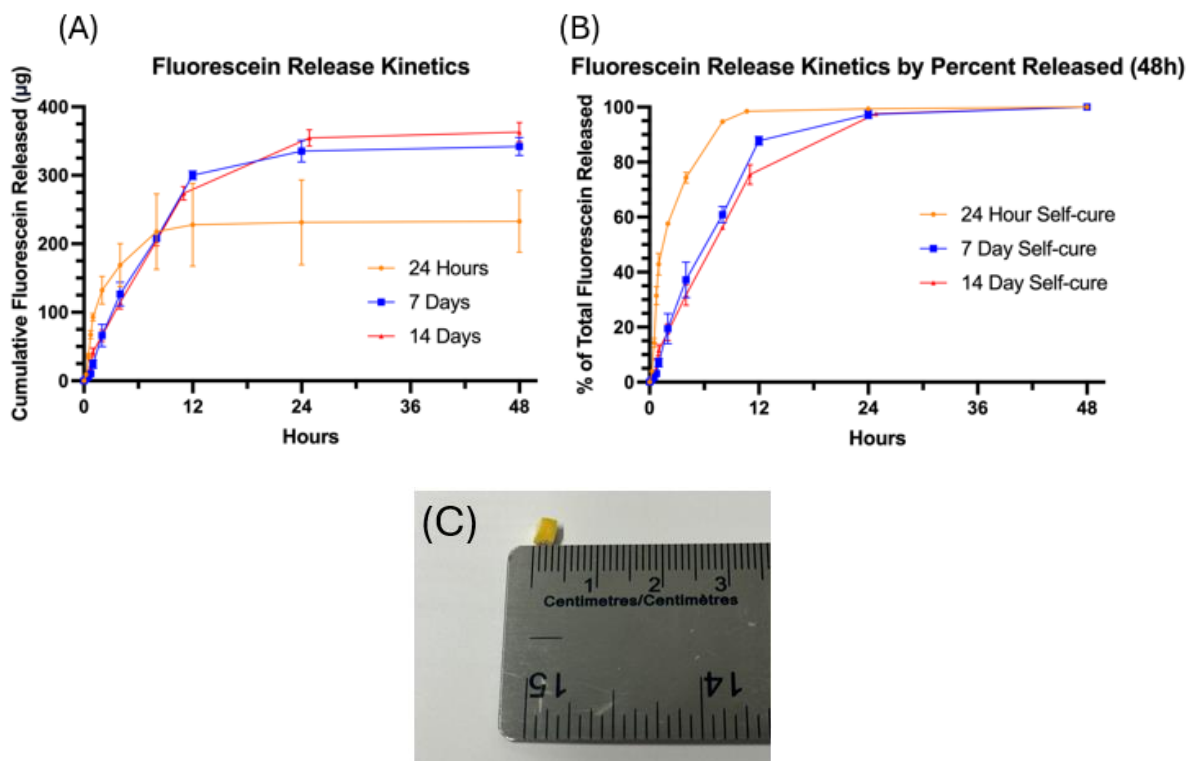


**Figure 24: Fluorescein Release Kinetics from CSBP after 48 Hours in PBS (pH 7.2, 37°C).**

**(A) Fluorescein release kinetics by total released. (B) Fluorescein release kinetics by percent released. (C) Fluorescein-loaded CSBP scaffold. Data represents the mean +/- SD (n=3).**

A small amount of fluorescein was integrated into the CSBP formulation at a percent weight of 0.633% of the entire CSBP paste formulation. Using the results obtained from the weight loss of self-cured CSBP after 7 days at 10% RH (59.3%), it can be estimated that the theoretical total fluorescein in a 50mg fluorescein-loaded self-cured CSBP sample was 316.81µg.

By looking at the release kinetics of fluorescein from CSBP in Figure 24, CSBP self-cured for 7- and 14-days exhibits a rapid release within the first 24 hours of immersion, while 24-hour self-cured CSBP releases most of its payload in the first 12 hours of immersion. Looking at the quantities of fluorescein released, the cumulative release of 7- and 14-day self-cured CSBP after 48 hours, 342.06 +/- 13.13µg and 363.13 +/- 13.87µg respectively, are above fluorescein's

theoretical weight of 316.81µg. The reason for this discrepancy is that the CSBP formulation was mixed manually, which means that fluorescein was likely not homogenously dispersed throughout the paste. The use of a mechanical stirrer or homogenizer in future studies can correct this deviation from theoretical and should provide a homogenous distribution of fluorescein throughout the CSBP formulation.

The fluorescein release from 24-hour self-cured CSBP scaffolds (232.93 +/- 45.21 µg) was much below the theoretical value of 316.81µg and with a high standard deviation, which is likely a combination of the overcorrection of the self-curing weight change value used in the calculation of theoretical fluorescein content as well as formulation inconsistencies from manual mixing. To calculate the theoretical fluorescein content of the CSBP scaffolds, the total CSBP weight was scaled in accordance with the mean self-cured weight loss for 7-day self-cured CSBP to account for the difference in weight between fluorescein-loaded CSBP paste and the resulting scaffold used for release studies. An example of this calculation is provided below:

$$\textit{Theoretical Fluorescein Content} = \left( \frac{\textit{fluorescein content}}{\left( \frac{\textit{total CSBP paste weight}}{\textit{CSBP Self cure weight loss}} \right)} \right) \times \textit{Scaffold weight}$$

Using the above formula appears to lead to an approximate theoretical total fluorescein content for 7- and 14- day self-cured CSBP but may fail to accurately account for the effect of refrigeration (storage of samples at 4°C, 20% RH) on the self-curing of CSBP in the first 24 hours. Due to the manufacturer’s recommendation of storage at 4°C for fluorescein in solution to prevent degradation, samples were stored in a 4°C fridge and protected from light exposure during self-curing. However, in doing so, this may have impacted the resulting self-curing by decelerating the self-curing of CSBP, most notably by slowing down the evaporation of water. Generally, the temperature, humidity, and air velocity of the surrounding atmosphere will dictate the evaporation of water.<sup>181</sup> The lower temperature of the self-curing conditions may have contributed to slower

evaporation of water and a lower degree of CSBP weight loss in the first 24 hours of self-curing, which means that the formula used would not be accurate for 24-hour CSBP. Therefore, the theoretical fluorescein content in future studies needs to be calculated in accordance with first re-characterizing the weight loss of self-curing CSBP at 4°C and 20% RH to account for any changes in self-curing reductions.

Looking at the release kinetics of fluorescein from self-cured CSBP in terms of percent released in the first 48 hours allows for a clear representation of the release kinetics of fluorescein as a function of CSBP's self-cure time. The percent release of fluorescein from self-cured CSBP in Figure 24B produces the expected result of increasing cure time, as the CSBP scaffolds set to cure for longer exhibit a more delayed release of fluorescein. The solidification of CSBP from paste to final object through self-curing allows for more gradual release of fluorescein, as long self-cure times produce a stronger scaffold that in turn is more resistant to force and swelling in water.

Comparing the release kinetics of fluorescein from CSBP to that of other SPI-based materials that have recently been developed to explore the potential of protein-based materials in drug delivery, the release kinetics are generally similar. Research conducted by Song and Zhang, Chien et al., and Vaz et al. focused on soy protein-based DDS exhibit a release profile within the first 48 hours similar to that of the 7- and 14- day self-cured CSBP.<sup>100,105,120</sup>

### **3.8 Heat Cured CSBP Mechanical Properties**

As discussed throughout this study, CSBP can be cured with the use of heat opposed to allowing it to self-cure, however, this drastically alters both the resulting material and interactions within CSBP. Mechanical testing conducted on heat cured CSBP show a compressive strength of 22.9006 +/- 1.2881 MPa, and an ultimate tensile strength of 1.235 +/- 0.11 MPa. Since soy protein

plastics are historically known to be brittle and have low ductility when processed at high temperatures, tensile strength was determined through the use of ASTM D638 which is designed for rigid plastics.<sup>85,182</sup> Heat cured CSBP produces a much more rigid and brittle final object compared to self-cured CSBP. A comparison of self-cured and heat cured CSBP mechanical properties is provided in Figure 25, using the 10% 14-day self-cured CSBP results to represent self-curing.

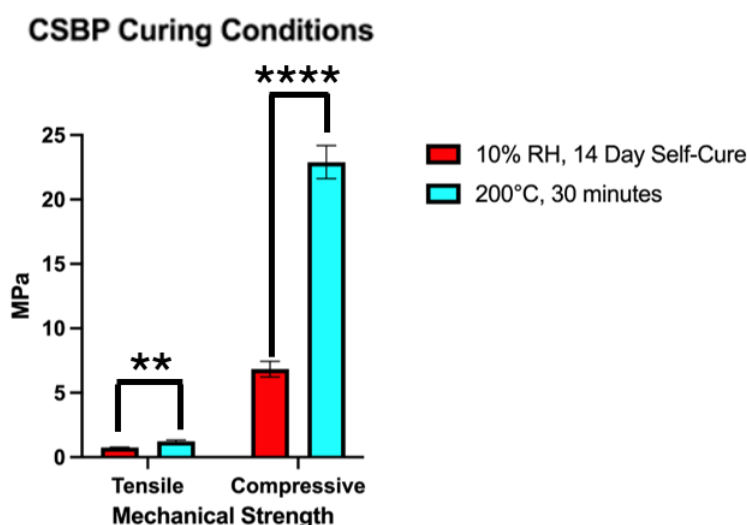


**Figure 25: Comparison of CSBP Mechanical Properties by Curing Condition. The comparison between compressive strength is not direct, and instead between compressive strength at 35% deformation for self-cured CSBP and compressive strength of heat cured CSBP. \*\*p<0.01, \*\*\*\*p<0.0001.**

A comparison of self-cured and heat cured CSBP shows that the use of Maillard-type reactions and crosslinking produces an object with stronger mechanical properties than that of self-cured CSBP. As heat cured CSBP is processed above the thermal degradation of the two additives glycerol and citric acid, it does not rely on these formulation components directly and instead induces Maillard-type reactions between SPI, MCC, and potentially degradation products. The increased mechanical strength of CSBP through the use of heat curing was an expected result, as

the use of Maillard-type reaction in biomaterial synthesis is known to increase the resulting mechanical properties.<sup>77</sup>

Although the tensile strength values of CSBP for self-curing (0.749 +/- 0.047 MPa) is close to that of heat cured CSBP (1.235 +/- 0.11 MPa), the behavior varies significantly. Heat cured CSBP is much firmer and more brittle than self-cured CSBP, and snaps quickly under load. Self-cured CSBP is instead more viscoelastic and has a greater degree of elasticity and resilience than heat cured CSBP. The difference in tensile behavior of these two curing variations may be better characterized quantitatively using an extensometer during tensile testing.

### **3.9 CSBP Characterization Summary**

Multiple studies were conducted to explore the baseline properties of CSBP and to help gauge the potential real-world applications of this biomaterial, which will be expanded upon in section 3.10. Overall, CSBP contains fully GRAS components and relies on a synergistic approach of SPI-MCC film formation, crosslinking, and solvent evaporation to form a self-curable solid object. The processes involved in CSBP formulation and 3D printing are void of the use of heat and other high energy processes when self-curing is employed. Further, heat cured CSBP was characterized alongside self-cured CSBP for multiple studies to provide a comparison between the two conditions of CSBP curing. A summary table of the characteristics of CSBP discussed in sections 3.1-3.8 is provided below:

**Table 5: Summary of CSBP Characterizations**

<b>Characteristic</b>	<b>Self-cured CSBP</b>	<b>Heat Cured CSBP</b>
3D Printable using a syringe-based mechanism	Yes	Yes
Natural Biodegradability (soil)	98.13% weight loss in 80 days	Unknown
Optimal Degradation Temperature	342.1°C	342.1°C
Microstructure	Porous, SPI-MCC film formation	Unknown
Water Properties	Hydrophilic, 47.49% water uptake at 95% RH	Hydrophilic, 11.73% water uptake at 95% RH
Cytotoxicity	Non-cytotoxic	Unknown
Release Kinetics	Rapid release in first 24 hours	Unknown
Compressive Strength	2.4894 MPa at 10% RH, 14 days	22.9006 MPa
Tensile Strength	0.749 MPa at 10% RH, 14 days	1.235 MPa.

### **3.10 CSBP Applications**

#### **3.10.1 Paper-Based Adhesive**

From working through the 3D printing and characterizations of CSBP, it was observed that CSBP paste has a sticky texture and self-curing behavior, which suggested there may be potential use as a sustainable adhesive. The preliminary adhesive strength of CSBP was tested as well as two dilutions for the impact of higher water content, and the results are summarized in Table 6.

**Table 6: CSBP Preliminary Adhesive Strength by Dilution**

<b>Dilution</b>	<b>Failure Weight (lbs)</b>
None (100% CSBP)	>3.3
10% (9 parts CSBP, 1 part water)	≤2.20
25% (3 parts CSBP, 1 part water)	≤0.956

The preliminary adhesive strength tests of CSBP show that without dilution, CSBP can endure over 3.3 pounds of weight without failure when adhered with a 1x1 inch application of CSBP paste onto a cardboard strip. Since a small box was used for the preliminary adhesive

strength testing, no additional weight could be fit into the box to test higher weights beyond 3.3 pounds. The dilution of CSBP using DI water greatly reduced the resulting failure weight of the samples, which was to be expected as the dilution of CSBP reduces the molecular interactions in self-curing and therefore decreases bond strength. Although the dilution of CSBP decreases the resulting bond strength, it dilutes CSBP into a more fluid state, which may be beneficial for adhesive applications that require a fluid adhesive to be extruded from a thin nozzle. The potential of SPI-based materials as an adhesive for a wide range of products has been a very recent expansion of SPI material development explored by some researchers, however, due to the nature of the preliminary adhesive testing of CSBP the results can not be effectively compared to the findings of others at this time.<sup>183-185</sup> The purchase and use of UTM attachments designed for peel adhesive strength tests alongside protocol such as those outlined in ASTM D903: Peel or Stripping Strength of Adhesive Bonds would allow for an exact and rigorous determination of the adhesive strength of CSBP and should be conducted to provide a better quantitative assessment of CSBP adhesive strength.

### **3.10.2 Sustainable and Biodegradable Packaging Alternative**

As the self-curing of CSBP produces a non-rigid final object, there is the potential for applications in the packaging industry as a sustainable alternative to foams currently used. Most foams are made up of polystyrene, a synthetic polymer created from petroleum-based resources and known to be non-biodegradable.<sup>186,187</sup> Thus, if CSBP can be manufactured to produce packaging objects like those being created with polystyrene, there is great potential for reducing plastic usage in packaging. As a proof-of-concept for CSBP's potential packaging applications, the creation of a small packaging peanut like those made of polystyrene and used in shipping boxes was created and compared.

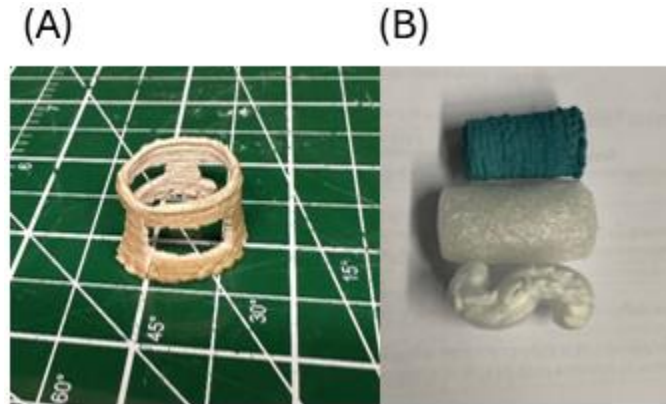


**Figure 26: Preliminary CSBP Packing Peanut Design. (A) Air-based CSBP packing peanut with inserts removed (B) Comparison of CSBP packing peanut size, prior to insert removal, to other common polystyrene packaging peanuts.**

The CSBP packaging peanut design shown in Figure 26A differs in appearance from that of polystyrene packing peanuts, as an air-based design is used to mimic the exact properties of packing peanuts. The CSBP 3D printed peanut has rectangular inserts carefully removed post curing, for two main reasons. Firstly, the use of this air-based design and insert removal allows for CSBP to create low density structures, as the typical density of CSBP ( $0.9631 \pm 0.032 \text{ mg/mm}^3$ ) is much higher than that of common packaging solutions. The use of a hollow structure and the removal of small rectangular inserts allows for a near tenfold reduction in density for CSBP packing peanuts (Table 7), which although the resulting density remains approximately ten times higher than polystyrene packing peanuts, is a major improvement. Second, the use of an air-based design for CSBP packaging applications allows for the modulation of the resulting compressive strength to a value equal to that of polystyrene packing peanuts, as displayed in Table 7. Different size and shape removals from the hollow cylindrical structure of CSBP may be used to meet any specific requirements (density, compressive strength, recovery) needed for CSBP packaging applications, to better match the properties of other foams.

**Table 7: CSBP Preliminary Packaging Results**

<b>Material</b>	<b>Density (mg/mm<sup>3</sup>)</b>	<b>35% Deformation Compressive Strength (MPa)</b>
Typical CSBP	0.9631 +/- 0.032	Dependent on cure conditions
CSBP Packing Peanut	0.1138 +/- 0.037	0.0194
Polystyrene Packing Peanut	0.01127 +/- 0.0021	0.0153

Qualitatively, the performance of the CSBP packaging peanuts tested for compression showed excellent shape recovery after compression, a property that is promising for use as an alternative to foams. Future studies may be conducted to quantify and compare the recovery of CSBP peanuts to other common packaging materials. The application of CSBP for use in packaging, namely as a sustainable alternative to polystyrene packing peanuts, provides insight on how the tunable properties of CSBP may be applied to the real-world. The findings of this study can greatly be expanded upon by evaluating how different insert removal shapes and dimensions, hollow gap space and other parameters to this air-based structure may reduce the discrepancy in the density of CSBP and currently used foams in the packaging industry.

### **3.10.2 Microneedles for Drug Delivery**

The creation of microneedle patches with CSBP was performed to assess the potential of CSBP in the fabrication of an established DDS. Firstly, CSBP microneedles were created using a casting method (outlined in section 2.5.3) opposed to 3D printing, which required three key changes to the CSBP formulation. Since a casting method was required to pour and fill the microneedle molds, the MCC content of CSBP was reduced to 50% of the original formulation to reduce the viscosity of the paste into a free-flowing liquid. However, the reduction of the MCC content of CSBP in turn reduced the mechanical strength of the microneedles and increased the flexibility, because of the lower MCC fibre content for film formation. To resolve the decreased rigidity of the CSBP microneedles, PVA was added to the formulation at a ratio of 90:10 CSBP to

PVA. PVA was selected to resolve the decreased mechanical strength of the CSBP-PVA microneedles as it is a common polymer used in microneedle fabrication, known for its superior strength and skin penetration when compared to other microneedle polymers.<sup>188,189</sup> The use of 70°C heat during PVA addition was to facilitate the dissolution of PVA into the CSBP binder, to ensure a homogenous blend was prepared for casting.

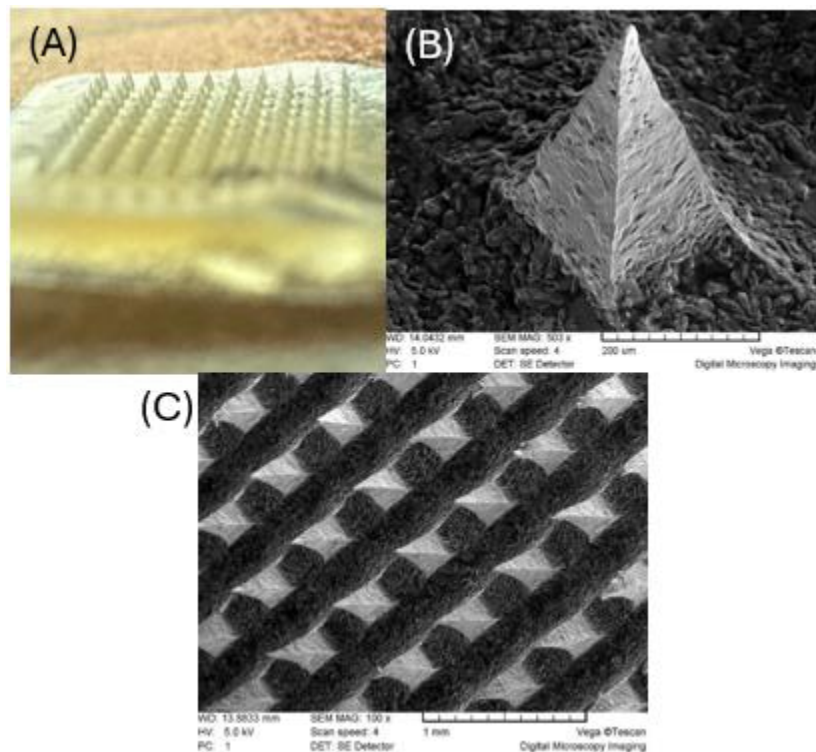


**Figure 27: CSBP-PVA Microneedle Macroscopic Appearance and SEM Imaging. (A) Image of the CSBP-PVA microneedles using an iPhone 3x optical zoom. (B) SEM image of the CSBP-PVA microneedle with a magnification of 503x. (C) Image of an array of the CSBP-PVA's microneedles at a magnification of 100x.**

The CSBP-PVA microneedles in Figure 27 show the successful creation of sharp microneedle tips, and a similar porous microstructure seen with the CSBP SEM conducted earlier. The appearance of some of the microneedle tips appear to be slightly bent, which is due to the microneedles being removed from the mold whilst still in a soft state, causing deformation. It is

also possible that damage occurred to the microneedle samples during transportation to the SEM, as microneedles were fully removed from the mold prior to transportation which left them susceptible to damage. Allowing for a longer self-curing period (beyond 48 hours) within the microneedle mold prior to removing the microneedle would prevent this issue on future microneedles made using CSBP, as well as keeping the microneedles fixed in the mold up until imaging is to be conducted. To test the mechanical integrity of the CSBP-PVA microneedles and ensure that there is sufficient penetration of the skin, insertion analysis was conducted using Parafilm M and porcine stratum corneum. The use of Parafilm M in the insertion analysis of microneedles is a technique employed for evaluating microneedle insertion, and the penetration of three successive layers is regarded as sufficient for dermal applications.<sup>127,190</sup> The results shown in Figure 28 demonstrate CSBP-PVA microneedles' capability to penetrate 3 layers of parafilm and the porcine stratum corneum, signifying that sufficient strength has been achieved for dermal penetration.

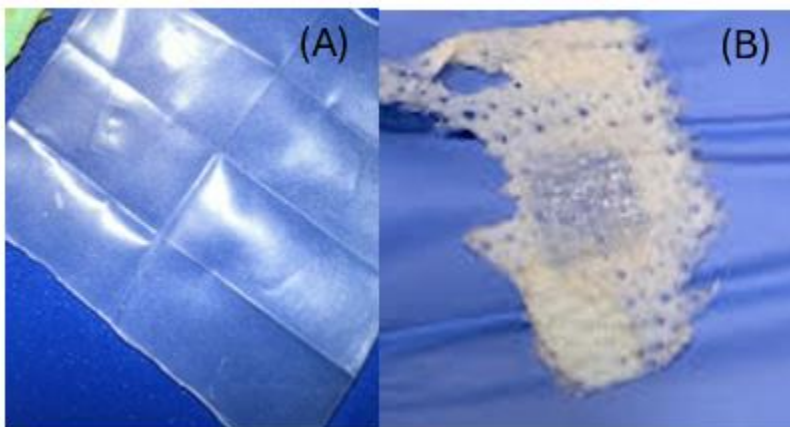


**Figure 28: Insertion Analysis of CSBP-PVA Microneedles. (A) Penetration of 3 layers of Parafilm M with a CSBP-PVA microneedle. (B) Penetration of porcine stratum corneum with CSBP-PVA microneedle.**

Cumulatively, the preliminary work done on creating microneedles using CSBP demonstrates the ability to successfully fabricate microneedles with precise needle formation and

sufficient mechanical strength for dermal applications. Release studies should be performed using CSBP-PVA microneedles to evaluate how the different formulation, preparation method, as well as surface area of these microneedles may change the release profile when compared to the release kinetics of CSBP characterized in this study. Under the assumption that CSBP-PVA microneedles will exhibit a similar release profile to that of CSBP characterized in this study (section 3.7), applications for the 24 hour delivery of macromolecules such as skin treatment may be explored.<sup>191</sup> Alternatively, the potential for CSBP microneedles for sustained release may be investigated by exploring CSBP's formulation versatility and the integration of other polymers in attempt to slow down the release profile of the resulting DDS.

## 4. CONCLUSIONS AND FUTURE DIRECTION

### 4.1 Conclusions

This study successfully created a novel cellulose-based soy biopolymer, coined CSBP, with a thorough exploration of the preliminary characteristics and applications of this new biomaterial. CSBP works through a synergistic combination of protein crosslinking, film formation, and solvent evaporation to become one of, if not the first, 3D-printable soy protein biomaterials for non-edible applications. The CSBP formulation also shows a degree of interchangeability through the potential for varying cellulose components and additives with similar functional groups. The integration of CSBP with 3D printing was accomplished using a syringe-based mechanism for extrusion and printing up to a 20Ga needle diameter in combination with self or heat curing to form a final object. The maximum self-cured tensile and 35% deformation compressive strength of CSBP,  $0.7487 \pm 0.0474$  MPa and  $6.843 \pm 0.608$  MPa respectively, occurred after 14 days of self-curing at 10% RH. The impact of atmospheric water content, in the form of RH, had a significant impact on the resulting mechanical properties of self-cured CSBP. Cytotoxicity testing of CSBP revealed that the elution of CSBP for up to 30 days in media produces no significant decrease in cell viability, as expected. Evaluating the biodegradability of CSBP with TGA and soil burial tests allowed a determination of the ODT of CSBP ( $342.1 \pm 0.948^\circ\text{C}$ ) and the natural biodegradation of CSBP in soil ( $98.13 \pm 0.63\%$  weight loss in 80 days). The water properties of CSBP were designed to characterize the absorptive ability of self-cured CSBP ( $47.49 \pm 1.55\%$  water uptake), as well as to evaluate how changes in curing temperature may affect the water properties of CSBP. It was determined through both water uptake and contact angle that the use of heat in the curing of CSBP produces a less hydrophilic and absorptive final object. The release kinetics of fluorescein from self-cured CSBP showed the rapid release of fluorescein within 24

hours of PBS immersion, with slightly delayed release in this timeframe for longer periods of self-curing. A trend common throughout many of the time-based characterizations of self-cured CSBP is the lack of significant change beyond 14 days of self-curing, suggesting that 14 days is an ideal timepoint to obtain the maximum properties of self-cured CSBP.

With established natural biodegradability, biocompatibility, and environmentally friendly synthesis, through low energy production methods, ambient-active molecular interactions and potential for the integration of post consumer recycled paper, CSBP can create a sustainable alternative to various materials and processes amongst multiple industries. For each of the three potential industries for CSBP evaluated in this study, adhesive use, packaging, and pharmacy, the preliminary results are an encouraging starting point to the use of CSBP as a sustainable and naturally biodegradable biomaterial in the real-world.

The findings of this study may also provide a sustainable alternative to thermoplastic usage and FDM printing, thereby reducing the need for non-renewable resources in 3D printing. Compared to currently used filaments in FDM processes such as ABS, PET and PLA, CSBP offers some of the following advantages:

1. Low power consumption: The energy consumption of FDM printers is of concern for the long term sustainability of 3D printing, as they require high amounts of energy to continually heat and print using a hot-head mechanism.<sup>192,193</sup> With the development of CSBP feedstock relying only on the application of heat as a pre-print denaturation step and optional post-print modification for heat curing, the overall power consumption of CSBP production is considerably lower than that of current FDM processes. The exact difference in power consumption could be calculated in a future study.

2. Petroleum-free alternative for FDM printing: The created CSBP paste does not rely on the use of petroleum products or raw material and is comprised of renewable and recycled materials that are GRAS and demonstrated to be noncytotoxic.
3. Biodegradability: Being that CSBP is reliant on the crosslinking of plant proteins and does not involve synthetic polymers, it is naturally biodegradable without the restrictions of highly specific conditions such as those required to degrade PLA.<sup>47,51</sup> The natural biodegradability of CSBP was directly evaluated in Section 3.5.2, and greatly outperformed common FDM polymers ABS and PLA.
4. Recyclability of waste: Unique to CSBP, the recyclability of paper can be incorporated into the formulation to develop the resulting paste. With paper fibres accounting for the 36% of Canada's total waste diverted by material, this material may be used help to reduce and reuse paper waste.<sup>59</sup> Although only brown and white paper were evaluated in this study, the role of paper in CSBP's formulation shows some interchangeability, and there may be capacity for this biomaterial to recycle other common waste materials that can interact with soy protein. Other forms of paper fibres, such as those that are not recyclable (paper that has been treated, coated, waxed, laminated etc.) may be a compatible substitution into the CSBP formulation and should be evaluated in a future study to expand the recyclability potential of this material.
5. Soy: CSBP is reliant on the use of soy for protein crosslinking and film formation. While soy production is still prominent globally due to its use in soybean oils, the uses of soy in human food is very low at 9.21 tons in 2019.<sup>194</sup> When comparing the use of soybean in food products to that of corn, the raw material of PLA, approximately 147 million tons of corn is used for direct human food<sup>195</sup>. Therefore, the use of soy protein as a future bioplastic requires much

less consideration of the impact it may have on global food staples if mass production is required, due to greatly reduced use in foods when compared to PLA and corn usage.

## **4.2 Limitations**

The limitations of CSBP pertain to typical limitations associated with plant-protein plastics as well as syringe-based 3D printing mechanisms. Firstly, it should be noted that the strength of CSBP was expected to be inferior to that of PLA and petroleum-based plastics, as the goal of this project was to synthesize a sustainable and safe material as an alternative to these polymers, opposed to a direct replacement. The lower mechanical properties of CSBP does not dismiss the potential for various applications of CSBP, as various objects can still be produced with sufficient mechanical properties for end-user applications. The water-soluble nature of CSBP was characterized through the water properties and mechanical strength characterizations and showed that self-cured CSBP has greatly reduced performance when exposed to water, either directly or within the surrounding environment. This is a potential limitation to the end use of CSBP with self-curing as variable performance in response to humidity and water content may be problematic with certain applications of this material.

With respect to the 3D printing of CSBP, the use of a syringe-based mechanism presents limitations in design and production as mentioned in section 1.1.3, as well as less detailed prints resulting from a larger syringe nozzle diameter. The shelf-life of uncured CSBP paste is finite as it undergoes self-curing, and storage in an air-tight container is necessary to prevent CSBP paste from solidifying. Thus far, CSBP samples stored in an air-tight container at 4°C have shown no fungal growth and can be 3D printed without any noticeable changes in viscosity up to 6 months after synthesis, however, there is the potential for expiry beyond this. The methodology used to

prepare CSBP was not optimized in this study and needs to be further explored by evaluating differing ratios of each formulation component.

### **4.3 Future Directions**

Ultimately, through the completion of this project a sustainable alternative to current 3D printing has been developed and characterized, as well as preliminary insights into the potential applications of this new material. There is a wide variety of biopolymer characterizations that can be performed to evaluate CSBP and cannot be covered in this study alone. A list of potential studies that can be performed to expand upon the properties of CSBP is listed in Table 8.

To address the biggest potential limitation of CSBP, future work should work towards reducing CSBP's susceptibility to water. Although a carnauba wax coating was successfully used as a negative control in this study and prevented CSBP's uptake of water, this wax coating may alter the materials other properties and instead other alternatives should be explored. The most promising potential solution, the use of a heat cure for CSBP, was employed throughout this study and should be explored fully for how it may be used to reduce CSBP's water properties.

**Table 8: A List of Potential Future Characterizations for CSBP**

<b>Characterization</b>	<b>Rationale</b>	<b>Method / Equipment</b>
Geometry	Determine the specific bonds and interactions present in CSBP	NMR Spectroscopy
Porosity	Obtain porosity values for CSBP	Pycnometer
Heat cured CSBP	Perform studies conducted on self-cured CSBP on heat cured CSBP	N/A
Compressive recovery	Recovery properties of self-cured CSBP	UTM and ASTM D3574
Accelerated stability testing	Identify potential shelf-life of CSBP as an object or paste	Environmental Chamber
Mechanical strength and water resistance	Evaluate how the use of heat in the curing of CSBP may prevent a decline in mechanical strength with water exposure	UTM
Additional Mechanical Properties	Evaluate mechanical properties useful in characterization of non-rigid materials such as hardness	UTM and more

The potential pharmaceutical applications of this material include the creation of medical devices such as regenerative medicine or drug delivery platforms that can be evaluated in a future study to expand upon the biocompatibility, water properties and release kinetics evaluated in this study. The versatility of CSBP fabrication, through methods such as 3D printing or molding, makes it a great candidate for the fabrication of a wide variety of drug delivery systems, such as the microneedles fabricated in this study. Stemming from the applications evaluated in this study, there is also potential for future applications of CSBP in the real-world, as this material may be used as a safe and sustainable alternative in industries such as AM, adhesives, and packaging. Future studies tailored towards evaluating one specific application of CSBP would be beneficial, as this study focussed namely on evaluating the baseline characteristics and applications of a general CSBP formulation. Within the synthesis of CSBP, there exists multiple changes that can be made to the formulation and process to optimize CSBP towards a specific application.

## REFERENCES

- (1) Huang, S. H.; Liu, P.; Mokasdar, A.; Hou, L. Additive Manufacturing and Its Societal Impact: A Literature Review. *Int. J. Adv. Manuf. Technol.* **2013**, *67* (5–8), 1191–1203. <https://doi.org/10.1007/s00170-012-4558-5>.
- (2) Thomas, D. Costs, Benefits, and Adoption of Additive Manufacturing: A Supply Chain Perspective. *Int. J. Adv. Manuf. Technol.* **2016**, *85* (5), 1857–1876. <https://doi.org/10.1007/s00170-015-7973-6>.
- (3) Mathew, J. J.; Sakhale, C. N.; Shelare, S. D. Latest Trends in Sheet Metal Components and Its Processes—A Literature Review. In *Advances in Computing and Intelligent Systems*; Sharma, H., Govindan, K., Poonia, R. C., Kumar, S., El-Medany, W. M., Eds.; Algorithms for Intelligent Systems; Springer: Singapore, **2020**; pp 565–574. [https://doi.org/10.1007/978-981-15-0222-4\\_54](https://doi.org/10.1007/978-981-15-0222-4_54).
- (4) Chan, H. K.; Griffin, J.; Lim, J. J.; Zeng, F.; Chiu, A. S. F. The Impact of 3D Printing Technology on the Supply Chain: Manufacturing and Legal Perspectives. *Int. J. Prod. Econ.* **2018**, *205*, 156–162. <https://doi.org/10.1016/j.ijpe.2018.09.009>.
- (5) Gao, W.; Zhang, Y.; Ramanujan, D.; Ramani, K.; Chen, Y.; Williams, C. B.; Wang, C. C. L.; Shin, Y. C.; Zhang, S.; Zavattieri, P. D. The Status, Challenges, and Future of Additive Manufacturing in Engineering. *Comput.-Aided Des.* **2015**, *69*, 65–89. <https://doi.org/10.1016/j.cad.2015.04.001>.
- (6) Jandyal, A.; Chaturvedi, I.; Wazir, I.; Raina, A.; Ul Haq, M. I. 3D Printing – A Review of Processes, Materials and Applications in Industry 4.0. *Sustainable Operations and Computers* **2022**, *3*, 33–42. <https://doi.org/10.1016/j.susoc.2021.09.004>.

- (7) Ranjan, R.; Kumar, D.; Kundu, M.; Chandra Moi, S. A Critical Review on Classification of Materials Used in 3D Printing Process. *Mater. Today Proc.* **2022**, *61*, 43–49. <https://doi.org/10.1016/j.matpr.2022.03.308>.
- (8) Liu, Z.; Wang, Y.; Wu, B.; Cui, C.; Guo, Y.; Yan, C. A Critical Review of Fused Deposition Modeling 3D Printing Technology in Manufacturing Polylactic Acid Parts. *Int. J. Adv. Manuf. Technol.* **2019**, *102* (9), 2877–2889. <https://doi.org/10.1007/s00170-019-03332-x>.
- (9) Kristiawan, R. B.; Imaduddin, F.; Ariawan, D.; Ubaidillah; Arifin, Z. A Review on the Fused Deposition Modeling (FDM) 3D Printing: Filament Processing, Materials, and Printing Parameters. *Open Eng.* **2021**, *11* (1), 639–649. <https://doi.org/10.1515/eng-2021-0063>.
- (10) Okwuosa, T. C.; Stefaniak, D.; Arafat, B.; Isreb, A.; Wan, K.-W.; Alhnan, M. A. A Lower Temperature FDM 3D Printing for the Manufacture of Patient-Specific Immediate Release Tablets. *Pharm. Res.* **2016**, *33* (11), 2704–2712. <https://doi.org/10.1007/s11095-016-1995-0>.
- (11) Choi, W. J.; Hwang, K. S.; Kwon, H. J.; Lee, C.; Kim, C. H.; Kim, T. H.; Heo, S. W.; Kim, J.-H.; Lee, J.-Y. Rapid Development of Dual Porous Poly(Lactic Acid) Foam Using Fused Deposition Modeling (FDM) 3D Printing for Medical Scaffold Application. *Mater. Sci. Eng. C* **2020**, *110*, 110693. <https://doi.org/10.1016/j.msec.2020.110693>.
- (12) Daminabo, S. C.; Goel, S.; Grammatikos, S. A.; Nezhad, H. Y.; Thakur, V. K. Fused Deposition Modeling-Based Additive Manufacturing (3D Printing): Techniques for Polymer Material Systems. *Mater. Today Chem.* **2020**, *16*, 100248. <https://doi.org/10.1016/j.mtchem.2020.100248>.
- (13) Tümer, E. H.; Erbil, H. Y. Extrusion-Based 3D Printing Applications of PLA Composites: A Review. *Coatings* **2021**, *11* (4), 390. <https://doi.org/10.3390/coatings11040390>.

- (14) Greco, A.; Ferrari, F. Thermal Behavior of PLA Plasticized by Commercial and Cardanol-Derived Plasticizers and the Effect on the Mechanical Properties. *J. Therm. Anal. Calorim.* **2021**, *146* (1), 131–141. <https://doi.org/10.1007/s10973-020-10403-9>.
- (15) Moore, J. D. Acrylonitrile-Butadiene-Styrene (ABS) - a Review. *Composites* **1973**, *4* (3), 118–130. [https://doi.org/10.1016/0010-4361\(73\)90585-5](https://doi.org/10.1016/0010-4361(73)90585-5).
- (16) Liu, Y.; Qian, J.; Wang, J. Pyrolysis of Polystyrene Waste in a Fluidized-Bed Reactor to Obtain Styrene Monomer and Gasoline Fraction. *Fuel Process. Technol.* **2000**, *63* (1), 45–55. [https://doi.org/10.1016/S0378-3820\(99\)00066-1](https://doi.org/10.1016/S0378-3820(99)00066-1).
- (17) Szykiedans, K.; Credo, W.; Osiński, D. Selected Mechanical Properties of PETG 3-D Prints. *Procedia Eng.* **2017**, *177*, 455–461. <https://doi.org/10.1016/j.proeng.2017.02.245>.
- (18) Rett, J. P.; Traore, Y. L.; Ho, E. A. Sustainable Materials for Fused Deposition Modeling 3D Printing Applications. *Adv. Eng. Mater.* **2021**, *23* (7), 2001472. <https://doi.org/10.1002/adem.202001472>.
- (19) Latko-Durałek, P.; Dydek, K.; Boczkowska, A. Thermal, Rheological and Mechanical Properties of PETG/rPETG Blends. *J. Polym. Environ.* **2019**, *27* (11), 2600–2606. <https://doi.org/10.1007/s10924-019-01544-6>.
- (20) Le-Bail, A.; Maniglia, B. C.; Le-Bail, P. Recent Advances and Future Perspective in Additive Manufacturing of Foods Based on 3D Printing. *Curr. Opin. Food Sci.* **2020**, *35*, 54–64. <https://doi.org/10.1016/j.cofs.2020.01.009>.
- (21) Sun, J.; Peng, Z.; Yan, L.; Fuh, J. Y. H.; Hong, G. S. 3D Food Printing an Innovative Way of Mass Customization in Food Fabrication. *Int. J. Bioprinting* **2015**, *1* (1). <https://doi.org/10.18063/IJB.2015.01.006>.

- (22) Attarin, S.; Attaran, M. Food Printing: Evolving Technologies, Challenges, Opportunities, and Best Adoption Strategies. *J. Int. Technol. Inf. Manag.* **2020**, *29* (1), 25–55. <https://doi.org/10.58729/1941-6679.1442>.
- (23) Angelats Lobo, D.; Ginestra, P. Cell Bioprinting: The 3D-Bioplotter™ Case. *Materials* **2019**, *12* (23), 4005. <https://doi.org/10.3390/ma12234005>.
- (24) Jiang, C.-P.; Chen, Y.-Y. Biofabrication of Hybrid Bone Scaffolds Using a Dual-Nozzle Bioplotter and in-Vitro Study of Osteoblast Cell. *Int. J. Precis. Eng. Manuf.* **2014**, *15*, 1947–1953. <https://doi.org/10.1007/s12541-014-0549-9>.
- (25) Chiesa, I.; Ligorio, C.; Bonatti, A. F.; De Acutis, A.; Smith, A. M.; Saiani, A.; Vozzi, G.; De Maria, C. Modeling the Three-Dimensional Bioprinting Process of  $\beta$ -Sheet Self-Assembling Peptide Hydrogel Scaffolds. *Front. Med. Technol.* **2020**, *2*. <https://doi.org/10.3389/fmedt.2020.571626>.
- (26) Boularaoui, S.; Al Hussein, G.; Khan, K. A.; Christoforou, N.; Stefanini, C. An Overview of Extrusion-Based Bioprinting with a Focus on Induced Shear Stress and Its Effect on Cell Viability. *Bioprinting* **2020**, *20*, e00093. <https://doi.org/10.1016/j.bprint.2020.e00093>.
- (27) Sarker, Md.; Chen, X. B. Modeling the Flow Behavior and Flow Rate of Medium Viscosity Alginate for Scaffold Fabrication With a Three-Dimensional Bioplotter. *J. Manuf. Sci. Eng.* **2017**, *139* (8). <https://doi.org/10.1115/1.4036226>.
- (28) Chen, J.; Mu, T.; Goffin, D.; Blecker, C.; Richard, G.; Richel, A.; Haubruge, E. Application of Soy Protein Isolate and Hydrocolloids Based Mixtures as Promising Food Material in 3D Food Printing. *J. Food Eng.* **2019**, *261*, 76–86. <https://doi.org/10.1016/j.jfoodeng.2019.03.016>.

- (29) Pusch, K.; Hinton, T. J.; Feinberg, A. W. Large Volume Syringe Pump Extruder for Desktop 3D Printers. *HardwareX* **2018**, *3*, 49–61. <https://doi.org/10.1016/j.ohx.2018.02.001>.
- (30) Samokhin, A. S. Syringe Pump Created Using 3D Printing Technology and Arduino Platform. *J. Anal. Chem.* **2020**, *75* (3), 416–421. <https://doi.org/10.1134/S1061934820030156>.
- (31) Baas, S.; Saggiomo, V. Ender3 3D Printer Kit Transformed into Open, Programmable Syringe Pump Set. *HardwareX* **2021**, *10*, e00219. <https://doi.org/10.1016/j.ohx.2021.e00219>.
- (32) Kewuyemi, Y. O.; Kesa, H.; Adebo, O. A. Trends in Functional Food Development with Three-Dimensional (3D) Food Printing Technology: Prospects for Value-Added Traditionally Processed Food Products. *Crit. Rev. Food Sci. Nutr.* **2022**, *62* (28), 7866–7904. <https://doi.org/10.1080/10408398.2021.1920569>.
- (33) Demircan, E.; Özçelik, B. Development of Affordable 3D Food Printer with an Exchangeable Syringe-Pump Mechanism. *HardwareX* **2023**, *14*, e00430. <https://doi.org/10.1016/j.ohx.2023.e00430>.
- (34) Darling, C.; Smith, D. A. Syringe Pump Extruder and Curing System for 3D Printing of Photopolymers. *HardwareX* **2021**, *9*, e00175. <https://doi.org/10.1016/j.ohx.2021.e00175>.
- (35) Guo, C.-F.; Zhang, M.; Bhandari, B. A Comparative Study between Syringe-Based and Screw-Based 3D Food Printers by Computational Simulation. *Comput. Electron. Agric.* **2019**, *162*, 397–404. <https://doi.org/10.1016/j.compag.2019.04.032>.
- (36) Zhang, J. Y.; Pandya, J. K.; McClements, D. J.; Lu, J.; Kinchla, A. J. Advancements in 3D Food Printing: A Comprehensive Overview of Properties and Opportunities. *Crit. Rev. Food Sci. Nutr.* **2022**, *62* (17), 4752–4768. <https://doi.org/10.1080/10408398.2021.1878103>.

- (37) Bom, S.; Ribeiro, R.; Ribeiro, H. M.; Santos, C.; Marto, J. On the Progress of Hydrogel-Based 3D Printing: Correlating Rheological Properties with Printing Behaviour. *Int. J. Pharm.* **2022**, *615*, 121506. <https://doi.org/10.1016/j.ijpharm.2022.121506>.
- (38) Fazzini, G.; Paolini, P.; Paolucci, R.; Chiulli, D.; Barile, G.; Leoni, A.; Muttillio, M.; Pantoli, L.; Ferri, G. Print On Air: FDM 3D Printing Without Supports. In *2019 II Workshop on Metrology for Industry 4.0 and IoT (MetroInd4.0&IoT)*; **2019**; pp 350–354. <https://doi.org/10.1109/METROI4.2019.8792846>.
- (39) Despeisse, M.; Baumers, M.; Brown, P.; Charnley, F.; Ford, S.; Garmulewicz, A.; Knowles, S.; Minshall, T.; Mortara, L.; Reed-Tsochas, F.; Rowley, J. *Unlocking Value for a Circular Economy through 3D Printing: A Research Agenda*; **2016**. <https://doi.org/10.13140/RG.2.1.4618.9685>.
- (40) Liu, Z.; Jiang, Q.; Zhang, Y.; Li, T.; Zhang, H.-C. Sustainability of 3D Printing: A Critical Review and Recommendations. In *Volume 2: Materials; Biomanufacturing; Properties, Applications and Systems; Sustainable Manufacturing*; American Society of Mechanical Engineers: Blacksburg, Virginia, USA, **2016**; p V002T05A004. <https://doi.org/10.1115/MSEC2016-8618>.
- (41) Hopewell, J.; Dvorak, R.; Kosior, E. Plastics Recycling: Challenges and Opportunities. *Philos. Trans. R. Soc. B Biol. Sci.* **2009**, *364* (1526), 2115–2126. <https://doi.org/10.1098/rstb.2008.0311>.
- (42) Kabeyi, D.; Olanrewaju, O. Review and Design Overview of Plastic Waste-to-Pyrolysis Oil Conversion with Implications on the Energy Transition. *J. Energy* **2023**, *2023*, 1–25. <https://doi.org/10.1155/2023/1821129>.

- (43) *AR6 Synthesis Report: Climate Change 2023*. <https://www.ipcc.ch/report/ar6/syr/> (accessed 2023-03-21).
- (44) Song, R.; Telenko, C. Material Waste of Commercial FDM Printers under Realistic Conditions; **2016**.
- (45) Canada, E. and C. C. *Plastic waste and pollution reduction*. <https://www.canada.ca/en/environment-climate-change/services/managing-reducing-waste/reduce-plastic-waste.html> (accessed 2023-03-21).
- (46) Lai, B.; Zhou, Y.; Qin, H.; Wu, C.; Pang, C.; Lian, Y.; Xu, J. Pretreatment of Wastewater from Acrylonitrile–Butadiene–Styrene (ABS) Resin Manufacturing by Microelectrolysis. *Chem. Eng. J.* **2012**, *179*, 1–7. <https://doi.org/10.1016/j.cej.2010.12.089>.
- (47) Tokiwa, Y.; Calabia, B. P. Biodegradability and Biodegradation of Poly(Lactide). *Appl. Microbiol. Biotechnol.* **2006**, *72* (2), 244–251. <https://doi.org/10.1007/s00253-006-0488-1>.
- (48) Zhang, J.; Wang, X.; Gong, J.; Gu, Z. A Study on the Biodegradability of Polyethylene Terephthalate Fiber and Diethylene Glycol Terephthalate. *J. Appl. Polym. Sci.* **2004**, *93* (3), 1089–1096. <https://doi.org/10.1002/app.20556>.
- (49) Raj, T.; Chandrasekhar, K.; Naresh Kumar, A.; Kim, S.-H. Lignocellulosic Biomass as Renewable Feedstock for Biodegradable and Recyclable Plastics Production: A Sustainable Approach. *Renew. Sustain. Energy Rev.* **2022**, *158*, 112130. <https://doi.org/10.1016/j.rser.2022.112130>.
- (50) *Plastic by the Numbers*. Plastic Action Centre. <https://plasticactioncentre.ca/directory/plastic-by-the-numbers/> (accessed 2023-03-21).
- (51) Choe, S.; Kim, Y.; Won, Y.; Myung, J. Bridging Three Gaps in Biodegradable Plastics: Misconceptions and Truths About Biodegradation. *Front. Chem.* **2021**, *9*.

- (52) Ciriminna, R.; Pagliaro, M. Biodegradable and Compostable Plastics: A Critical Perspective on the Dawn of Their Global Adoption. *ChemistryOpen* **2020**, *9* (1), 8–13. <https://doi.org/10.1002/open.201900272>.
- (53) Zhu, J.; Wang, C. Biodegradable Plastics: Green Hope or Greenwashing? *Mar. Pollut. Bull.* **2020**, *161*, 111774. <https://doi.org/10.1016/j.marpolbul.2020.111774>.
- (54) Pakkanen, J.; Manfredi, D.; Minetola, P.; Iuliano, L. About the Use of Recycled or Biodegradable Filaments for Sustainability of 3D Printing. In *Sustainable Design and Manufacturing 2017*; Campana, G., Howlett, R. J., Setchi, R., Cimatti, B., Eds.; Smart Innovation, Systems and Technologies; Springer International Publishing: Cham, **2017**; Vol. 68, pp 776–785. [https://doi.org/10.1007/978-3-319-57078-5\\_73](https://doi.org/10.1007/978-3-319-57078-5_73).
- (55) Wojtyła, S.; Klama, P.; Baran, T. Is 3D Printing Safe? Analysis of the Thermal Treatment of Thermoplastics: ABS, PLA, PET, and Nylon. *J. Occup. Environ. Hyg.* **2017**, *14* (6), D80–D85. <https://doi.org/10.1080/15459624.2017.1285489>.
- (56) Azimi, P.; Zhao, D.; Pouzet, C.; Crain, N. E.; Stephens, B. Emissions of Ultrafine Particles and Volatile Organic Compounds from Commercially Available Desktop Three-Dimensional Printers with Multiple Filaments. *Environ. Sci. Technol.* **2016**, *50* (3), 1260–1268. <https://doi.org/10.1021/acs.est.5b04983>.
- (57) Farcas, M. T.; McKinney, W.; Qi, C.; Mandler, K. W.; Battelli, L.; Friend, S. A.; Stefaniak, A. B.; Jackson, M.; Orandle, M.; Winn, A.; Kashon, M.; LeBouf, R. F.; Russ, K. A.; Hammond, D. R.; Burns, D.; Ranpara, A.; Thomas, T. A.; Matheson, J.; Qian, Y. Pulmonary and Systemic Toxicity in Rats Following Inhalation Exposure of 3-D Printer Emissions from Acrylonitrile Butadiene Styrene (ABS) Filament. *Inhal. Toxicol.* **2020**, *32* (11–12), 403–418. <https://doi.org/10.1080/08958378.2020.1834034>.

- (58) Stephens, B.; Azimi, P.; El Orch, Z.; Ramos, T. Ultrafine Particle Emissions from Desktop 3D Printers. *Atmos. Environ.* **2013**, *79*, 334–339. <https://doi.org/10.1016/j.atmosenv.2013.06.050>.
- (59) Yunis, J.; Aliakbari, E. Generation and Management of Municipal Solid Waste: How's Canada Doing? *Fraser Inst.* **2021**.
- (60) Kumar, V. Recycling of Waste and Used Papers: A Useful Contribution in Conservation of Environment: A Case Study. *Asian J. Water Environ. Pollut.* **2017**, *14* (4), 31–36. <https://doi.org/10.3233/AJW-170034>.
- (61) Valente, M.; Tirillò, J.; Quitadamo, A. Industrial Paper Recycling Process: Suitable Micronization for Additive Polymer Application. *CSE - City Saf. Energy* **2016**, *0* (2), 145–152. <https://doi.org/10.12896/cse20150020071>.
- (62) Gupta, R.; Garg, V. K. Vermiremediation and Nutrient Recovery of Non-Recyclable Paper Waste Employing *Eisenia Fetida*. *J. Hazard. Mater.* **2009**, *162* (1), 430–439. <https://doi.org/10.1016/j.jhazmat.2008.05.055>.
- (63) Sutcu, M.; del Coz Díaz, J. J.; Álvarez Rabanal, F. P.; Gencel, O.; Akkurt, S. Thermal Performance Optimization of Hollow Clay Bricks Made up of Paper Waste. *Energy Build.* **2014**, *75*, 96–108. <https://doi.org/10.1016/j.enbuild.2014.02.006>.
- (64) Jagadeesh, D.; Kanny, K.; Prashantha, K. A Review on Research and Development of Green Composites from Plant Protein-Based Polymers. *Polym. Compos.* **2017**, *38* (8), 1504–1518. <https://doi.org/10.1002/pc.23718>.
- (65) Scheller, J.; Conrad, U. Plant-Based Material, Protein and Biodegradable Plastic. *Curr. Opin. Plant Biol.* **2005**, *8* (2), 188–196. <https://doi.org/10.1016/j.pbi.2005.01.010>.

- (66) Mooney, B. P. The Second Green Revolution? Production of Plant-Based Biodegradable Plastics. *Biochem. J.* **2009**, *418* (2), 219–232. <https://doi.org/10.1042/BJ20081769>.
- (67) Galiotta, G.; Di Gioia, L.; Guilbert, S.; Cuq, B. Mechanical and Thermomechanical Properties of Films Based on Whey Proteins as Affected by Plasticizer and Crosslinking Agents. *J. Dairy Sci.* **1998**, *81* (12), 3123–3130. [https://doi.org/10.3168/jds.S0022-0302\(98\)75877-1](https://doi.org/10.3168/jds.S0022-0302(98)75877-1).
- (68) Martinez, A. W.; Caves, J. M.; Ravi, S.; Li, W.; Chaikof, E. L. Effects of Crosslinking on the Mechanical Properties, Drug Release and Cytocompatibility of Protein Polymers. *Acta Biomater.* **2014**, *10* (1), 26–33. <https://doi.org/10.1016/j.actbio.2013.08.029>.
- (69) Feeney, R. E.; Whitaker, J. R. Importance of Cross-Linking Reactions in Proteins. *Adv. Cereal Sci. Technol. USA* **1987**.
- (70) Ullsten, N. H.; Gällstedt, M.; Hedenqvist, M. S. *Plasticizers for Protein-Based Materials*; IntechOpen, **2016**. <https://doi.org/10.5772/64073>.
- (71) Gerrard, J. A. Protein–Protein Crosslinking in Food: Methods, Consequences, Applications. *Trends Food Sci. Technol.* **2002**, *13* (12), 391–399. [https://doi.org/10.1016/S0924-2244\(02\)00257-1](https://doi.org/10.1016/S0924-2244(02)00257-1).
- (72) Zarina, S.; Zhao, H.-R.; Abraham, E. Advanced Glycation End Products in Human Senile and Diabetic Cataractous Lenses. *Mol. Cell. Biochem.* **2000**, *210* (1), 29–34. <https://doi.org/10.1023/A:1007015416572>.
- (73) Gupta, M. N.; Perwez, M.; Sardar, M. Protein Crosslinking: Uses in Chemistry, Biology and Biotechnology. *Biocatal. Biotransformation* **2020**, *38* (3), 178–201. <https://doi.org/10.1080/10242422.2020.1733990>.

- (74) Heck, T.; Faccio, G.; Richter, M.; Thöny-Meyer, L. Enzyme-Catalyzed Protein Crosslinking. *Appl. Microbiol. Biotechnol.* **2013**, *97* (2), 461–475. <https://doi.org/10.1007/s00253-012-4569-z>.
- (75) Zhang, W.; Azizi-Lalabadi, M.; Roy, S.; Salim, S. A.; Castro-Muñoz, R.; Jafari, S. M. Maillard-Reaction (Glycation) of Biopolymeric Packaging Films; Principles, Mechanisms, Food Applications. *Trends Food Sci. Technol.* **2023**, *138*, 523–538. <https://doi.org/10.1016/j.tifs.2023.06.026>.
- (76) Moreira, A. S. P.; Nunes, F. M.; Domingues, M. R.; Coimbra, M. A. Coffee Melanoidins: Structures, Mechanisms of Formation and Potential Health Impacts. *Food Funct.* **2012**, *3* (9), 903–915. <https://doi.org/10.1039/c2fo30048f>.
- (77) Abedin Zadeh, M.; Alany, R. G.; Satarian, L.; Shavandi, A.; Abdullah Almousa, M.; Brocchini, S.; Khoder, M. Maillard Reaction Crosslinked Alginate-Albumin Scaffolds for Enhanced Fenofibrate Delivery to the Retina: A Promising Strategy to Treat RPE-Related Dysfunction. *Pharmaceutics* **2023**, *15* (5), 1330. <https://doi.org/10.3390/pharmaceutics15051330>.
- (78) Rowat, S. JA.; Legge, R. L.; Moresoli, C. Plant Protein in Material Extrusion 3D Printing: Formation, Plasticization, Prospects, and Challenges. *J. Food Eng.* **2021**, *308*, 110623. <https://doi.org/10.1016/j.jfoodeng.2021.110623>.
- (79) Chen, Y.; Zhang, M.; Bhandari, B. 3D Printing of Steak-like Foods Based on Textured Soybean Protein. *Foods* **2021**, *10* (9), 2011. <https://doi.org/10.3390/foods10092011>.
- (80) Xu, Y.; Han, Y.; Chen, M.; Li, J.; Li, J.; Luo, J.; Gao, Q. A Soy Protein-Based Film by Mixed Covalent Cross-Linking and Flexibilizing Networks. *Ind. Crops Prod.* **2022**, *183*, 114952. <https://doi.org/10.1016/j.indcrop.2022.114952>.

- (81) Jahangirian, H.; Azizi, S.; Rafiee-Moghaddam, R.; Baratvand, B.; Webster, T. J. Status of Plant Protein-Based Green Scaffolds for Regenerative Medicine Applications. *Biomolecules* **2019**, *9* (10), 619. <https://doi.org/10.3390/biom9100619>.
- (82) Paliwal, R.; Palakurthi, S. Zein in Controlled Drug Delivery and Tissue Engineering. *J. Controlled Release* **2014**, *189*, 108–122. <https://doi.org/10.1016/j.jconrel.2014.06.036>.
- (83) Jing, L.; Sun, J.; Liu, H.; Wang, X.; Huang, D. Using Plant Proteins to Develop Composite Scaffolds for Cell Culture Applications. *Int. J. Bioprinting* **2020**, *7* (1), 298. <https://doi.org/10.18063/ijb.v7i1.298>.
- (84) Shurtleff, W.; Aoyagi, A. *Henry Ford and His Researchers - History of Their Work with Soybeans, Soyfoods and Chemurgy (1928-2011): Extensively Annotated Bibliography and Sourcebook*; Soyinfo Center, **2011**.
- (85) Swain, S. N.; Biswal, S. M.; Nanda, P. K.; Nayak, P. L. Biodegradable Soy-Based Plastics: Opportunities and Challenges. *J. Polym. Environ.* **2004**, *12* (1), 35–42. <https://doi.org/10.1023/B:JOOE.0000003126.14448.04>.
- (86) Kumar, R.; Choudhary, V.; Mishra, S.; Varma, I. K.; Mattiason, B. Adhesives and Plastics Based on Soy Protein Products. *Ind. Crops Prod.* **2002**, *16* (3), 155–172. [https://doi.org/10.1016/S0926-6690\(02\)00007-9](https://doi.org/10.1016/S0926-6690(02)00007-9).
- (87) Nishinari, K.; Fang, Y.; Guo, S.; Phillips, G. O. Soy Proteins: A Review on Composition, Aggregation and Emulsification. *Food Hydrocoll.* **2014**, *39*, 301–318. <https://doi.org/10.1016/j.foodhyd.2014.01.013>.
- (88) Gitlin-Domagalska, A.; Maciejewska, A.; Dębowski, D. Bowman-Birk Inhibitors: Insights into Family of Multifunctional Proteins and Peptides with Potential Therapeutical Applications. *Pharmaceuticals* **2020**, *13* (12), 421. <https://doi.org/10.3390/ph13120421>.

- (89) Major, I. T.; Constabel, C. P. Functional Analysis of the Kunitz Trypsin Inhibitor Family in Poplar Reveals Biochemical Diversity and Multiplicity in Defense against Herbivores. *Plant Physiol.* **2008**, *146* (3), 888–903. <https://doi.org/10.1104/pp.107.106229>.
- (90) Álvarez-Castillo, E.; Aguilar, J. M.; Bengoechea, C.; López-Castejón, M. L.; Guerrero, A. Rheology and Water Absorption Properties of Alginate-Soy Protein Composites. *Polymers* **2021**, *13* (11), 1807. <https://doi.org/10.3390/polym13111807>.
- (91) Jiang, K.; Lei, Z.; Maoyu, Y.; Lv, W.; Jing, M.; Feng, Q.; Tan, H.; Chen, Y.; Xiao, H. Improved Performance of Soy Protein Adhesive with Melamine–Urea–Formaldehyde Prepolymer. *RSC Adv.* **2021**, *11*, 27126–27134. <https://doi.org/10.1039/D1RA00850A>.
- (92) Caillard, R.; Remondetto, G. E.; Mateescu, M. A.; Subirade, M. Characterization of Amino Cross-Linked Soy Protein Hydrogels. *J. Food Sci.* **2008**, *73* (5), C283-291. <https://doi.org/10.1111/j.1750-3841.2008.00780.x>.
- (93) Wang, Y.; Mo, X.; Sun, X. S.; Wang, D. Soy Protein Adhesion Enhanced by Glutaraldehyde Crosslink. *J. Appl. Polym. Sci.* **2007**, *104* (1), 130–136. <https://doi.org/10.1002/app.24675>.
- (94) Denavi, G.; Tapia-Blácido, D. R.; Añón, M. C.; Sobral, P. J. A.; Mauri, A. N.; Menegalli, F. C. Effects of Drying Conditions on Some Physical Properties of Soy Protein Films. *J. Food Eng.* **2009**, *90* (3), 341–349. <https://doi.org/10.1016/j.jfoodeng.2008.07.001>.
- (95) Rebezov, M.; Oboturova, N.; Statsenko, E.; Bachukin, V.; Katkova, E.; Khayrullin, M.; Neverova, O.; Zinina, O. Crosslinking Methods for Improving the Properties of Soy-Protein Based Films for Meat Packaging: A Review. *Potravinarstvo Slovak J. Food Sci.* **2023**, *17*, 635–648. <https://doi.org/10.5219/1892>.

- (96) Song, F.; Tang, D.-L.; Wang, X.-L.; Wang, Y.-Z. Biodegradable Soy Protein Isolate-Based Materials: A Review. *Biomacromolecules* **2011**, *12* (10), 3369–3380. <https://doi.org/10.1021/bm200904x>.
- (97) Chien, K. B.; Makridakis, E.; Shah, R. N. Three-Dimensional Printing of Soy Protein Scaffolds for Tissue Regeneration. *Tissue Eng. Part C Methods* **2013**, *19* (6), 417–426. <https://doi.org/10.1089/ten.tec.2012.0383>.
- (98) Zhang, H.; Wang, L.; Li, H.; Chi, Y.; Zhang, H.; Xia, N.; Ma, Y.; Jiang, L.; Zhang, X. Changes in Properties of Soy Protein Isolate Edible Films Stored at Different Temperatures: Studies on Water and Glycerol Migration. *Foods* **2021**, *10* (8), 1797. <https://doi.org/10.3390/foods10081797>.
- (99) O'Dell, J.; Hunt, C.; Frihart, C. Heat Resistant Sustainable Adhesives Based on Soy. In *33rd Annual Meeting of The Adhesion Society*; Daytona Beach, FL, **2010**; p 5.
- (100) Song, F.; Zhang, L.-M. Gelation Modification of Soy Protein Isolate by a Naturally Occurring Cross-Linking Agent and Its Potential Biomedical Application. *Ind. Eng. Chem. Res.* **2009**, *48* (15), 7077–7083. <https://doi.org/10.1021/ie801372f>.
- (101) Wang, S.; Liu, S. 3D Printing of Soy Protein- and Gluten-Based Gels Facilitated by Thermosensitive Cocoa Butter in a Model Study. *ACS Food Sci. Technol.* **2021**, *1* (10), 1990–1996. <https://doi.org/10.1021/acsfoodscitech.1c00311>.
- (102) Carranza, T.; Guerrero, P.; Caba, K. de la; Etxabide, A. Texture-Modified Soy Protein Foods: 3D Printing Design and Red Cabbage Effect. *Food Hydrocoll.* **2023**, *145*, 109141. <https://doi.org/10.1016/j.foodhyd.2023.109141>.
- (103) Zheng, Z. Insights into Soy Protein-Based Drug Delivery Vehicles via Molecular Dynamic Simulation. *J. Mol. Liq.* **2023**, *388*, 122818. <https://doi.org/10.1016/j.molliq.2023.122818>.

- (104) Mehra, S.; Nisar, S.; Chauhan, S.; Singh, V.; Rattan, S. Soy Protein-Based Hydrogel under Microwave-Induced Grafting of Acrylic Acid and 4-(4-Hydroxyphenyl)Butanoic Acid: A Potential Vehicle for Controlled Drug Delivery in Oral Cavity Bacterial Infections. *ACS Omega* **2020**, *5* (34), 21610–21622. <https://doi.org/10.1021/acsomega.0c02287>.
- (105) Vaz, C. M.; van Doeveren, P. F. N. M.; Reis, R. L.; Cunha, A. M. Soy Matrix Drug Delivery Systems Obtained by Melt-Processing Techniques. *Biomacromolecules* **2003**, *4* (6), 1520–1529. <https://doi.org/10.1021/bm034050i>.
- (106) Liu, F.; Liu, C.; Zheng, B.; He, J.; Liu, J.; Chen, C.; Lee, I.; Wang, X.; Liu, Y. Synergistic Effects on Incorporation of  $\beta$ -Tricalcium Phosphate and Graphene Oxide Nanoparticles to Silk Fibroin/Soy Protein Isolate Scaffolds for Bone Tissue Engineering. *Polymers* **2020**, *12* (1), 69. <https://doi.org/10.3390/polym12010069>.
- (107) Baranes-Zeevi, M.; Goder, D.; Zilberman, M. Novel Drug-Eluting Soy-Protein Structures for Wound Healing Applications. *Polym. Adv. Technol.* **2019**, *30* (10), 2523–2538. <https://doi.org/10.1002/pat.4673>.
- (108) Varshney, N.; Singh, P.; Rai, R.; Vishwakarma, N. K.; Mahto, S. K. Superporous Soy Protein Isolate Matrices as Superabsorbent Dressings for Successful Management of Highly Exuding Wounds: In Vitro and in Vivo Characterization. *Int. J. Biol. Macromol.* **2023**, *253* (Pt 6), 127268. <https://doi.org/10.1016/j.ijbiomac.2023.127268>.
- (109) Zhang, J.; Mungara, P.; Jane, J. Mechanical and Thermal Properties of Extruded Soy Protein Sheets. *Polymer* **2001**, *42* (6), 2569–2578. [https://doi.org/10.1016/S0032-3861\(00\)00624-8](https://doi.org/10.1016/S0032-3861(00)00624-8).

- (110) Wang, S.; Sue, H.-J.; Jane, J. Effects of Polyhydric Alcohols on the Mechanical Properties of Soy Protein Plastics. *J. Macromol. Sci. Part A* **1996**, *33* (5), 557–569. <https://doi.org/10.1080/10601329608010878>.
- (111) Alavarse, A. C.; Frachini, E. C. G.; da Silva, R. L. C. G.; Lima, V. H.; Shavandi, A.; Petri, D. F. S. Crosslinkers for Polysaccharides and Proteins: Synthesis Conditions, Mechanisms, and Crosslinking Efficiency, a Review. *Int. J. Biol. Macromol.* **2022**, *202*, 558–596. <https://doi.org/10.1016/j.ijbiomac.2022.01.029>.
- (112) Krishnakumar, G. S.; Sampath, S.; Muthusamy, S.; John, M. A. Importance of Crosslinking Strategies in Designing Smart Biomaterials for Bone Tissue Engineering: A Systematic Review. *Mater. Sci. Eng. C* **2019**, *96*, 941–954. <https://doi.org/10.1016/j.msec.2018.11.081>.
- (113) Soboyejo, W. *Mechanical Properties of Engineered Materials*; CRC Press: Boca Raton, **2002**. <https://doi.org/10.1201/9780203910399>.
- (114) Akinwande, D.; Brennan, C. J.; Bunch, J. S.; Egberts, P.; Felts, J. R.; Gao, H.; Huang, R.; Kim, J.-S.; Li, T.; Li, Y.; Liechti, K. M.; Lu, N.; Park, H. S.; Reed, E. J.; Wang, P.; Yakobson, B. I.; Zhang, T.; Zhang, Y.-W.; Zhou, Y.; Zhu, Y. A Review on Mechanics and Mechanical Properties of 2D Materials—Graphene and Beyond. *Extreme Mech. Lett.* **2017**, *13*, 42–77. <https://doi.org/10.1016/j.eml.2017.01.008>.
- (115) Cai, C.; Zhou, K. Chapter 7 - Metal Additive Manufacturing. In *Digital Manufacturing*; Patel, C. D., Chen, C.-H., Eds.; Elsevier, **2022**; pp 247–298. <https://doi.org/10.1016/B978-0-323-95062-6.00005-X>.

- (116) Chua, C. K.; Wong, C. H.; Yeong, W. Y. Chapter Eight - Benchmarking for Additive Manufacturing. In *Standards, Quality Control, and Measurement Sciences in 3D Printing and Additive Manufacturing*; Chua, C. K., Wong, C. H., Yeong, W. Y., Eds.; Academic Press, **2017**; pp 181–212. <https://doi.org/10.1016/B978-0-12-813489-4.00008-8>.
- (117) Pires, J. R. A.; Souza, V. G. L.; Fuciños, P.; Pastrana, L.; Fernando, A. L. Methodologies to Assess the Biodegradability of Bio-Based Polymers—Current Knowledge and Existing Gaps. *Polymers* **2022**, *14* (7), 1359. <https://doi.org/10.3390/polym14071359>.
- (118) Ye, Q.; Han, Y.; Zhang, J.; Zhang, W.; Xia, C.; Li, J. Bio-Based Films with Improved Water Resistance Derived from Soy Protein Isolate and Stearic Acid *via* Bioconjugation. *J. Clean. Prod.* **2019**, *214*, 125–131. <https://doi.org/10.1016/j.jclepro.2018.12.277>.
- (119) Li, F.; Zhao, G.; Tian, G. A New Method for Evaluating Sirolimus Actual Release Kinetics of Degradable Polymer Matrix via Numerical Convolution. *J. Drug Deliv. Sci. Technol.* **2023**, *81*, 104275. <https://doi.org/10.1016/j.jddst.2023.104275>.
- (120) Chien, K. B.; Chung, E. J.; Shah, R. N. Investigation of Soy Protein Hydrogels for Biomedical Applications: Materials Characterization, Drug Release, and Biocompatibility. *J. Biomater. Appl.* **2014**, *28* (7), 1085–1096. <https://doi.org/10.1177/0885328213497413>.
- (121) Paarakh, M. P.; Jose, P. A.; Setty, C.; Peterchristoper, G. V. RELEASE KINETICS – CONCEPTS AND APPLICATIONS. *Int. J. Pharm. Res. Technol. IJPRT* **2018**, *8* (1), 12–20. <https://doi.org/10.31838/ijprt/08.01.02>.
- (122) Godfray, H. C. J.; Beddington, J. R.; Crute, I. R.; Haddad, L.; Lawrence, D.; Muir, J. F.; Pretty, J.; Robinson, S.; Thomas, S. M.; Toulmin, C. Food Security: The Challenge of Feeding 9 Billion People. *Science* **2010**, *327* (5967), 812–818. <https://doi.org/10.1126/science.1185383>.

- (123) Tümer, E. H.; Erbil, H. Y. *Extrusion-Based 3D Printing Applications of PLA Composites: A Review. Coatings* **2021**, *11* (4), 390. <https://doi.org/10.3390/coatings11040390>.
- (124) Chaunier, L.; Guessasma, S.; Belhabib, S.; Della Valle, G.; Lourdin, D.; Leroy, E. Material Extrusion of Plant Biopolymers: Opportunities & Challenges for 3D Printing. *Addit. Manuf.* **2018**, *21*, 220–233. <https://doi.org/10.1016/j.addma.2018.03.016>.
- (125) Armbruster, D. A.; Pry, T. Limit of Blank, Limit of Detection and Limit of Quantitation. *Clin. Biochem. Rev.* **2008**, *29* (Suppl 1), S49–S52.
- (126) Babity, S.; Polomska, A. K.; Couture, F.; Bonmarin, M.; Fehr, D.; Detmar, M.; Brambilla, D. Rational Design of a Fluorescent Microneedle Tattoo for Minimally Invasive Monitoring of Lymphatic Function. *J. Control. Release Off. J. Control. Release Soc.* **2020**, *327*, 350–359. <https://doi.org/10.1016/j.jconrel.2020.08.017>.
- (127) Larrañeta, E.; Moore, J.; Vicente-Pérez, E. M.; González-Vázquez, P.; Lutton, R.; Woolfson, A. D.; Donnelly, R. F. A Proposed Model Membrane and Test Method for Microneedle Insertion Studies. *Int. J. Pharm.* **2014**, *472* (1), 65–73. <https://doi.org/10.1016/j.ijpharm.2014.05.042>.
- (128) Arboleda, J. C.; Niemi, N.; Kumpunen, J.; Lucia, L. A.; Rojas, O. J. Soy Protein-Based Polyelectrolyte Complexes as Biobased Wood Fiber Dry Strength Agents. *ACS Sustain. Chem. Eng.* **2014**, *2* (10), 2267–2274. <https://doi.org/10.1021/sc500399d>.
- (129) Yue, L.; Meng, Z.; Yi, Z.; Gao, Q.; Mao, A.; Li, J. Effects of Different Denaturants on Properties and Performance of Soy Protein-Based Adhesive. *Polymers* **2019**, *11* (8), 1262. <https://doi.org/10.3390/polym11081262>.

- (130) Jiang, S.; Carroll, L.; Mariotti, M.; Hägglund, P.; Davies, M. J. Formation of Protein Cross-Links by Singlet Oxygen-Mediated Disulfide Oxidation. *Redox Biol.* **2021**, *41*, 101874. <https://doi.org/10.1016/j.redox.2021.101874>.
- (131) Bulleid, N. J. Disulfide Bond Formation in the Mammalian Endoplasmic Reticulum. *Cold Spring Harb. Perspect. Biol.* **2012**, *4* (11), a013219. <https://doi.org/10.1101/cshperspect.a013219>.
- (132) Bukartyk, M.; Zholobko, O.; Wu, X.-F. Green Synthesis of Soy Protein Nanocomposites: Effects of Cross-Linking and Clay Nanoparticles on the Mechanical Performance. *ACS Omega* **2022**, *7* (7), 5883–5893. <https://doi.org/10.1021/acsomega.1c06002>.
- (133) Tian, H.; Guo, G.; Xiang, A.; Zhong, W.-H. Intermolecular Interactions and Microstructure of Glycerol-Plasticized Soy Protein Materials at Molecular and Nanometer Levels. *Polym. Test.* **2018**, *67*, 197–204. <https://doi.org/10.1016/j.polymertesting.2018.03.002>.
- (134) Xu, H.; Shen, L.; Xu, L.; Yang, Y. Low-Temperature Crosslinking of Proteins Using Non-Toxic Citric Acid in Neutral Aqueous Medium: Mechanism and Kinetic Study. *Ind. Crops Prod.* **2015**, *74*, 234–240. <https://doi.org/10.1016/j.indcrop.2015.05.010>.
- (135) Yan, Z.; Li, Q.; Zhang, P. Soy Protein Isolate and Glycerol Hydrogen Bonding Using Two-Dimensional Correlation (2D-COS) Attenuated Total Reflection Fourier Transform Infrared (ATR FT-IR) Spectroscopy. *Appl. Spectrosc.* **2017**, *71* (11), 2437–2445. <https://doi.org/10.1177/0003702817710249>.
- (136) Pattanaik, S.; Sutar, A.; Maharana, T. Graft Copolymerization of Soy Protein Isolate with Polylactide via Ring Opening Polymerization. *IOP Conf. Ser. Mater. Sci. Eng.* **2018**, *410*, 012011. <https://doi.org/10.1088/1757-899X/410/1/012011>.

- (137) Zhang, Z.; Liu, Z.; Xue, C.; Chen, H.; Han, X.; Ren, Y. Amorphous Porous Organic Polymers Containing Main Group Elements. *Commun. Chem.* **2023**, *6* (1), 1–22. <https://doi.org/10.1038/s42004-023-01063-5>.
- (138) Lubis, M.; Harahap, M.; Ginting, M. H. S.; Maysarah, S.; Gana, A. Short Communication: The Effect of Ethylene Glycol as Plasticizer against Mechanical Properties of Bioplastic Originated from Jackfruit Seed Starch and Cocoa Pod Husk. *Nusant. Biosci.* **2018**, *10*, 76–80. <https://doi.org/10.13057/nusbiosci/n100202>.
- (139) Tayeb, A. H.; Hubbe, M. A.; Tayeb, P.; Pal, L.; Rojas, O. J. Soy Proteins As a Sustainable Solution to Strengthen Recycled Paper and Reduce Deposition of Hydrophobic Contaminants in Papermaking: A Bench and Pilot-Plant Study. *ACS Sustain. Chem. Eng.* **2017**, *5* (8), 7211–7219. <https://doi.org/10.1021/acssuschemeng.7b01425>.
- (140) Barkay-Olami, H.; Zilberman, M. Novel Porous Soy Protein-Based Blend Structures for Biomedical Applications: Microstructure, Mechanical, and Physical Properties. *J. Biomed. Mater. Res. B Appl. Biomater.* **2016**, *104* (6), 1109–1120. <https://doi.org/10.1002/jbm.b.33459>.
- (141) Ahmad, K.; Din, Z.; Ullah, H.; Ouyang, Q.; Rani, S.; Jan, I.; Alam, M.; Rahman, Z.; Kamal, T.; Ali, S.; Khan, A.; Shahwar, D.; Gul, F.; Ibrahim, M.; Nawaz, T. Preparation and Characterization of Bio-Based Nanocomposites Packaging Films Reinforced with Cellulose Nanofibers from Unripe Banana Peels. **2022**.
- (142) Langlet, M.; Nadaud, F.; Mohammed, B.; Pezron, I.; Saleh, K.; Guigon, P.; Metlas-Komunjer, L. Kinetics of Dissolution and Recrystallization of Sodium Chloride at Controlled Relative Humidity. *KONA Powder Part. J.* **2011**, *29*, 168–179. <https://doi.org/10.14356/kona.2011019>.

- (143) Tamanna, N.; Mahmood, N. Food Processing and Maillard Reaction Products: Effect on Human Health and Nutrition. *Int. J. Food Sci.* **2015**, *2015*, 526762. <https://doi.org/10.1155/2015/526762>.
- (144) Sun, X. S. 9 - THERMAL AND MECHANICAL PROPERTIES OF SOY PROTEINS. In *Bio-Based Polymers and Composites*; Wool, R. P., Sun, X. S., Eds.; Academic Press: Burlington, **2005**; pp 292–326. <https://doi.org/10.1016/B978-012763952-9/50010-1>.
- (145) Guerrero, P.; Retegi, A.; Gabilondo, N.; de la Caba, K. Mechanical and Thermal Properties of Soy Protein Films Processed by Casting and Compression. *J. Food Eng.* **2010**, *100* (1), 145–151. <https://doi.org/10.1016/j.jfoodeng.2010.03.039>.
- (146) Jensen, R. P.; Strongin, R. M.; Peyton, D. H. Solvent Chemistry in the Electronic Cigarette Reaction Vessel. *Sci. Rep.* **2017**, *7* (1), 42549. <https://doi.org/10.1038/srep42549>.
- (147) Barbooti, M. M.; Al-Sammerrai, D. A. Thermal Decomposition of Citric Acid. *Thermochim. Acta* **1986**, *98*, 119.
- (148) Sánchez-Sánchez, R.; Rodríguez-Rego, J. M.; Macías-García, A.; Mendoza-Cerezo, L.; Díaz-Parralejo, A. Relationship between Shear-Thinning Rheological Properties of Bioinks and Bioprinting Parameters. *Int. J. Bioprinting* **2023**, *9* (2), 687. <https://doi.org/10.18063/ijb.687>.
- (149) Li, Y.; Chen, F.; Zhang, L.; Yao, Y. Effect of Surface Changes of Soy Protein Materials on Water Resistance. *Mater. Lett.* **2015**, *149*, 120–122. <https://doi.org/10.1016/j.matlet.2015.02.034>.
- (150) Gao, G.; Xu, F.; Xu, J.; Liu, Z. Study of Material Color Influences on Mechanical Characteristics of Fused Deposition Modeling Parts. *Materials* **2022**, *15* (19), 7039. <https://doi.org/10.3390/ma15197039>.

- (151) Lamp, A.; Kaltschmitt, M.; Dethloff, J. Options to Improve the Mechanical Properties of Protein-Based Materials. *Molecules* **2022**, *27* (2), 446. <https://doi.org/10.3390/molecules27020446>.
- (152) Friesen, K.; Chang, C.; Nickerson, M. Incorporation of Phenolic Compounds, Rutin and Epicatechin, into Soy Protein Isolate Films: Mechanical, Barrier and Cross-Linking Properties. *Food Chem.* **2015**, *172*, 18–23. <https://doi.org/10.1016/j.foodchem.2014.08.128>.
- (153) Gopalakrishnan, S.; Xu, J.; Zhong, F.; Rotello, V. M. Strategies for Fabricating Protein Films for Biomaterials Applications. *Adv. Sustain. Syst.* **2021**, *5* (1), 2000167. <https://doi.org/10.1002/adsu.202000167>.
- (154) Basiak, E.; Lenart, A.; Debeaufort, F. How Glycerol and Water Contents Affect the Structural and Functional Properties of Starch-Based Edible Films. *Polymers* **2018**, *10* (4), 412. <https://doi.org/10.3390/polym10040412>.
- (155) Mercadé-Prieto, R.; Zhao, H.; Zhang, M.; Li, H.; Zhao, L.; Chen, X. D. Dissolution and Swelling of Soy Protein Isolate Hydrogels in Alkali. *Food Hydrocoll.* **2016**, *56*, 285–291. <https://doi.org/10.1016/j.foodhyd.2015.12.014>.
- (156) Peng, C.; Chow, A. H. L.; Chan, C. K. Hygroscopic Study of Glucose, Citric Acid, and Sorbitol Using an Electrodynamic Balance: Comparison with UNIFAC Predictions. *Aerosol Sci. Technol.* **2001**, *35* (3), 753–758. <https://doi.org/10.1080/02786820152546798>.
- (157) East, A. L. L. On the Hydrolysis Mechanisms of Amides and Peptides. *Int. J. Chem. Kinet.* **2018**, *50* (10), 705–709. <https://doi.org/10.1002/kin.21194>.

- (158) Robins, L. I.; Fogle, E. J.; Marlier, J. F. Mechanistic Investigations of the Hydrolysis of Amides, Oxoesters and Thioesters via Kinetic Isotope Effects and Positional Isotope Exchange. *Biochim. Biophys. Acta BBA - Proteins Proteomics* **2015**, *1854* (11), 1756–1767. <https://doi.org/10.1016/j.bbapap.2014.12.016>.
- (159) Li, W.; Zhou, J.; Xu, Y. Study of the in Vitro Cytotoxicity Testing of Medical Devices (Review). *Biomed. Rep.* **2015**, *3* (5), 617–620. <https://doi.org/10.3892/br.2015.481>.
- (160) Awa, K.; Shinzawa, H.; Ozaki, Y. The Effect of Microcrystalline Cellulose Crystallinity on the Hydrophilic Property of Tablets and the Hydrolysis of Acetylsalicylic Acid as Active Pharmaceutical Ingredient Inside Tablets. *AAPS PharmSciTech* **2015**, *16* (4), 865–870. <https://doi.org/10.1208/s12249-014-0276-7>.
- (161) Sweis, I. E.; Cressey, B. C. Potential Role of the Common Food Additive Manufactured Citric Acid in Eliciting Significant Inflammatory Reactions Contributing to Serious Disease States: A Series of Four Case Reports. *Toxicol. Rep.* **2018**, *5*, 808–812. <https://doi.org/10.1016/j.toxrep.2018.08.002>.
- (162) Azelee, N. I. W.; Ramli, A. N. M.; Manas, N. H. A.; Salamun, N.; Man, R. C.; Enshasy, H. E. Glycerol In Food, Cosmetics And Pharmaceutical Industries: Basics And New Applications. **2019**, *8* (12).
- (163) Gupta, A. J.; Gruppen, H.; Maes, D.; Boots, J.-W.; Wierenga, P. A. Factors Causing Compositional Changes in Soy Protein Hydrolysates and Effects on Cell Culture Functionality. *J. Agric. Food Chem.* **2013**, *61* (45), 10613–10625. <https://doi.org/10.1021/jf403051z>.

- (164) Olami, H.; Zilberman, M. Microstructure and in Vitro Cellular Response to Novel Soy Protein-Based Porous Structures for Tissue Regeneration Applications. *J. Biomater. Appl.* **2016**, *30* (7), 1004–1015. <https://doi.org/10.1177/0885328215614713>.
- (165) Chang, Z.; Zhang, S.; Li, F.; Wang, Z.; Li, J.; Xia, C.; Yu, Y.; Cai, L.; Huang, Z. Self-Healable and Biodegradable Soy Protein-Based Protective Functional Film with Low Cytotoxicity and High Mechanical Strength. *Chem. Eng. J.* **2021**, *404*, 126505. <https://doi.org/10.1016/j.cej.2020.126505>.
- (166) Zhao, Y.; Huang, Z.; Zhang, J.; Wu, W.; Wang, M.; Fan, L. Thermal Degradation of Sodium Alginate- Incorporated Soy Protein Isolate/Glycerol Composite Membranes. **2010**.
- (167) Wyrzykowski, D.; Hebanowska, E.; Nowak-Wicz, G.; Makowski, M.; Chmurzyński, L. Thermal Behaviour of Citric Acid and Isomeric Aconitic Acids. *J. Therm. Anal. Calorim.* **2011**, *104* (2), 731–735. <https://doi.org/10.1007/s10973-010-1015-2>.
- (168) Almazrouei, M.; Samad, T. E.; Janajreh, I. Thermogravimetric Kinetics and High Fidelity Analysis of Crude Glycerol. *Energy Procedia* **2017**, *142*, 1699–1705. <https://doi.org/10.1016/j.egypro.2017.12.552>.
- (169) Rasheed, M.; Jawaid, M.; Karim, Z.; Abdullah, L. C. Morphological, Physiochemical and Thermal Properties of Microcrystalline Cellulose (MCC) Extracted from Bamboo Fiber. *Molecules* **2020**, *25* (12), 2824. <https://doi.org/10.3390/molecules25122824>.
- (170) Novak Babič, M.; Gunde-Cimerman, N. Water-Transmitted Fungi Are Involved in Degradation of Concrete Drinking Water Storage Tanks. *Microorganisms* **2021**, *9* (1), 160. <https://doi.org/10.3390/microorganisms9010160>.
- (171) Vranova, V.; Rejsek, K.; Formanek, P. Proteolytic Activity in Soil: A Review. *Appl. Soil Ecol.* **2013**, *70*, 23–32. <https://doi.org/10.1016/j.apsoil.2013.04.003>.

- (172) El-Gendi, H.; Saleh, A. K.; Badierah, R.; Redwan, E. M.; El-Maradny, Y. A.; El-Fakharany, E. M. A Comprehensive Insight into Fungal Enzymes: Structure, Classification, and Their Role in Mankind's Challenges. *J. Fungi* **2021**, *8* (1), 23. <https://doi.org/10.3390/jof8010023>.
- (173) Datta, R. Enzymatic Degradation of Cellulose in Soil: A Review. *Heliyon* **2024**, *10* (1), e24022. <https://doi.org/10.1016/j.heliyon.2024.e24022>.
- (174) Wen, J.; Stacey, S. P.; McLaughlin, M. J.; Kirby, J. K. Biodegradation of Rhamnolipid, EDTA and Citric Acid in Cadmium and Zinc Contaminated Soils. *Soil Biol. Biochem.* **2009**, *41* (10), 2214–2221. <https://doi.org/10.1016/j.soilbio.2009.08.006>.
- (175) Inayati; Pamungkas, D. J.; Matovanni, M. P. N. Effect of Glycerol Concentration on Mechanical Characteristics of Biodegradable Plastic from Rice Straw Cellulose. *AIP Conf. Proc.* **2019**, *2097* (1), 030110. <https://doi.org/10.1063/1.5098285>.
- (176) Vossoughi, M.; Alemzadeh, I.; Heydari, A. Influence of Glycerol and Clay Contents on Biodegradability of Corn Starch Nanocomposites. *Int. J. Eng.* **2014**, *27* (2), 203–214.
- (177) Wei, N.; Liao, M.; Xu, K.; Qin, Z. High-Performance Soy Protein-Based Films from Cellulose Nanofibers and Graphene Oxide Constructed Synergistically via Hydrogen and Chemical Bonding. *RSC Adv.* **2021**, *11* (37), 22812–22819. <https://doi.org/10.1039/D1RA02484A>.
- (178) Chen, W. L.; Guo, D. W.; Shen, Y. Y.; Guo, S. R.; Ruan, K. P. Effects of Highly Hygroscopic Excipients on the Hydrolysis of Simvastatin in Tablet at High Relative Humidity. *Indian J. Pharm. Sci.* **2012**, *74* (6), 527–534. <https://doi.org/10.4103/0250-474X.110587>.

- (179) Capezza, A. J.; Robert, E.; Lundman, M.; Newson, W. R.; Johansson, E.; Hedenqvist, M. S.; Olsson, R. T. Extrusion of Porous Protein-Based Polymers and Their Liquid Absorption Characteristics. *Polymers* **2020**, *12* (2), 459. <https://doi.org/10.3390/polym12020459>.
- (180) Malafaya, P. B.; Silva, G. A.; Reis, R. L. Natural-Origin Polymers as Carriers and Scaffolds for Biomolecules and Cell Delivery in Tissue Engineering Applications. *Adv. Drug Deliv. Rev.* **2007**, *59* (4–5), 207–233. <https://doi.org/10.1016/j.addr.2007.03.012>.
- (181) Hisatake, K.; Tanaka, S.; Aizawa, Y. Evaporation Rate of Water in a Vessel. *J. Appl. Phys.* **1993**, *73* (11), 7395–7401. <https://doi.org/10.1063/1.354031>.
- (182) Crist, B. The Ultimate Strength and Stiffness of Polymers. *Annu. Rev. Mater. Sci.* **1995**, *25* (1), 295–323. <https://doi.org/10.1146/annurev.ms.25.080195.001455>.
- (183) Bai, M.; Zhang, Y.; Bian, Y.; Gao, Q.; Shi, S. Q.; Cao, J.; Zhang, Q.; Li, J. A Novel Universal Strategy for Fabricating Soybean Protein Adhesive with Excellent Adhesion and Anti-Mildew Performances. *Chem. Eng. J.* **2023**, *452*, 139359. <https://doi.org/10.1016/j.cej.2022.139359>.
- (184) Li, H.; Wang, Y.; Xie, W.; Tang, Y.; Yang, F.; Gong, C.; Wang, C.; Li, X.; Li, C. Preparation and Characterization of Soybean Protein Adhesives Modified with an Environmental-Friendly Tannin-Based Resin. *Polymers* **2023**, *15* (10), 2289. <https://doi.org/10.3390/polym15102289>.
- (185) Podlena, M.; Böhm, M.; Saloni, D.; Velarde, G.; Salas, C. Tuning the Adhesive Properties of Soy Protein Wood Adhesives with Different Coadjutant Polymers, Nanocellulose and Lignin. *Polymers* **2021**, *13* (12), 1972. <https://doi.org/10.3390/polym13121972>.

- (186) Koerner, G. R.; Hsuan, Y. G.; Koerner, R. M. 3 - The Durability of Geosynthetics. In *Geosynthetics in Civil Engineering*; Sarsby, R. W., Ed.; Woodhead Publishing Series in Textiles; Woodhead Publishing, 2007; pp 36–65. <https://doi.org/10.1533/9781845692490.1.36>.
- (187) Pasek, J.; Vörös, F. The Present and the Future of Polystyrene Foam in Construction. *Adv. Mater. Res.* **2014**, *1020*, 43–48. <https://doi.org/10.4028/www.scientific.net/AMR.1020.43>.
- (188) Nguyen, H. X.; Bozorg, B. D.; Kim, Y.; Wieber, A.; Birk, G.; Lubda, D.; Banga, A. K. Poly (Vinyl Alcohol) Microneedles: Fabrication, Characterization, and Application for Transdermal Drug Delivery of Doxorubicin. *Eur. J. Pharm. Biopharm.* **2018**, *129*, 88–103. <https://doi.org/10.1016/j.ejpb.2018.05.017>.
- (189) McGrath, M. G.; Vucen, S.; Vrdoljak, A.; Kelly, A.; O’Mahony, C.; Crean, A. M.; Moore, A. Production of Dissolvable Microneedles Using an Atomised Spray Process: Effect of Microneedle Composition on Skin Penetration. *Eur. J. Pharm. Biopharm. Off. J. Arbeitsgemeinschaft Pharm. Verfahrenstechnik EV* **2014**, *86* (2), 200–211. <https://doi.org/10.1016/j.ejpb.2013.04.023>.
- (190) Mir, M.; Permana, A. D.; Ahmed, N.; Khan, G. M.; Rehman, A. ur; Donnelly, R. F. Enhancement in Site-Specific Delivery of Carvacrol for Potential Treatment of Infected Wounds Using Infection Responsive Nanoparticles Loaded into Dissolving Microneedles: A Proof of Concept Study. *Eur. J. Pharm. Biopharm.* **2020**, *147*, 57–68. <https://doi.org/10.1016/j.ejpb.2019.12.008>.
- (191) Bariya, S. H.; Gohel, M. C.; Mehta, T. A.; Sharma, O. P. Microneedles: An Emerging Transdermal Drug Delivery System. *J. Pharm. Pharmacol.* **2012**, *64* (1), 11–29. <https://doi.org/10.1111/j.2042-7158.2011.01369.x>.

- (192) Shahrubudin, N.; Lee, T. C.; Ramlan, R. An Overview on 3D Printing Technology: Technological, Materials, and Applications. *Procedia Manuf.* **2019**, *35*, 1286–1296. <https://doi.org/10.1016/j.promfg.2019.06.089>.
- (193) Annibaldi, V.; Rotilio, M. Energy Consumption Consideration of 3D Printing. In *2019 II Workshop on Metrology for Industry 4.0 and IoT (MetroInd4.0&IoT)*; **2019**; pp 243–248. <https://doi.org/10.1109/METROI4.2019.8792856>.
- (194) Fraanje, W.; Garnett, T. *Soy: food, feed, and land use change | TABLE Debates*. <https://tabledebates.org/building-blocks/soy-food-feed-and-land-use-change> (accessed 2024-06-26).
- (195) Erenstein, O.; Jaleta, M.; Sonder, K.; Mottaleb, K.; Prasanna, B. M. Global Maize Production, Consumption and Trade: Trends and R&D Implications. *Food Secur.* **2022**, *14* (5), 1295–1319. <https://doi.org/10.1007/s12571-022-01288-7>.